2014

Layer-by-Layer Assemblies for Membrane-Based Enzymatic Catalysis

Andrew R. Tomaino
University of Kentucky, andrew.tomaino@gmail.com

STUDENT AGREEMENT:

I represent that my thesis or dissertation and abstract are my original work. Proper attribution has been given to all outside sources. I understand that I am solely responsible for obtaining any needed copyright permissions. I have obtained needed written permission statement(s) from the owner(s) of each third-party copyrighted matter to be included in my work, allowing electronic distribution (if such use is not permitted by the fair use doctrine) which will be submitted to UKnowledge as Additional File.

I hereby grant to The University of Kentucky and its agents the irrevocable, non-exclusive, and royalty-free license to archive and make accessible my work in whole or in part in all forms of media, now or hereafter known. I agree that the document mentioned above may be made available immediately for worldwide access unless an embargo applies.

I retain all other ownership rights to the copyright of my work. I also retain the right to use in future works (such as articles or books) all or part of my work. I understand that I am free to register the copyright to my work.

REVIEW, APPROVAL AND ACCEPTANCE

The document mentioned above has been reviewed and accepted by the student's advisor, on behalf of the advisory committee, and by the Director of Graduate Studies (DGS), on behalf of the program; we verify that this is the final, approved version of the student's thesis including all changes required by the advisory committee. The undersigned agree to abide by the statements above.

Andrew R. Tomaino, Student

Dr. Dibakar Bhattacharyya, Major Professor

Dr. Thomas Dziubla, Director of Graduate Studies

LAYER-BY-LAYER ASSEMBLIES FOR MEMBRANE-BASED ENZYMATIC CATALYSIS

THESIS

A thesis submitted in partial fulfillment of the
requirements for the degree of Master of Science in
Chemical Engineering in the
College of Engineering
at the University of Kentucky

By

Andrew R. Tomaino

Lexington, Kentucky

Co-directors: Dr. Dibakar Bhattacharyya, Professor of Chemical Engineering
and Dr. Thomas Dziubla, Professor of Chemical Engineering

Lexington, Kentucky

2014

ABSTRACT OF THESIS

LAYER-BY-LAYER ASSEMBLIES FOR MEMBRANE-BASED ENZYMATIC CATALYSIS

While considerable progress has been made towards understanding the effect that membrane-based layer-by-layer (LbL) immobilizations have on the activity and stability of enzymatic catalysis, detailed work is required in order to fundamentally quantify and optimize the functionalization and operating conditions that define these properties. Transport mechanisms were studied by use of pressure-induced, flow-driven enzymatic catalysis of LbL-functionalized hydrophilized poly(vinyldiene) (PVDF)-poly(acrylic acid) (PAA)-poly(allylamine hydrochloride) (PAH)-glucose oxidase (GOx) membranes. These membranes were coupled in a sealed series following cellulose acetate (CA) membranes for the elimination of product accumulation within the feed-side solution during operation. The enzymatic catalysis of LbL-immobilized GOx from *Aspergillus niger* performed remarkably well in comparison to the homogeneous-phase catalysis within an analogous aqueous solution. On average, the enzymatic turnover was 0.0123 and 0.0076 mmol/(mg-GOx)(min) for the homogeneous-phase catalysis and the LbL-immobilized catalysis, respectively. Replicate permeations resulted in repeatable kinetic results with $R^2 > 0.95$. Over the course of a three week trial period, permeation of functionalized membranes maintained >90% normalized activity when membranes were removed when not in use and stored at -20°C, whereas the homogenous-phase kinetics dropped below 90% normalized activity in under one day.

KEYWORDS: Layer-by-layer, microfiltration, membrane, enzyme immobilization, enzymatic catalysis.

Andrew R. Tomaino

October 14, 2014

LAYER-BY-LAYER ASSEMBLIES FOR MEMBRANE-BASED ENZYMATIC CATALYSIS

By

Andrew R. Tomaino

Dr. Dibakar Bhattacharyya

Director of Thesis

Dr. Thomas Dziubla

Director of Graduate Studies

October 14, 2014

Date

Dedication

This thesis is dedicated to my fiancé, Ashley Sofia, whose perseverance and patience guided me through my academic journey; and my mother and brother, who together, with their love and guidance, taught me how to read at an early age.

Acknowledgements

Primarily, I would like to give a warm thanks to Prof. Dibakar “DB” Bhattacharyya. He has been very caring and patient with my graduate education over the last few years, and I am personally very grateful to have been assigned under such a wonderful advisor. Dr. DB has not only been an excellent advisor, but he has also become a dear friend of mine over the months. His energy, drive, and motivation have allowed him to become a role model in my mind, as I intend to mimic these qualities in my own studies. I have learned countless amounts of scholarly and professional qualities from him - things that I intend to carry with me throughout my life. In addition, I would like to thank my co-advisor, Dr. Tom Dziubla, who was able to assist me with a variety of experimental topics and practices when my primary advisor was not available.

I am also greatly thankful for the wonderful lab-mates and fellow IGERT trainees that I have has over the years for assisting me with my studies and having rigorous scientific conversations with. Thanks to Li Xiao, Minghui Gui, Dr. Vasile Smuleac, Noah Meeks, Sebastián Hernández, Ruo He, Dave Cochran, Dan Schlipf, and Jacob Lilly. I would also like to take the opportunity to thank Jim Begley from the UK Imaging Facility for help with confocal imaging, Jia Ye from the UK Electron Microscopy Center for help with SEM imaging, and John May and Tricia Coakley from UK Environmental Training and Research Laboratory (ERTL) for help with ICP-AES.

I would also like to thank my fiancé, Ashley Sofia, for her never-ending support and

love during my years at UK. I would not have been able to become a successful graduate student were it not for her patience and concern for my education. I am truly grateful to have such a wonder person in my life, as she is someone who keeps me focused and passionate. An extended thanks to my family members that have supported me including my brother and sisters, Ron Jr., Tara, and Ashley, and my parents, Ron Sr., Lori, and Barbara for their continued help and support. Finally, thank you to everyone else that has supported and helped me over the years.

This study was supported by NSF-IGERT program in Bioactive Interfaces and Devices and NIEHS (National Institute of Environmental Health Science) funding grant P42ES07380. Functionalized membranes used in this research were developed through joint research with Ultura Corporation (formerly Sepro Memranes), Oceanside, CA.

Table of Contents

Acknowledgements iii

Table of Contents v

List of Tables viii

List of Figures ix

Chapter 1. Introduction 1

Chapter 2. Objectives 4

2.1 Overview 4

2.2 Specific aims 4

Chapter 3. Literature Review 5

3.1 Microfiltration 5

3.2 Layer-by-Layer (LbL) functionalization 6

3.3 Enzyme and protein immobilization within microporous media 9

3.4 Glucose oxidase 9

Chapter 4. Experimental Section 13

4.1 Overview 13

4.2 Materials 13

4.3 Microporous Media Functionalization Methods 14

4.4 Membrane Permeation Experiments and Layer-by-Layer Functionalization 15

4.4.1 Immobilization and Quantification of LbL Polyelectrolyte Layers 16

4.4.2 Immobilization and Quantification of LbL Enzymatic Layers 17

4.5 Quantification of Glucose Oxidase 18

4.6 Enzymatic Catalysis Studies 19

Chapter 5. Mathematical Modeling 25

5.1 Overview 25

5.2 Reaction Kinetics 25

5.3 Determination of Effective Boundary Properties within a Microporous Domain 27

5.4 Mass Transport Phenomena within a PFR 29

5.5 Residence Time within a Microporous Domain and Reactor Modeling 32

Chapter 6. Results and Discussion 36

6.1 Overview 36

6.2 pH-Responsive Behavior of Membrane-Functionalized PVDF-PAA Films 38

6.3 Characterization of Functionalized PVDF Membranes 41

6.4 Effect of Operating Pressure on the Permeate Flux of LbL-Functionalized PVDF Membranes 57

6.5 Effect of Immobilized Enzymatic Mass on Membrane Permeability 61

6.6 Short-Term Reproducibility of Kinetic Data 63

6.7 Long-Term Stability of Immobilized Enzymatic Activity 65

6.8 Effect of Feed Solution Dissolved Oxygen Concentration on Permeate H_2O_2 Concentration 67

6.9 Effect of Barrier Membranes on Time-Dependent Permeate H_2O_2 Concentration 69

6.10 Effect of Functionalized Membrane Characteristics on Steady-State Membrane Permeability during Enzymatic Catalysis 74

6.11 Effect of Permeate Residence Time on Permeate H_2O_2 Concentration 79

6.12 Effect of Initial Glucose Substrate Concentration on Reaction Rate 86

6.13 Effect of Immobilized Mass of Enzyme on Activity 90

Chapter 7. Conclusions 92

Appendix A. MATLAB Program Code 95

References 97

Vita 102

List of Tables

Table 6.1 Compilation of relative EDS data represented in Figure 6.6.....49

Table 6.2 Compilation of relative EDS data represented in Figure 6.7.....50

Table 6.3 Table overview of sample La3+ mass balance data for experiment outlined in this section.....51

Table 6.4 Summary of the effects that different storage conditions used in this study had on the long-term activity of GOx.....66

Table 6.5 Effect of feed-side pressure of substrate concentrations of the production of H_2O_2 for ΔP =1.22 bar. 68

List of Figures

Figure 3.1 Schematic depicting the (top) LbL functionalization procedure implemented in this work and (bottom) the enzymatic oxidation of glucose and oxygen to H_2O_2 and gluconic acid.……..8

Figure 3.2 Three-dimensional structure of the enzyme glucose oxidase ……..12

Figure 6.1 Effect of pH on permeate flux of D.I.U.F. H_2O. ……..40

Figure 6.2 SEM surface image of a PVDF400HE-PAA-AA membrane under 10 kV. ……..44

Figure 6.3 SEM surface image of a PVDF400HA-PAA membrane under 20 kV ……..45

Figure 6.4 SEM cross-section image of a PVDF400HE-PAA-AA membrane under 10 kV ……..46

Figure 6.5 SEM cross-section image of a PVDF400HA-PAA membrane under 10 kV ……..47

Figure 6.6 EDS spectrum showing the Kα peaks for Na, Ca, and La based off of relative intensities for an SEM surface analysis of a PVDF-PAA-La^{3+} membrane. ……..49

Figure 6.7 EDS spectrum showing the Kα peaks for Na, Ca, and La based off of relative intensities for an SEM surface analysis for a bare PVDF membrane ……..50

Figure 6.8 SEM image of a (Millipore) PVDF-PAA-La^{3+} membrane surface at 20 kV. ……..52

Figure 6.9 CLSM image of the top surface of a PVDF400HE-PAA-AA-PAH-GOx membrane at 488 nm. ……..54

Figure 6.10 CLSM image of the bottom surface of a PVDF400HE-PAA-AA-PAH-GOx membrane at 488 nm. ……..55

Figure 6.11 CLSM image of the PVDF domain in a PVDF400HE-PAA-AA-PAH-GOx membrane at 488 nm and a penetration depth of approximately 15 μm from the top surface. ……..56

Figure 6.12 Effect of applied pressure gradient on permeate flux of D.I.U.F. H_2O for a number of layers in LbL functionalization for the determination of effective membrane geometries for a PVDF400HA-PAA-(PAH) membrane. ……..59

Figure 6.13 Effect of applied pressure gradient on permeate flux of D.I.U.F. H_2O for a number of layers in LbL functionalization for the determination of effective membrane geometries for a PVDF400HA-PAA-PAH-(GOx)-(GOx) membrane. ……..60

Figure 6.14 Membrane permeability of D.I.U.F. H_2O as a function of the amount of GOx immobilized within PVDF400HA-PAA-PAH-GOx membranes. ……..62

Figure 6.15 Concentration of H_2O_2 in the permeate as a function of permeation time for three consecutive runs. ……..64

Figure 6.16 Schematic of the different “barrier” membrane set-ups used during this experiment.. ……72

Figure 6.17 Time-dependent data analysis that demonstrates the steady-state enzymatic catalysis of GOx for CA:PVDF400HE-PAA-AA-PAH-GOx (Setup C) and dual PVDF400HE: PVDF400HE-PAA-AA-PAH-GOx (Setup B) composite membrane systems, when compared to a single PVDF400HE-PAA-AA-PAH-GOx (Setup A) membrane alone. ……..73

Figure 6.18 Effect of applied pressure gradient on functionalized membrane permeability during enzymatic catalysis of GOx for a CA:PVDF400HE-PAA-AA-PAH-GOx membrane system. ……..77

Figure 6.19 Effect of applied pressure gradient on functionalized membrane permeability during enzymatic catalysis of GOx for a CA:PVDF400HE-PAA-AA-PAH-GOx membrane system. ……..78

Figure 6.20 Effect of estimated steady-state permeate residence time on immobilized GOx enzymatic kinetics for LbL-functionalized CA:PVDF400HA-PAA-PAH-GOx membrane systems (0.90 mg GOx)……..80

Figure 6.21 Effect of estimated steady-state permeate residence time on immobilized GOx enzymatic kinetics for LbL-functionalized CA:PVDF400HA-PAA-PAH-GOx membrane systems (0.90 mg GOx, CSTR linear approximation)……..81

Figure 6.22 Effect of estimated steady-state permeate residence time on immobilized GOx enzymatic kinetics for LbL-functionalized CA:PVDF400HA-PAA-PAH-GOx membrane systems (1.53 mg GOx)……..82

Figure 6.23 Effect of estimated steady-state permeate residence time on immobilized GOx enzymatic kinetics for LbL-functionalized CA:PVDF400HA-PAA-PAH-GOx membrane systems (1.53 mg GOx, CSTR linear approximation)……..83

Figure 6.24 Effect of estimated steady-state permeate residence time on immobilized GOx enzymatic kinetics for LbL-functionalized CA:PVDF400HA-PAA-PAH-GOx membrane systems (3.19 mg GOx)……..84

Figure 6.25 Effect of estimated steady-state permeate residence time on immobilized GOx enzymatic kinetics for LbL-functionalized CA:PVDF400HA-PAA-PAH-GOx membrane systems (3.19 mg GOx, CSTR linear approximation)……..85

Figure 6.26 Effect of initially-charged glucose concentration on immobilized GOx enzymatic kinetics for LbL-functionalized CA:PVDF400HA-PAA-PAH-GOx membrane systems. (These data were generated from the linear regressions in Figure 6.21.)……..,,,……..87

Figure 6.27 Effect of initially-charged glucose concentration on immobilized GOx enzymatic kinetics for LbL-functionalized CA:PVDF400HA-PAA-PAH-GOx membrane systems. (These data were generated from the linear regressions in Figure 6.23.)……..88

Figure 6.28 Effect of initially-charged glucose concentration on immobilized GOx enzymatic kinetics for LbL-functionalized CA:PVDF400HA-PAA-PAH-GOx membrane systems. (These data were generated from the linear regressions in Figure 6.25.)……..89

Figure 6.29 Comparison of volume-denormalized enzymatic loading on between immobilized GOx enzymatic kinetics for LbL-functionalized CA:PVDF400HA-PAA-PAH-GOx membrane systems and homogeneous-phase kinetics of the same kind. ……..91

Chapter 1. Introduction

The techniques of immobilizing enzymes within the porous domain of functionalized, porous media are thoroughly-studied approaches for the synthesis of novel catalytic membrane reactors, and have numerous applications in intelligent enzymatic catalysis and separations. This type of technology is highly attractive because a porous template is ideal for enzyme immobilization: First, the internal membrane structure provides a semi-protective barrier against denaturizing external vectors, which include mineral and biological fouling / contamination; second, relatively high porosity allows for an intrinsically large internal surface area, and therefore a high maximum magnitude of functional loading; third, the reaction and transport conditions of membrane operation can be optimized for prolonged enzymatic stability and increased reactor robustness; and finally, the ease and relative cost of fabrication and operation are noteworthy and competitive. An additional benefit of this technology is realized when enzyme immobilization is coupled with responsive polymeric systems for powerful, biomimetic approaches to separations and reactions.

Many have demonstrated that the relative activity by weight of immobilized enzymes within a flow reactor is a strong function of the particular enzyme immobilization technique employed, which directly affects active site accessibility and dynamic structure folding [2]. It is important to note that by normalizing the relative enzymatic activity by the weight of the immobilized mass, these qualities may be compared between different immobilization techniques. Of these techniques, it has been indicated that layer-by-layer assemblies (LbLs) provide a biomimetic

and, thus, an optimally electrostatic environment for enzymatic immobilization as opposed to, for instance, direct covalent attachment of functional species [3-5]. For this reason, LbL-functionalized membranes have permitted recent advances in numerous areas of research, including fuel cell technologies, [1, 6, 7] responsive sensors [8-10], controlled novel films [11-13], selective and biomimetic separations and devices [14-18], and enhanced-stability reactors [19, 20] – the latter two of which are applications encompassed within the scope of this work. The fundamental LbL fabrication principles are relatively simple, which concerns the alternatingly electrostatic immobilization of oppositely-charged species in successive layers. This network of polyionic layers is thoroughly stabilized between immobilization steps *via* aqueous-phase washing phases at a designated pH temperature, and ionic strength for the removal of unstable species. In this work, the charged layers are immobilized within the pores of a hydrophilized poly(vinylidene fluoride) (PVDF) membrane template that has been functionalized with a crosslinked network of poly(acrylic acid) (PAA), which initially results in a net negative membrane charge at pH = 6. Successive functional charged layers used in this work are composed of poly(allylamine hydrochloride) (PAH) glucose oxidase (GOx).

While considerable progress has been made towards the maximization of catalytic, LbL-functionalized membrane effectiveness, much more work is required in order to fully understand the mechanisms that control and preserve the activity of membrane-immobilized species [21-23]. Essentially, it is necessary to show that the relative enzymatic activity is a strong function of active site accessibility, particularly when enzymes are immobilized in a non-hindering, electrostatic fashion.

Enzymatic active site accessibility can be observed as a function of feed solution membrane flux by varying the driving potentials across the membrane, in a similar way that is done for flow reactors.

Chapter 2. Objectives

2.1 Overview

It is of key interest to synthesize reproducible, biomimetic materials for the electrostatic immobilization of enzymes in order to gain an understanding of the effect that the LbL functionalization procedure has on enzymatic activity and stability. Microfiltration media gives an advantageous platform for LbL functionalization due to the benefits listed in the previous section. With a better understanding of the nature of these interactions, the LbL methods may be improved upon for optimal results. In order to achieve this ultimate goal, the following specific aims are proposed:

2.2 Specific aims

1.) production of LbL-functionalized PVDF membranes *via in situ* polymerization of PAA, and subsequent aqueous-phase electrostatic interactions of polyelectrolytes and enzymes *via* convective modulations;

2.) examination of the effects that membrane residence time and substrate concentration have on the oxidation of glucose for LbL-immobilized GOx;

3.) assessment of the issues associated with LbL-immobilized GOx active site accessibility *via* variation of the amount of GOx immobilized within the functionalized PVDF membranes; and

4.) comparison of the accessibility derived from (3.) to batch-phase enzymatic accessibility by quantification of a mass-normalized enzymatic turnover.

Chapter 3. Literature Review

3.1 Microfiltration

Microfiltration is a widely-used class of liquid-phase filtration techniques that have various applications in the modern world, specifically in wastewater treatment, for the purpose of the capture of particulate suspensions, resins, and biological masses. The application scope of microfiltration is greater than in any other filtration field, with applications in the medical, food processing, gas phase processing, and bioprocessing fields. Typical materials and operating specifications for microfiltration membranes and their applications are as follows: A pore diameter range of 0.1 – 0.5 μm; a pore geometry ranging from the relatively uniform and monodispersely-porous materials like track-etched polycarbonate (PC), to the highly-disperse, "sponge-like" materials with tortuous pores, such as PVDF; and a commercial operating pressure range dependent on the particular application, such as the typical range of 0.3 – 3 bar in bioprocessing [24]. The typical materials separated by microfiltration processes range from several micrometers to 100 nm in characteristic length [25, 26]. As mentioned, microfiltration plays a crucial role in the bioprocessing sector. Specific applications include downstream cellular recovery, biomolecule purification, and immobilized enzymatic catalysis. It is the latter application that is concerned with our group's research in that we wish to study the particular mechanisms associated with enzymatic immobilization within a porous domain.

3.2 Layer-by-Layer (LbL) functionalization

As is well-known, the LbL approach is a strong candidate for biofunctional electrostatic depositions within the porous domain of microporous media [27]. This can be attributed to the pseudo-random electrical environment that a biomolecule encounters when electrostatically immobilized near an LbL-functionalized surface. As has been shown, this randomly-charged, crosslinked polymeric network of allows for favorable interactions between biomolecules and immobilization surfaces due to the minimization of conformational shifts and of the steric blockage of the active sites. This is especially prevalent when the enzymatic substrate is convectively introduced, as diffusion limitations become less prevalent [2].

The LbL approach of polyelectrolyte deposition is simply the pressure-induced permeation of alternating polycationic and polyanionic species in order to grow a thin film that is functionalized, robust, and, in this case, stimuli-responsive. The latter mentioned quality has gained substantial attention in recent years [28, 29]. Figure 3.1 illustrates a simple diagram of the procedure associated with LbL assembly within a porous domain.

Relevant to this research is the study of the effect of membrane functionalization on the immobilization of biomolecules within a porous domain. As described in the materials and methods section, this study focuses on the effects that a pH-sensitive, highly crosslinked polymeric network of poly(acrylic acid) (PAA), which is formed in both the porous and surface domains of a PVDF microfiltration membrane, has on the immobilization of biomolecules. This polymeric network forms the negatively-charged base onto which the LbL method is

propagated in subsequent layers. The polymerization of PAA from monomeric acrylic acid (AA) and an ethylene glycol (EG) crosslinker occurs at 90^{o}C under the presence of a potassium persulfate ($K_2S_2O_8$) initiator. The polymer density is a strong function of the molar ratio of ethylene glycol to acrylic acid.

PAA is a superabsorbent material, in that it has the capability of absorbing several times its own weight in water. It has many applications in aqueous-phase absorbance, and is the reason why it has such applications as a sanitary superabsorbent. It is also a pH-responsive material with a pKa in the range of 4 to 4.5 [30]. Within this range, the carboxyl groups on the backbone of PAA become protonated, and above this range they are negatively-charged. In the presence of cationic strength, the net negative charge forces the hydrated state of PAA to swell into a chelated salt form, thus displaying a significant difference in polyelectrolyte structure with a change in pH. Therefore, it is of interest to add the subsequent layer of polycation (such as PAH) when PAA is fully ionized (pH > 5.5) for maximum adsorption.

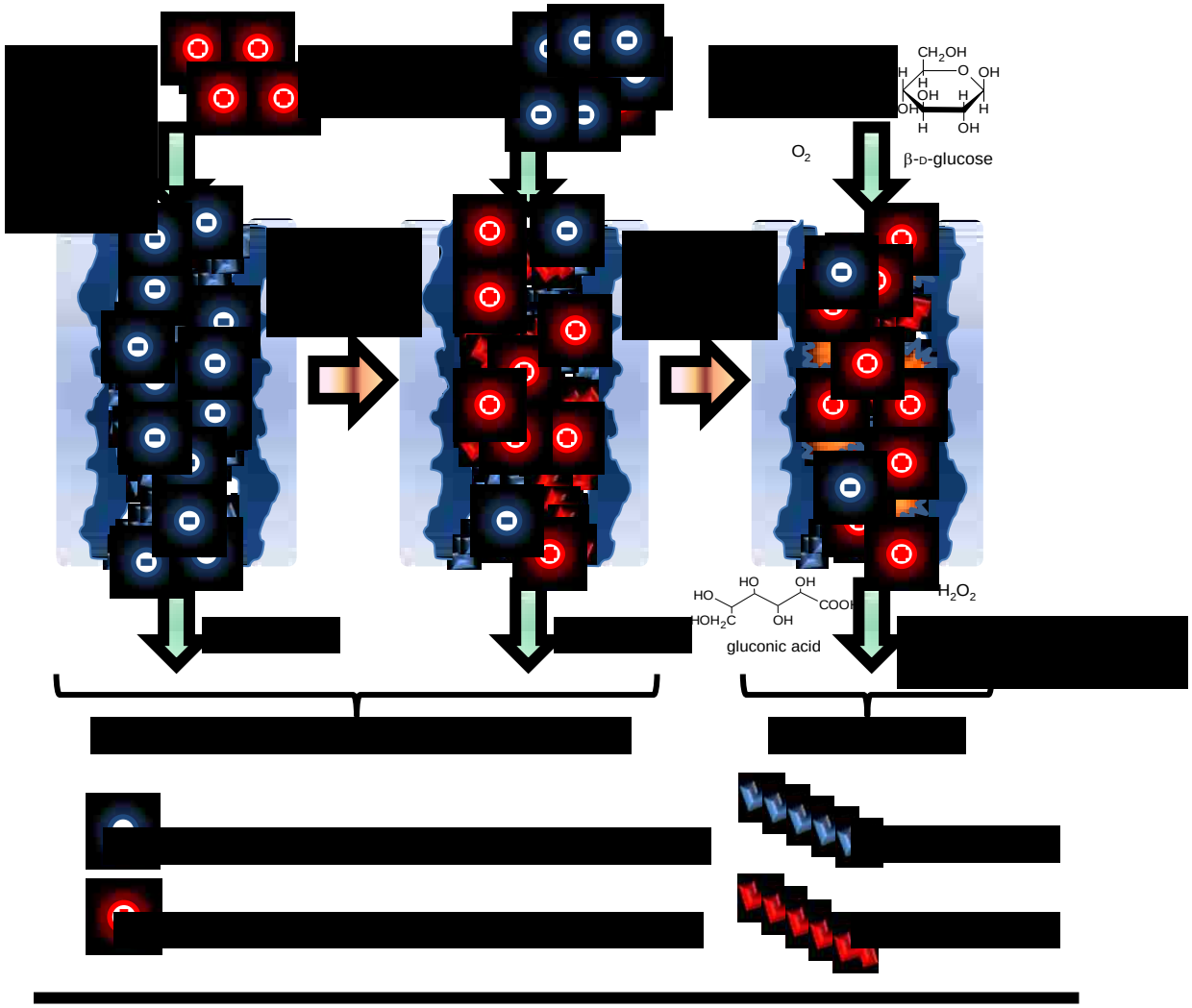

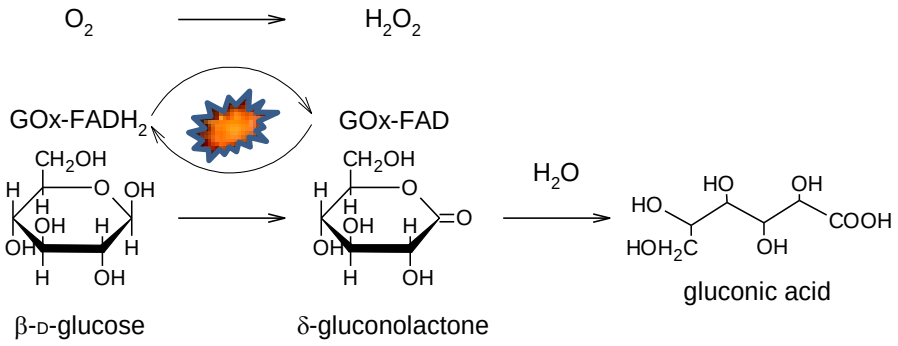

Figure 3.1 Schematic depicting the (top) LbL functionalization procedure implemented in this work and (bottom) the enzymatic oxidation of glucose and oxygen to H_2O_2 and gluconic acid.

3.3 Enzyme and protein immobilization within microporous media

Biofunctionalization of microporous media is a well-studied, classic approach for solution-phase reactions. For several decades, researchers have been able to successfully develop membranes with immobilized enzymes. Membranes have even been developed that incorporate a number of different enzymatic species, such as both glucose oxidase and catalase [31], or glucose oxidase and inorganics [32]. Many papers have addressed the problems associated with enzymatic immobilization. Rios, et al. give an excellent review of the status of the pros and cons of protein immobilization within membranes, and suggests that the main problems associated with enzymatic immobilization are the reduction of enzyme reactivity, the heterogeneity of the reaction conditions (which this work attempts to address and define), the presence of the polarization layer (which creates mass transfer limitations), and membrane fouling [33]. Recent work has suggested that the immobilization of biomolecules onto functionalized and responsive materials, such as PVDF-PAA, may lead to novel and effective applications.

3.4 Glucose oxidase

Glucose oxidase (GOx) is a well-studied dimeric enzyme that catalyzes the reaction between β-D-glucose and O_2. It is a common extracellular enzyme found in eukaryotic species that aerobically metabolize β-D-glucose for further cellular processing. For laboratory and commercial use, GOx is usually derived from mold extracts, particularly *Aspergillus niger* and various Penicillium species such as *Penicillium notatum* [34] [35]. The formation of hydrogen peroxide product from the glucose oxidase catalysis has many important applications, namely in the area of

biological-based decontamination. Among other applications, the produced hydrogen peroxide can then be used to either induce apoptosis in infectious bacteria via oxidative stress or to degrade environmental contaminants via redox reactions. Previous work by Lewis, et al. has shown that the electrostatic immobilization and catalysis of GOx within an electrically-charged micropore can ultimately form hydroxyl free radicals in the presence of Fe^{2+}, which have the ability to oxidize certain dense non-aqueous liquid phase (DNAPL) contaminants, such as trichloroethylene (TCE) [32]. In order to fundamentally understand the mechanism behind this latter application, it is of great interest to understand the electric, structural, functional, and higher-order conformational nature of GOx.

The enzymatic catalysis of the β-D-glucose substrate under the presence of O_2 produces the intermediate metabolite δ-gluconolactone via a half-reaction, which has a slow reaction with water to produce gluconic acid. In addition, H_2O_2 is produced as a result of a counter half-reaction with O_2. These half-reactions are the result of the oxidation and reduction of the two flavin adenine dinucleotide (FAD)-binding domains located within the deep pocket between the enzyme dimers. Each monomer is covalently linked to the other through disulfide bonding, and one noncovalently-bonded FAD domain exists for each monomeric subunit. The reduced form of the FAD cofactor accepts two electrons and protons and is thus known as $FADH_2$. In the presence of a proton acceptor, such as oxygen, $FADH_2$ will oxidize and return to FAD due to an increase in the cofactor thermodynamic stability [36] [37].

GOx has an isoelectric point (pI) of approximately 4.2, a molecular weight of 160 kDa (80 kDa per monomeric unit), and has an approximate molecular

composition of 74% amino acids, 16% amino-carbohydrate complexes, and 2% amino acid-carbohydrate complexes. In addition to two moles of FAD per mole of GOx, there also exists two moles of iron [38] [37]. GOx has a measurable activity in the range of pH = 4 to 8, with an apparent maximum activity in the range of pH = 5.5 ± 0.5 in the homogenous phase and in the range of pH = 5.5 - 6 when immobilized near a surface [39] [40] [35] . See Figure 3.2 for a depiction of the structure of this enzyme.

Recently, GOx has gathered significant attention due to its biological role in reactive oxidative species (ROS) production [41]. Evidence has shown that elevated levels of glucose in the bloodstream directly results in the probably of an individual developing diabetes and/or cancer by means of metabolic mutation due to the direct formation of H_2O_2 and the subsequent formation of deregulated hydroxyl free-radicals, a particular species of ROS [42, 43]. These highly-reactive free-radicals readily and adversely interact with cellular structures, including proteins and carbohydrates, which cause cellular damage and mutation.

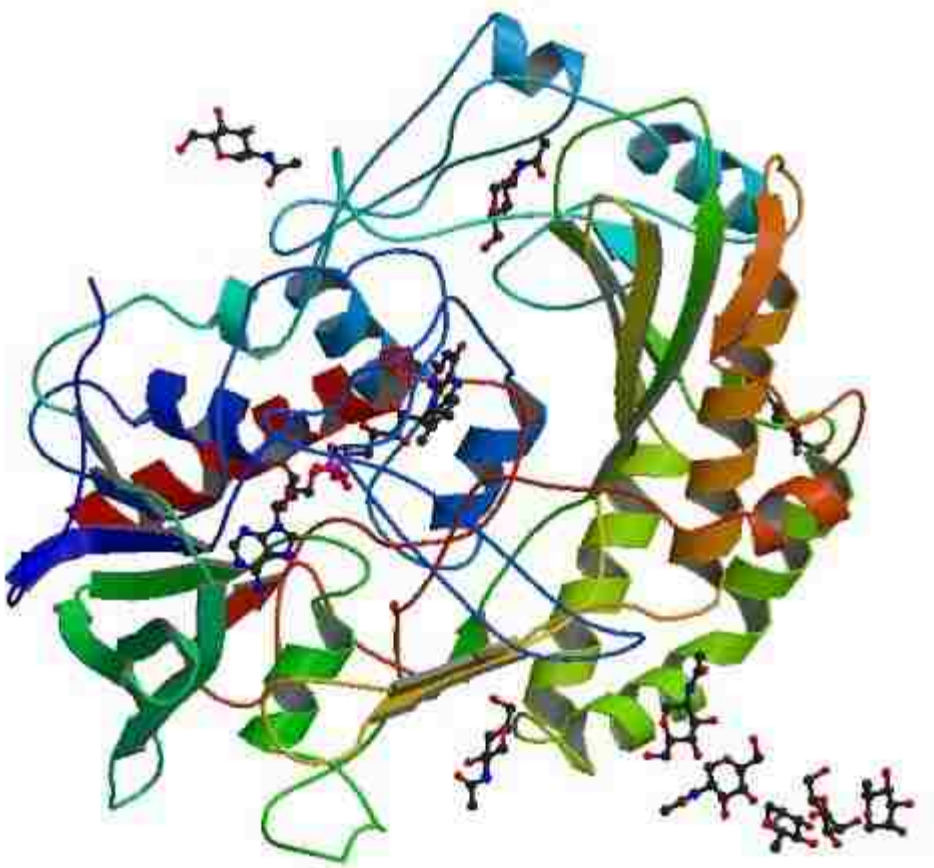

Figure 3.2 Three-dimensional structure of the enzyme glucose oxidase, courtesy of RCSB Protein Data Bank [35].

Chapter 4. Experimental Section

4.1 Overview

The following section includes an enumeration of the materials used / instruments used, and a detailed walkthrough of all of the experimental methods employed in this study for sample analyses and product material syntheses. Unless otherwise noted, chemicals were stored at room temperature in a normal atmospheric environment. Calibration techniques employed have listed statistical R^2 values for experimental precision.

4.2 Materials

Hydrogen peroxide (aq., 30% v/v) (Item # H341, Lot # 080210), sodium chloride (s.) (Item # S271, Lot # 120348A), dimethyl sulfoxide (Item # 108 M-1739, Lot # 108138), sodium hydroxide (aq., 1 N) (Item # SS266, Lot # 116551), hydrochloric acid (aq., 1 N) (Iterm # SA48, Lot # 095947), pH = 10 buffer solution (Item # SB115, Lot # 101681), pH = 7 buffer solution (Item # SB107, Lot # 110747), pH = 4 buffer solution (Item # SB101, Lot # 108305), and D.I.U.F. H_2O (Item # W2, Lot # 126295) were purchased from Fisher Scientific. Glucose oxidase (s, Type II, 17,300 U/g solid) (Item # G6125, Lot # 079K7450V), ő-(+)-glucose (s., 99.5%) (Item # 68270, Lot # 055K0025), acrylic acid (aq., 99% v/v) (Item # 147230, Lot # 04116EH), poly(allylamine hydrochloride) (s.) (Item # 283233, Lot # MKBI4274V), fluorescin isothiolcyanate (s.) (Item # F7350, Lot # SLBB8376V), and titanium (IV) oxylsulfate (H_2SO_4 solution, 99.99% v/v) (Item # 495379, Lot # MKBB3588) were purchased from Sigma-Aldrich.

Durapore® hydrophilized PVDF membrane filters (0.45 μm pore diameter, HV) (Item # HVLP09050, Lot # R2BA83074K) were purchased from Millipore. Potassium persulfate (s.) (Item # PX1560, Lot # 41303250) was purchased from EM Science (Merck, KGaA). Ethylene glycol (aq.) (Item # 5001, Lot # 5001 KVLA) was purchased from Mallinckrodt AR. Potassium carbonate (s.) (Item # 12609, Lot # G22M60) was purchased from Alfa-Aesar. Biorad Protein Assay dye reagent concentrate (Item # 500-0006, Lot # 200005613) was purchased from Bio-Rad Laboratories.

Full-scale composite hydrophilized PVDF membranes were developed by collaborative work with Ultura Corporation (Oceanside, CA) for joint-research purposes. In this study, four different membranes produced at that facility were used, as follows: Composite hydrophilized PVDF with polyester backing (Item # PVDF400HE, Lot # 12162), composite hydrophilized PVDF with polypropylene backing (Item # PVDF400HA), PAA-functionalized composite hydrrophilized PVDF with polyester backing (Item # PVDF400HE-PAA-AA), and PAA-functionalied composite hydrophilized PVDF with polypropylene backing (Item # PVDF400HA-PAA).

4.3 Microporous Media Functionalization Methods

The membranes enumerated in the previous section were functionalized with a variation of the method developed by Dickson, *et al*. The membranes were dip-coated in an oxygen-poor aqueous solution containing ethylene glycol (EG) as a cross-linking agent and acrylic acid (AA) at a constant molar ratio of 1:6.5, with potassium persulfate ($K_2S_2O_8$) as a free radical initiator. It has previously been

determined that this molar ratio gives substantial crosslinking for this particular application [22] [44]. Oxygen is a polymerization inhibitor in this reaction, and was purged as a result of constant nitrogen introduction during the polymerization. In addition, the aqueous solution used for the reaction was initially charged with nitrogen bubbling for 30 minutes in order to reduce in amount of dissolved oxygen before polymerization.

The polymerization procedure was scaled-up to full-scale with joint research at Ultura Corp., with the addition of a few proprietary adjustments to the solution composition and soaking methodologies. The functionalized PVDF-PAA-AA with polyester backing (Item ID #PVDF400HE-PAA-AA and #PVDF400HA-PAA-AA) microfiltration membrane sheets were used for subsequent LbL functionalization, enzymatic immobilizations, and enzymatic catalysis.

4.4 Membrane Permeation Experiments and Layer-by-Layer Functionalization

PAA-functionalized PVDF membranes were fastened in a convective flow pressure cell (Millipore) and introduced *via* permeation to alternating solutions of positively-charged and negatively-charged polyelectrolytes. Each immobilization phase was preceded by a standard wash phase, in which at least 500 mL of DIUF water at a pH of 6 was permeated through the functionalized membrane. Permeate samples were collected at the ends of each wash phase for appropriate solute analyses, depending on the type of . The first layer of attachment was performed with poly(allylamine hydrochloride) (PAH) (MW=58000, Sigma-Aldrich). 100 mL of an aqueous solution containing 0.03 g PAH with 0.1 M NaCl was convectively passed

through the functionalized membrane at a pH of 6. A subsequent layer 0.05 g of poly(styrene sulfonate) (PSS) was convectively passed through the membrane with 0.1 M NaCl at a pH of 6. Between each adsorption phase, fluxes vs. pressure data were recorded with pure water at a pH of 6. These data give insight into the presence of functionalization within the pore and the effective pore diameter. See the figure below for an illustration of these methods.

4.4.1 Immobilization and Quantification of LbL Polyelectrolyte Layers

PAA-functionalized PVDF membranes were fastened in a stirred tank pressure cell, 300 mL, (Millipore, "Solvent Resistant Stirred Cell", cat. no. XFUF 076 01) and introduced to alternating solutions of positively-charged and negatively-charged polyelectrolytes. The first layer of attachment was performed with PAH. An aqueous solution of 300 mL DIUF H_2O containing 0.03 g PAH with 0.1 M NaCl was convectively passed through the functionalized membrane at pH = 6. A subsequent layer 0.05 g of poly(styrene sulfonate) (PSS) was convectively passed through the membrane with 0.5 M NaCl. Between each convective layer, flux vs. pressure data were recorded with pure water at pH=5.85. These data give insight into the presence of functionalization within the pore and the effective pore diameter. See Figure 3.1 for a simple diagram of the functionalization methods used in this study.

Samples of both PAH and glucose were calibrated for concentration with serial dilutions for analysis in total organic carbon (TOC) (Shimadzu, TOC 5000 A) with $R^2 > 99\%$ between 50 and 250 mg/L for both glucose and PAH. A mass balance for PAH was conducted to determine the amount of polyelectrolyte that became immobilized within the membranes by taking the differences of feed solution

readings and total permeate solution readings, adjusted for any additional TOC measured in the permeate during the rinsing phases.

4.4.2 Immobilization and Quantification of LbL Enzymatic Layers

Immobilization of GOx upon the LbL matrix with the functionalized membranes was conducted at pH = 6 and T = 23°C. Approximately 8 mg of GOx were added to a solution of 40 mL DIUF H_2O in a 50 mL glass culture flask. On average, three 800 μL samples of this solution were removed using a pipette and collected for concentration analysis using either the Bradford assay at 595 nm or the I-125 – tyrosine radiolabelling assay (see below). The removal of this volume did not affect the concentration of the solution. Depending upon the mass of GOx desired for immobilization, 10 – 30 mL of the enzyme solution were poured into the feed compartment of the stirred cell and fully permeated at a pressure of 15 – 40 psi, depending upon the permeability of the membrane. The permeate volume was recorded and three 800 μL samples were collected for concentration analysis using either the Bradford assay at 595 nm or the I-125 – tyrosine radiolabelling assay.

Next, approximately 20 mL of DIUF H_2O at pH = 6 were permeated through the enzyme-functionalized membrane at 15 – 40 psi. This volume was fully collected and recorded, and three 800 μL samples were collected for concentration analysis using either the Bradford assay at 595 nm or the I-125 – tyrosine radiolabelling assay. The amounts of immobilized GOx were determined *via* mass balance about the feed, initial permeate, and the wash permeate batch solution volumes. Finally, permeability measurements were taken by measuring DIUF H_2O flux at pH = 6 for

various pressure gradients. The effective thickness of the enzymatic layer was determined using the Hagen-Poiseuille law of capillary flow, Equation (5.7).

4.5 Quantification of Glucose Oxidase

The concentration of GOx in aqueous solution was quantified using two well-known, yet separate, techniques in order to confirm with confidence the experimental values. It was confirmed that the results from both analyses agreed within ± 0.1 mg GOx. The two techniques employed are as follows.

4.5.1 Quantification of GOx – Bradford Assay

GOx was quantified using a well-known colorimetric dye complexing method developed in the literature [45]. The absorbance of samples of GOx were calibrated for concentration with serial dilutions for analysis at pH = 6 using the well-documented spectrophotometric Bradford protein assay at 595 nm, with $R^2 > 98\%$ between 2 and 25 mg/L (Varian, Cary 300). These measurements were referenced to a standard concentration curve using a standard BSA solution, which agreed with the assay literature. A mass balance for GOx was conducted to determine the amount of enzyme that became immobilized within the membrane by taking the differences of feed solution readings and total permeate solution readings, adjusted for any additional GOx measured in the permeate during the rinsing phases. It is very important to note that, before GOx immobilization, no TOC be measured in the prior rinse phase permeate. This is because PAH interferes with the Bradford assay due to the relatively high concentration of amine functionality.

4.5.2 Quantification of GOx – I-125 – Tyrosine Assay

. In order to measure the capability of the Bradford assay, an alternative method was implemented to quantify GOx. GOx were tagged *via* a well-documented radiotracing procedure using I-125 at approximately 25 μCi, which has an affinity for bonding to tyrosyl in a 1:1 ratio[46]. Samples of radiolabelled GOx were calibrated for concentration with serial dilutions for analysis in a gamma counter with $R^2 > 99\%$. It was found that, after calibration and in triplicate, the result of this method agreed with the Bradford assay within ± 0.1 mg.

4.6 Enzymatic Catalysis Studies

4.6.1 Quantification of H_2O_2 Produced

H_2O_2 was quantified using a well-known peroxotitanium complexing method reported in the literature [47]. 10 μL of an acidified titanium (IV) oxylsulfate solution were added to 1 mL samples of both homogenous reaction solution and permeates. The absorbance of light at 407 nm was calibrated again known series dilution concentrations of H_2O_2, and this calibration curve was used to quantify the concentration of H_2O_2 produced in the samples.

4.6.2 Batch Enzymatic Kinetic Measurements

Batch kinetic experiments were observed in an Erlenmeyer flask (100 mL) under constant stirring at pH = 6, T = 23^{o}C, and a normal atmosphere. Aqueous 10 mL solutions containing a variable concentration of GOx, in the range of 2-5 mg/mL, were formulated in a 50 mL glass culture flask that had been microwave-treated and

rigorously washed with DIUF H_2O to remove biological contaminants. The pH of the solutions was accordingly adjusted to 6 with diluted aqueous HCl or NaOH. The flask was capped and kept at constant convective conditions in a shaker tray before and after each use. The temperature of this solution was maintained constant at T = 23°C. Approximately 3 mL of this solution were analyzed using the Bradford assay at 595 nm, the removal of which did not affect the outcome of this experiment.

Second solutions of DIUF H_2O were prepared in an Erlenmeyer flask (105 mL) with pH = 6. Glucose substrates were added to the solutions, the concentration of which were kept within the range of 2.5 – 75 mM in order to observe the effect of substrate concentration on reaction rate. From this, 5 mL were sampled and analyzed using TOC analysis in order to experimentally determine the amount of glucose present in each solution. From the GOx stock solution, 1 mL volumes were transferred to the Erlenmeyer solution using a pipette while the latter was kept under constant stirring with a stir bar and a stir plate.

The instant that the GOx solution was added to the reaction solution, a timer was started. Samples of 1 mL were taken from the reaction solution using a pipette every two minutes for a total of ten minutes. Samples were immediately transferred from the reaction solution to 1 mL polystyrene cuvettes, and were subsequently vortex-mixed with 10 µL of an aqueous titanium (IV) oxysulfate solution for peroxotitanium analysis at 407 nm. Dilute sulfuric acid is present in the titanium (IV) oxysulfate solution, which renders the activity of GOx null. Therefore, these samples can be stored for up to an hour without significant changes in absorbance that would have otherwise been due to the continued enzymatic production of H_2O_2.

Data were experimentally analyzed according to the method of initial rates, which beneficially excludes zero-order kinetic effects generated by enzyme deactivation and substrate depletion.

4.6.3 Immobilized Enzymatic Kinetic Measurements under Convective Conditions

All convective mode enzymatic studies were performed at pH = 6 and T = 23^{o}C. Either industrial-grade air or ultra high purity grade O_2 was used to generate a pressure gradient across the membrane(s), which were fastened in the stirred cell vessel with an "O-ring". It has been previously reported that, under these conditions, an unintended effect takes place: The concentrations of H_2O_2 and gluconic acid within the batch feed of the pressurized vessel increase with respect to permeation time.[2] (Note that permeation time begins once the feed solution of glucose comes into contact with the membrane.) This is an adverse effect because the permeate concentrations of H_2O_2 and gluconic acid become dependent upon time. Therefore, it becomes very difficult to model the enzyme kinetics due to a number of reasons. First, the mass transfer rates between the feed solution and the intraporous solution are unknown; second, the effect of substrate depletion on the porous generation rates of products is difficult to measure; third, a large accumulation of products within the feed both damage the LbL functionalization and reduce GOx stability due being both increasingly acidic (pH < 4) and corrosive; and finally, all data collected become time-dependent, which adds more statistical uncertainty to experimental measurements. Thus, much effort was taken to prevent this feed-side accumulation.

It was discovered that the addition of a second, more permeable membrane in series before the reactive functionalized PVDF membrane circumvented this issue. Instead of having the functionalized membrane in direct contact with the feed solution, either a blank PVDF400HE or a cellulose acetate (CA) membrane was placed on top of the former. It was experimentally determined that the CA membrane performed much better in series with the functionalized membrane than did the PVDF400HE membrane due to the presence of flow channeling in the latter. Henceforth, these additional membranes are coined "barrier" membranes. The results that compare these experiments are discussed later. All convective mode kinetic data obtained were from the CA-functionalized membrane system.

It is very important that the membrane(s) be washed with enough DIUF H_2O before reactive use such that the measurable flux across either the functionalized membranes or the CA-functionalized membrane systems are stabilized, or reach steady-state. DIUF H_2O flux at pH = 6 was measured across single functionalized membranes until steady-state was reached, which usually required about 750 mL of permeate. The stirred cell vessel was opened, the "O-ring" was removed, the CA membranes were placed upon the functionalized membranes, the "O-ring" was placed upon the top CA membranes, the vessel was reassembled, and DIUF H_2O was permeated through the membrane systems at pH = 6 until the flux stabilized. For a typical stabilization procedure, approximately 1 L of DIUF H_2O permeation at pH = 6 was needed to stabilize flux for the CA-functionalized membrane system. It is important to note that the only present ionic strength of these solutions was due to the addition of dilute NaOH (aq.) for pH normalization.

Permeate flux stabilization for the CA-functionalized composite membrane system was facilitated by tightening the reaction vessel to its maximum capabilities. In order to accomplish this, Teflon tape was wrapped around the threading of the fastening bolts such that potential over-tightening of the cell did not damage threading. In a manner according to the literature, the fastening knobs were hand-secured, and then slowly secured with a wrench, with ½ turns alternating between each knob in a clockwise fashion, until maximum tightness was achieved. This reduced, and approximately eliminated, any observable adverse flow channeling around the functionalized membranes.

Reactive feed solutions containing variable glucose substrate concentrations were formulated with 300 mL DIUF H_2O at pH = 6. Approximately 15 mL of these feed solutions were collected and transferred to a disposable 15 mL polystyrene centrifuge vial for TOC analysis of glucose. For membranes with relatively low permeability, steady-state flux stabilization of this reactive solution was again necessary before permeate sampling could occur. Once the new level of flux stabilization had been reached (usually after passing 100 - 150 mL of the feed solution), permeate samples were collected over a time interval of several minutes in triplicate as a function of the applied pressure gradient. Permeate samples were collected in disposable 15 mL polystyrene centrifuge tubes for reaction product concentration analyses. The permeate sample collection tubes were stored within a laboratory drawer until the concentration analyses were conducted. This was done to prevent excessive sample exposure to light, since photons have the ability to degenerate H_2O_2. Permeate flux was also recorded for each data point.

Immobilized GOx kinetic rates were observed as a function of glucose substrate concentration, in the range of 2 – 50 mM; dissolved O_2 substrate concentration, estimated from gas-liquid partitioning of either air (21 % O_2) or 99.99 % O_2 at various pressures; porous residence time, varied by pressure modulations; and the magnitude of GOx immobilized for a given membrane; and the magnitude of GOx immobilized within the functionalized membrane, which affects porous volume and active site accessibility. Between consecutive runs, membrane systems were convectively rinsed with DIUF H_2O at pH = 6 until the permeate pH also reached a value of 6 and contained no measurable organic carbon (measured by TOC analysis). This rinsing phase is important due to the possibility of unwanted adsorbed reaction substrates or products, especially gluconic acid, which is negatively-charged at pH = 6, and has the ability to form electrostatic interactions with free amine groups from either PAH or GOx. Additionally, unreacted glucose may also become entrapped within the LbL matrix and give rise to unpredictable reaction startup kinetics during subsequent runs without first being rinsed from within the membrane pores.

When not in use, membranes were removed from the stirred cell vessel and stored in a Petri dish with a Parafilm® cover in a chest freezer at -20°C. It was assumed, and later proven, that at these storage conditions the loss of enzymatic activity with time is negligible for the time range observed in this work.

Chapter 5. Mathematical Modeling

5.1 Overview

The following chapter gives a comprehensive summary of the mathematical modeling applied in this work while enumerating the assumptions implied by the use of these models. The first section gives an derivation of the Michaelis-Menten (MM) model and the subsequent implications of this model used in this work. The following section derives the reactive space volume within a membrane pore based of the previous work conducted in this lab and amongst others. After this, there is a quick summary of the PFR derivation and the assumptions of this derivation as applied to this work. The final section of the theory connects the dots between the first three sections by using the space volume of the membrane to derive a form of an estimated mean residence time, which is used in a CSTR approximation of the PFR model in order to estimate the MM kinetic parameters.

5.2 Reaction Kinetics

It is well-established that the enzymatic catalysis of glucose and O_2 to H_2O_2 and gluconic acid in a batch reactor can be described using Michaelis-Menten (MM) kinetics. In the MM model, S is the enzymatic substrate, E is the free enzyme, $S * E$ is the enzyme-substrate complex, P is the reaction product, and $k_i: i = 1,2,3$ are the kinetic rates of the forward affinity, the reverse affinity, and the complex turnover, respectively:

$$S + E \overset{k_1}{\underset{k_2}{\longleftrightarrow}} S * E \qquad (5.1)$$

$$S * E \overset{k_3}{\rightarrow} E + P$$

(5. 2)

The intrinsic rate of the reaction, commonly expressed as $-r_S$, is defined in terms of and reaction parameters v_{max} and K_m and substrate concentration c_S:

$$-r_S = \frac{v_{max} c_S}{K_m + c_S}$$

(5. 3)

$$v_{max} \equiv k_3 E_t$$

(5. 4)

$$K_m \equiv \frac{k_2}{k_1} = c_S|_{v_{max}/2}$$

(5. 5)

where v_{max} is the maximum theoretically possible reaction rate for a given enzyme concentration E_t; K_m is the Michaelis-Menten constant, defined as the ratio of the forward reaction rate to the reverse reaction rate (affinity), and equal to the substrate concentration at which have of the maximum reaction rate is achieved; and k_3 is the reaction turnover number. Under batch conditions, E_t is equal to the volume concentration of reactive enzymes in solution. Note that $v_{max,obs} = v_{max}$ for a solution batch reaction. However, this is not the case for enzymes immobilized on a functionalized surface. That is, the accessible fraction of E_t is diminished due to the inherent effects of immobilization on enzymatic electrodistribution, folding, and active site accessibility. In fact, the quantification of v_{max} and K_m has proven to be an eluding matter in the area of enzymatic transport phenomena for immobilized enzymes.

The Michaelis-Menten rate equation can easily be linearized to give:

$$\frac{1}{-r_S} = \frac{K_m}{v_{max} c_S} + \frac{1}{v_{max}} \quad (5.6)$$

which is useful for the linear regression of the parameters K_m and v_{max}, and is commonly known as the Lineweaver-Burke method. For this method, $-r_S$ is estimated using the method of initial rates for a range of substrate concentrations. A review of the literature has indicated that, as approximate for GOx from *Aspergillus niger*, $K_m \approx 18$ mM and $v_{max} \approx 1$ to 1.5 mM/min [48, 49].

5.3 Determination of Effective Boundary Properties within a Microporous Domain

For the functionalization procedures presented in this work (LbL), the spatial characteristics with the porous domain of the microfiltration media are quantified via effective properties. The porous, highly tortuous, sponge-like internal domain of PVDF membranes, and thus functionalized PVDF membranes, is idealized as being highly ordered, evenly spaced, perfectly straight cylindrical pores – much like the porous domain of track-etched polycarbonate (PC) and uniformly-functionalized PC membranes. Thus, assuming constant Newtonian fluid properties, the Hagen-Poiseuille law of capillary flow can be applied as a first-pass estimate for measuring the equivalent membrane pore diameter of a functionalized membrane d_{ep}, chiefly:

$$d_{ep} = 2\left(\frac{8 J_v \mu L}{\pi N_{ep} \Delta P}\right)^{1/4} \quad (5.7)$$

where J_v, μ, L, N_{ep}, ΔP are the permeate flux at a specified pH and temperature, liquid viscosity, membrane thickness, number of equivalent membrane pores, and applied pressure gradient, respectively, of the media under dead-end filtration operating conditions. Roughly assuming that all else is held constant, it is implied that $d_{ep} \propto {J_v}^{1/4}$. Therefore, the equivalent pore diameter d_{ep} can be normalized *via* a known equivalent diameter, given known permeate flux at identical fluid properties flow conditions:

$$\frac{d_{ep}}{d_{ep0}} = \left(\frac{J_v}{J_{v0}}\Big|_{\Delta P}\right)^{1/4} \quad (5.8)$$

where d_{ep0} and J_{v0} are the equivalent pore diameter and permeate flux of a nonfunctionalized PVDF membrane, respectively. Since it is important to measure the effective reactor volume available for catalysis in enzymatic kinetics, the equivalent layer thickness δ_{ep} of layer n is a better-suited measurement for our purposes. This is defined as such:

$$\delta_{ep}\big|_n = \frac{(d_{ep}|_n - d_{ep}|_{n-1})}{2} \quad (5.9)$$

where $d_{ep}\big|_n$ and $d_{ep}\big|_{n-1}$ are the equivalent pore diameters of the nth and previous $(n-1)$th layer of functionalization, respectively, at the same pH and operating conditions.

Assuming that LbL functionalization uniformly accumulates perpendicular to bulk fluid flow within the pores, fluid permeation in PVDF membranes occurs

through both functionalized layer domains and a nonfunctionalized core domain. This latter permeation has been coined “core leakage”. Hence, it is relevant to consider the reactive volume of the membrane only as the functional layer where the catalyst resides. As is implied, the core leakage of a functionalized pore is much less than that of a nonfunctionalized pore due to a reduced value of d_{ep}, or, more accurately, a reduction in membrane porosity ε. The porosity can be adjusted for effective reactive domain volume calculations via the application of $\delta_{ep}\big|_n$ when n is an equivalent layer that is comprised of a reactive species, such as enzymes. The effective membrane volume V_e is estimated by:

$$V_e = \varepsilon \phi_e L A_C \qquad (5.10)$$

$$1 - \phi_e = \frac{\left(\frac{d_{ep0}}{2} - \sum_{i=1}^{N} \delta_{ep}\big|_n\right)^2}{\left(\frac{d_{ep0}}{2}\right)^2} \qquad (5.11)$$

where ϕ_e and A_C are, respectively, the porosity correction factor and cross-sectional membrane area for N functional layers of enzyme and polymer that make up the LbL matrix. Note that the term $1 - \phi_e$ is representative of the fraction of membrane porosity that includes the non-functionalized porous “core”.

5.4 Mass Transport Phenomena within a PFR

The transport modeling within an idealized PVDF PFR succeeds recent work in our lab [50] [22] [51]. A single membrane pore is idealized as a cylinder with an annular core bulk volume and a surrounding hollow cylindrical residence volume.

The reaction parameter v_{max} is first normalized by the mass concentration of enzymes that are immobilized within the pores of the membrane per effective reactive volume, V_e. This is known as the specific rate of enzymatic reaction. Thus,

$$v'_{max} \equiv \frac{v_{max}}{E_t} = k_{3,obs}(E_t)$$

(5. 12)

Here it is important to note that $k_{3,obs}$ is given in terms of a volume-normalized rate constant, which should remain the same for any magnitude of convection applied to the reactive membrane system. However, $k_{3,obs}$ may be a function of E_t due to multilayer deposition, active site blockage, and/or steric deactivation. Theoretically, for a batch reaction, $k_{3,obs} = k_3$ is a constant for all E_t. This may not be the case for immobilized enzymatic kinetics. Therefore, an overall membrane effectiveness factor of Ω is introduced and is defined as such:

$$\Omega = \frac{k_{3,obs}(E_t)}{k_3}$$

(5. 13)

For the general case involving a flow reactor with axial dispersion (the latter of which is included due to the presence of an assumedly non-functionalized core region within each pore), the following differential equation can be developed by performing a standard mass balance about an effective cylindrical volume within the porous domain and allowing $lim_{\Delta V \to 0}$:

$$D_S \frac{d^2 c_S}{dz^2} - U \frac{dc_S}{dz} - \Omega r_S \Psi(t) = 0$$

(5. 14)

$$z = 0, c_S = c_{S0}$$

(5. 15)

$$z = L, c_S = c_{S0}(1 - X)$$

(5. 16)

where D_a is the bulk axial dispersion coefficient of glucose substrate, U is the superficial fluid velocity normal to the membrane cross-section, and $\Psi(t)$ is the transient deactivation rate of the enzymatic mass. Note that all of the terms related to the enzymatic accessibility are encompassed by Ω, the theoretical implications of which are explained below. This equation makes a few important assumptions:

1.) Radial diffusion and convection are negligible because the driving force differentials only exist in the axial plane, and are insignificant in magnitude as compared to axial convection as a result.

2.) There is no generation of reaction products in the feed side of the membrane reactor, which allows for the steady-state generation of reaction products

3.) The overall enzymatic activity does not decrease with time - continued use or storage - such that $\Psi(t) = 1$.

4.) The recovery of H_2O_2 from glucose production is relatively close to 100%.

5.) Any mass transfer resistances encountered are encompassed by Ω.

6.) Axial diffusion is negligible compared to convection and reaction, such that $Da \gg 1$ (appropriate for LbL enzymatic immobilizations with relatively low mass transfer effects) and

$$D_S \frac{d^2 c_S}{dz^2} \ll U \frac{dc_S}{dz}$$

7.) The flow regime within the domain $0 \leq z \leq L$ is laminar, such that $Re = {\rho_l U d_e}/{\mu} \ll 2100$, where ρ_l and μ are the bulk solution fluid density and viscosity, respectively.

Due to these assumptions, Equations (5.14) to (5.16) can be simplified to a first-order nonlinear differential equation, which is similar to the model for the PFR, save the presence of the overall effectiveness term. As described later, the equation can ultimately be simplified into a CSTR model.

$$\frac{dc_S}{dz} = -\frac{\Omega \rho_B}{U} \frac{v'_{max} c_S}{K_m + c_S} \quad (5.17)$$

5.5 Residence Time within a Microporous Domain and Reactor Modeling

The effective reactor volume of the media is a useful parameter for calculating the residence time τ within the reactive porous domain for a substrate. The relationship between residence time and permeate flux is inversely proportional, and is defined as such, where V_e is the effective membrane reactor volume:

$$\tau \equiv \frac{V_e}{A_C J_v} \quad (5.18)$$

Therefore, the residence time can be varied by simply varying the permeate flux *via* applied pressure modulations. It is important to note that V_e is a function of the

nature of the porous LbL functionalization, and therefore also, in this case, solution pH.

When $Da \gg 1$, where Da is the reactive-convective Damköhler ratio for a continuous, steady-state reactor, and is defined as:

$$Da = \frac{reaction\ rate}{rate\ of\ mass\ transport\ (diffusive)}$$

This Damköhler ratio naturally arises from a differential elemental mass balance about an equivalent cylindrical volume within the porous domain of reactive microfiltration media. Noteworthy is that for $Da \gg 1$, $\Upsilon \ll 1$, where $\Upsilon = {\tau}/{\tau_{max}}$ is an absolute normalized residence time, τ is a given relative residence time, and τ_{max} is the maximum residence time measured for a particular relative scale. These implications are analogous to the use of the constantly-stirred tank reactor, CSTR, model. On the other hand, the plug flow reactor, PFR, model can be used to model all experimental data for $0 < \Upsilon < 1$.

It is well-established that the magnitude of residence time plays a primary role in the overall rate enzymatic catalysis. Flow through LbL-functionalized membrane reactors can be modeled as either a plug flow reactor (PFR), a constantly-stirred tank reactor (CSTR), or an idealized laminar-flow reactor (LFR) [2]. The PFR and CSTR models for a continuous reactor described by Michaelis-Menten kinetics are derived from an overall mass balance about the membrane pore. They are respectively given below in terms of the residence time within a pore τ for $Da \gg 1$ (negligible substrate diffusive mass transfer effects):

$$\tau = \frac{c_{S0}X}{v_{max}} - \frac{K_m}{v_{max}}\ln(1-X)$$

(5. 19)

$$\tau \approx \frac{c_{S0}X}{-r_S}$$

(5. 20)

where X is the steady-state conversion of glucose to hydrogen peroxide. First, note that the equation for the CSTR model is an approximation of the PFR model when $X \ll 1$. Even though τ is not dependent upon X (rather, the reverse is true), the previous equations are presented in this fashion in order to effectively display term degeneration under the following assumptions: When c_{S0} is sufficiently larger in magnitude than K_m, $lim_{c_{S0} \gg K_m}\, v = v_{max}$ and $c_{S0} \simeq c_S$. Hence, the second term of the PFR model degenerates and the CSTR model residence time can be correlated to the total accessible enzyme concentration by the following limiting case:

$$\tau \approx \frac{c_{S0}X}{k_{3,obs}E_t}$$

(5. 21)

In this study, data are collected that measure the steady-state concentration of hydrogen peroxide in the permeate solution $c_{PH_2O_2}$, which, assuming 100 % recovery of H_2O_2 and constant O_2 substrate concentration, is defined as such:

$$c_{PH_2O_2} \equiv\ c_{S0}X$$

(5. 22)

$$k_{3,obs} = \frac{c_{PH_2O_2}}{\tau E_t}\Big|_{v_{max}}$$

(5. 23)

Therefore, the total accessible enzyme concentration E_t can be varied to study the effect the magnitude of enzyme immobilization has on v_{max}, and to ultimately quantify this effect via the turnover number, k_3. This effect is described by the presence of an overall effectiveness factor, Ω, which is a coefficient that is placed in front of the reaction term for a PFR model described in the following section.

Chapter 6. Results and Discussion

6.1 Overview

This chapter reports the experimental findings of this study and evaluates those using scientific methods and chemical engineering principles. The theory for data evaluation has been enumerated in the previous section. It is of ultimate interest to observe and discuss the effect that enzymatic loading has on the observed specific activity of the immobilized enzymatic mass. In order to accomplish this, many theoretical assumptions must be made. The objective of this chapter is to report the relevant data and analyses for the justification of said assumptions. The results are reported in an order that makes it as easy as possibly to follow the rationale and justification for the assumptions made. Unless otherwise noted, all statistical errors reported of one standard deviation.

The order of result reporting begins with a larger scope, detailing the functional mechanisms of responsive polymers within microfiltration media, and then proceeds into the characterization of the membrane geometries. Next, the presence of functional PAA is qualitatively observed to ensure the existence of polyelectrolyte network functionalization. Succeeding this is another qualitative analysis used to observe the presence of GOx functionality. All of the LbL layers are then quantified by means of permeate flux measurements *via* pressure modulations. The permeate flux is also observed as a function of the magnitude of immobilized GOx in order to determine an effective immobilization “density” at a given pH.

After this, the kinetics of the membrane systems are measured as a function of a variety of processing variables. As mentioned before, it is key that there exist

relatively no feed-side production of enzymatic catalysis products (i.e., there be no measurable H_2O_2 in the feed) due to the adverse effects it has on membrane activity and stability, and experimental analyses. Therefore, the effect that the presence of a "barrier" membrane has on the steady-state production of H_2O_2 within GOx membrane reactor is observed as a function of permeation time. As will be shown, the presence of this "barrier" will allow for steady-state production of H_2O_2, and therefore non-falsified kinetics. Next, the kinetics are observed as a function of both short-term reproducibility for a number of consecutive runs and long-term stability for different storage conditions.

The enzymatic kinetics are also measured as a function of pressure gas composition in order to theoretically evaluate the effect that dissolved O_2 content within the feed-side solution has on the steady-state production of H_2O_2. During experimentation, it was observed that the feed solution composition (namely, whether glucose was present or not in the feed) played a role in the observed membrane permeability. Therefore, in addition, the effect of solution composition is observed as a function of immobilized enzymatic mass.

The enzymatic kinetics of GOx are then measured as a function of the production of H_2O_2. For a constant glucose substrate concentration, the permeate residence time is varied *via* pressure modulations and the permeate concentration of H_2O_2 is subsequently measured. This is done for a range of glucose concentrations in order to determine the Michaelis-Menten parameters associated with some quantified magnitude of enzymatic immobilization within the membrane.

The procedure in the previous paragraph is performed for a number of different GOx immobilization magnitudes, and the MM kinetics parameters are subsequently compared as a function of those immobilized masses. These results are finally compared to this analysis in aqueous batch solution at constant pH.

6.2 pH-Responsive Behavior of Membrane-Functionalized PVDF-PAA Films

As described earlier, PAA is an extremely hydrophilic and pH-responsive polymer due to the presence of a high concentration of carboxyl functionality. When it is cross-linked (in this case, with ethylene glycol) it is subject to aqueous-dependent swelling and collapsing behaviors, particularly as a function of solution pH. As is inherently a result of this behavior, when PAA is immobilized and stabilized within a membrane pore, it will expand and contract normal to the surface upon which it is immobilized. The direction of response is due to geometric constraint. Therefore, all else held constant, when the pH of the contact solution is varied, the effective pore size will either increase with lower pH or decrease with higher pH.

This phenomenon can be thought of in terms of ion exchange. For example, at pH < 3, the carboxyl groups within the immobilized PAA network will not be ionized such that they will exist in their hydrated –COOH form. At a relatively higher pH, for instance, pH = 6.5, many of the carboxyl groups will dissociate from the hydronium ion and ionize into their $–COO^-$ forms. This allows for ion exchange with any ions or polycations within the contacting solution. In this case, Na^+ will interact with the ionized carboxyl groups to form $–COO^- Na^+$ to form an ionic bond. Na^+ is present because it is the cation in the basic NaOH solution used to adjust the feed solution

pH. Since Na^+ is a larger ion that H^+, the PAA network will expand and the pore size will correspondingly decrease. At a constant operating pressure differential, this phenomenon results in a variably-observed permeate flux.

As shown in Figure 6.1, the pH-responsive flux variation is given as a function of permeate pH. The relative flux associated with permeate pH = 8-9 is roughly one-third of the flux measured at pH = 3-4. It is important to note that the feed solution pH does not determine the average local pH within the membrane. Instead, the effluent composition properties are a more effective indicator of the solution properties within the membrane volume (CSTR model). In addition, the parametric direction in which the pH is adjusted will have an effect on the curve represented in Figure 6.1 (i.e., low-to-high, as opposed to high-to-low). As is shown, the pKa of this particular PAA functionalization approximately occurs at pH = 5, which is within the reported range of crosslinked-PAA pKa.

The results from Figure 6.1 indicate that it is crucial to keep the pH constant within the membrane pores for LbL functionalization in terms of reproducibility. Since most of the experiments in this study were performed at pH = 6, it is imperative that the membranes be washed thoroughly enough (see Materials and Methods) to ensure that the permeate pH before and after each LbL immobilization phase is at pH = 6 ± 0.05. Any slight deviation from this range results in LbL functional loss, and subsequent immobilization configuration variability.

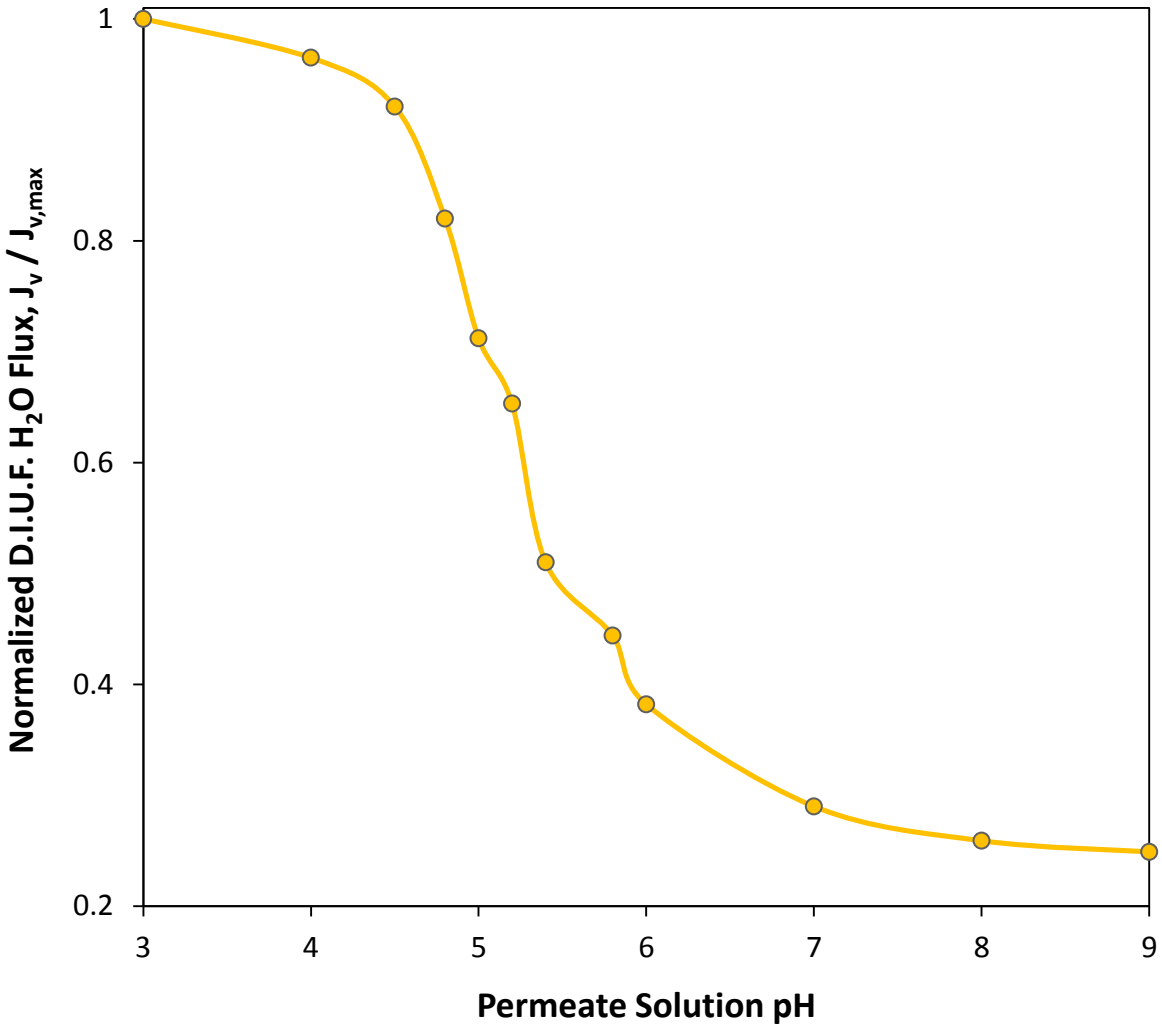

Figure 6.1. Effect of pH on permeate flux of D.I.U.F. H_2O. Note the direction of pH change from low to high, as this may not necessarily be the trend experienced in the opposite direction. Also note the inflection experienced at pH = 5, which is an approximate indicator of the PAA pKa in this case. T = 23°C, membrane cross-section = 31.7 cm^2.

6.3 Characterization of Functionalized PVDF Membranes

The two membranes used in this study (PVDF400HE, and PVDF400HA; see Materials and Methods) from Ultura Corp. were evaluated for surface porosity and PVDF layer thickness using a Hitachi-4300 Scanning Electron Microscope (SEM). The membranes were evaluated for the presence of carboxyl functionality using a Hitachi-4300 SEM coupled with Energy Dispersive X-Ray Spectroscopy (EDS) for elemental analysis. The membranes were evaluated for the presence of GOx functionality using a Leica SP5 Multiphoton Confocal Laser Scanning Microscope (CLSM).

6.3.1 Geometric Characterization of Membrane Surfaces and Cross-Sections using SEM

Before characterization, membranes were cut into areas of 31.7 cm^2 and fastened within a solvent-resistant stirred cell and subjected to pressure-driven, aqueous-phase convection until no observable carbon content (measured with TOC) was measured within the permeate. This was done to ensure that any loose PAA fragments would be dislodged from the membrane, particularly the membrane surface. Loose-chain PAA upon the surface of the membranes may give unreliable porosity results, and poor image quality especially when subject to relatively high (> 10 kV) electron acceleration voltages.

For SEM analysis, it is also important that the membranes be *extremely* dry, since the Hitachi 4300 does not have an environmental chamber. In order achieve this, samples were freeze-dried within a vacuum chamber for 4 days and directly taken to characterization. The relatively high hydrophilicity of PAA allows for a

hygroscopic effect to take place when the membranes have been dried. Membranes were sputter-coated with Au-Pt prior to analysis for conductive electrodeposition.

Even after these precautions were taken, image resolution still remained relatively poor, especially for the PVDF400HE-PAA membrane (Figure 6.3, which creates difficulties in determining the geometric membrane properties. Roughly speaking, porosity for both bare membranes was calculated to be in the range of 0.45 – 0.55 based upon an area-dependent averaging technique. The diameters of the darker sites upon the surfaces were measured using the calibrated scale provided by the software and the areas encompassed by these darker shades were estimated via a circular assumption. These circular areas were then subtracted from the total area in a differential section. Each section was summed and averaged to find the mean surface porosity [52].

Fortunately, the manufacturer provided average pore size information for the bare membranes. The reported average pore size was approximately 420 nm. As shown in previous and subsequent sections, the effective pore size for a functional LbL step can be calculated directly from membrane permeability data and the original bare membrane average pore size. This procedure is crucial for determining the porosity correction factor for a LbL-functionalized PVDF membrane.

The required image resolution for measuring the effective cross-sectional lengths of the membranes is three orders of magnitude less than surface analysis, and thus was not an issue. Figure 6.4 and Figure 6.5 depict the cross-sections of the PVDF400HE-PAA-AA and the PVDF400HA-PAA membranes, respectively. As was measured by the scale provided by the imaging software, each of the membranes

has an approximate PVDF (top) layer thickness of 70 μm. In the case of the PVDF400HE-PAA-AA membrane, the polyester - and in the case of the PVDF400HA-PAA membrane, the polypropylene – support backing are shown as the bottom layer. The geometric measurement of these backing layers is relatively unimportant, as the resistance to flow across them is miniscule as compared to that across the PVDF, and especially the functionalized PVDF, layer. In addition, while these backing layers may experience LbL-functionalized in addition to the PVDF layer, the hypothetical internal surface area of these is so small that the relative magnitude of immobilization is negligible. Thus, nearly all of the membrane reaction takes place within the PVDF layer.

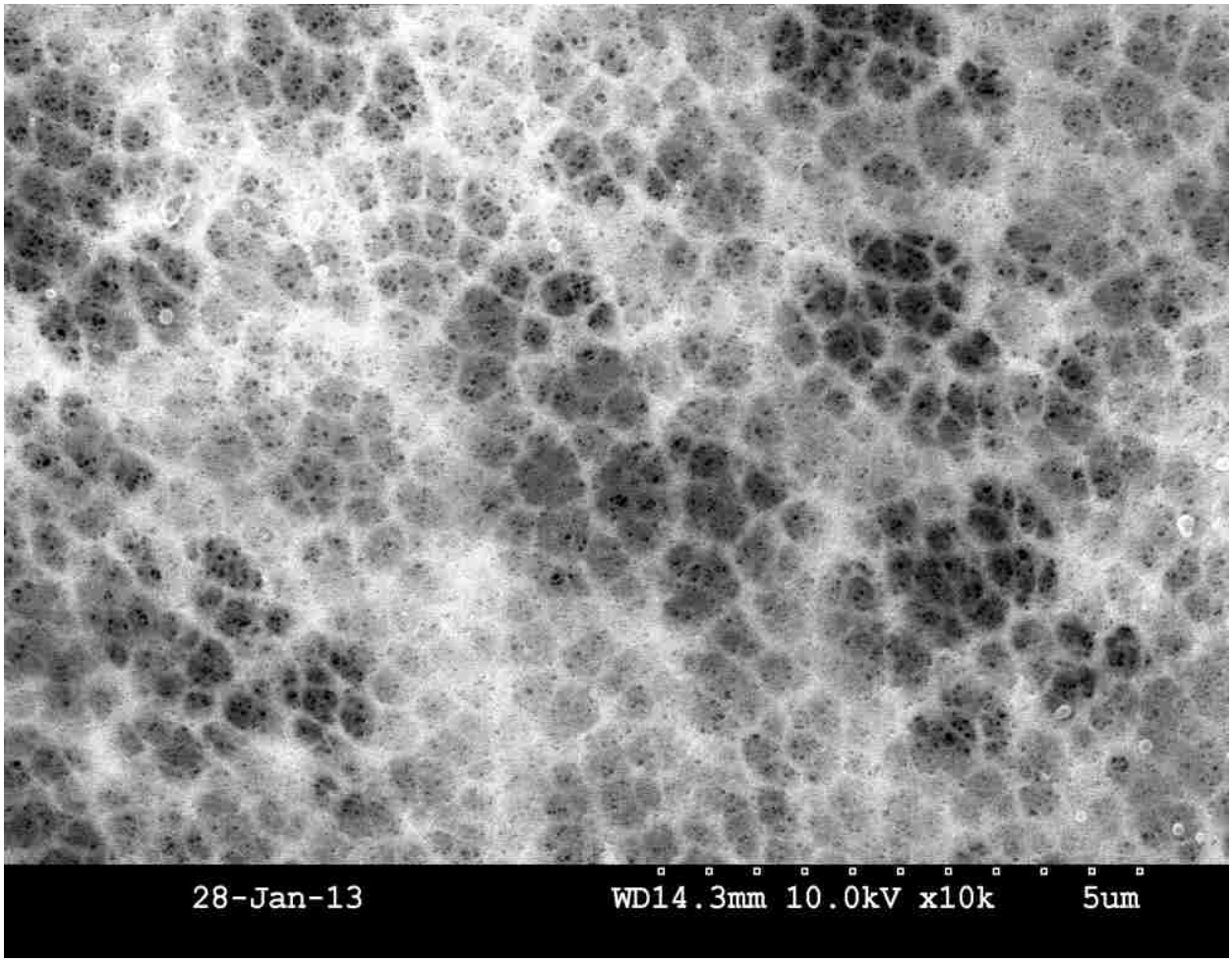

Figure 6.2. SEM surface image of a PVDF400HE-PAA-AA membrane under 10 kV. Note surface porosity and pore size. Pores are defined by small black holes that are freckled upon the image. *Courtesy of Minghui Gui*.

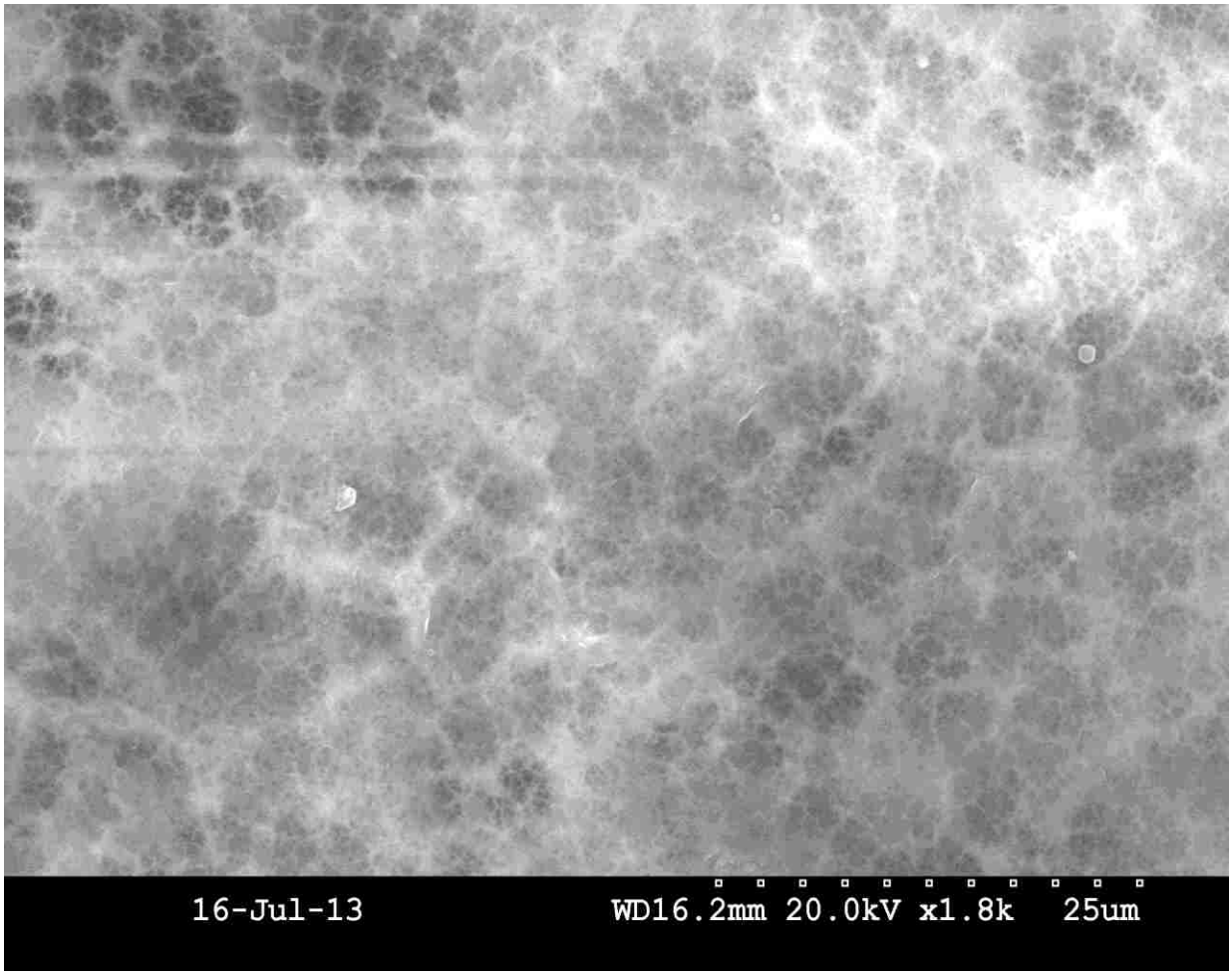

Figure 6.3. SEM surface image of a PVDF400HA-PAA membrane under 20 kV. Note relatively poor image resolution, apparently due to high surface functionality.

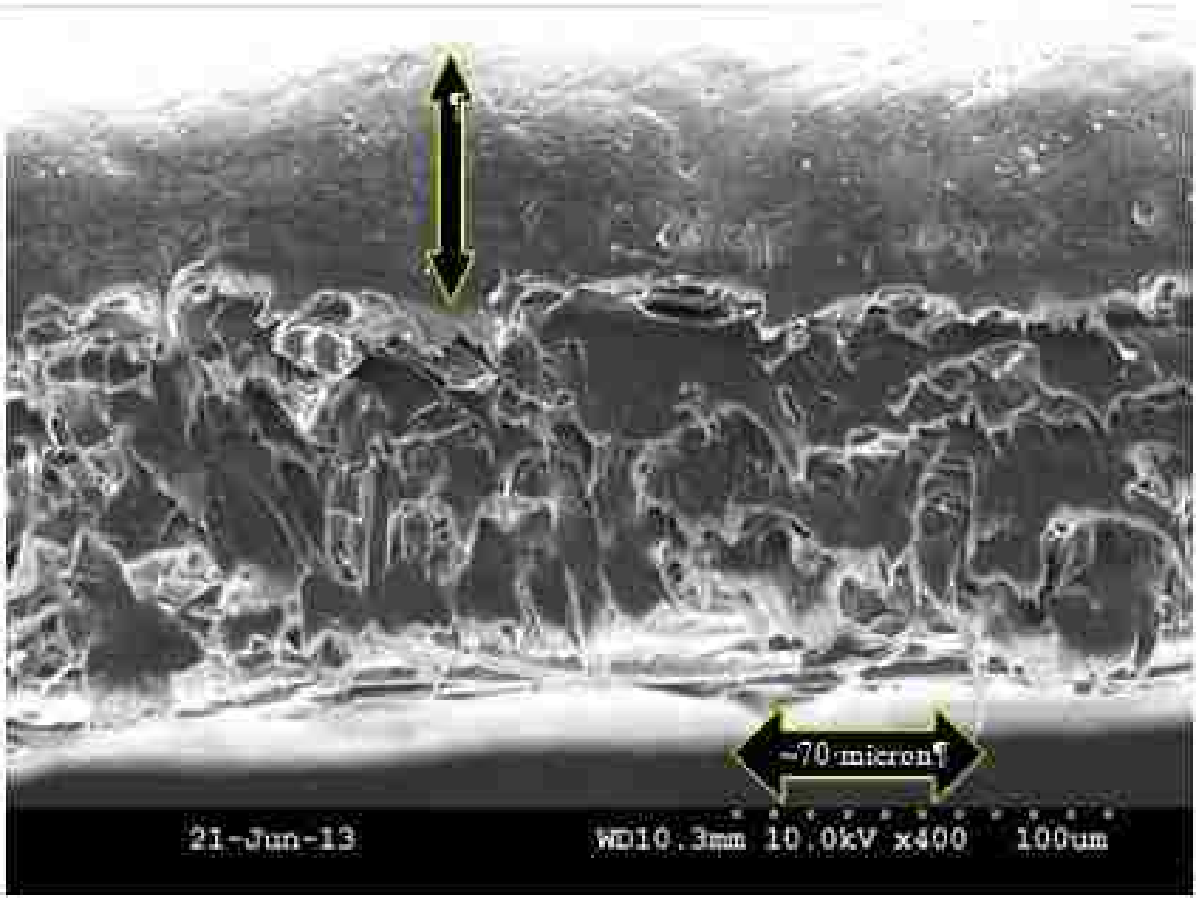

Figure 6.4. SEM cross-section image of a PVDF400HE-PAA-AA membrane under 10 kV. Note that the PVDF functional layer thickness is approximately 70 μm. The bottom layer is polyester.

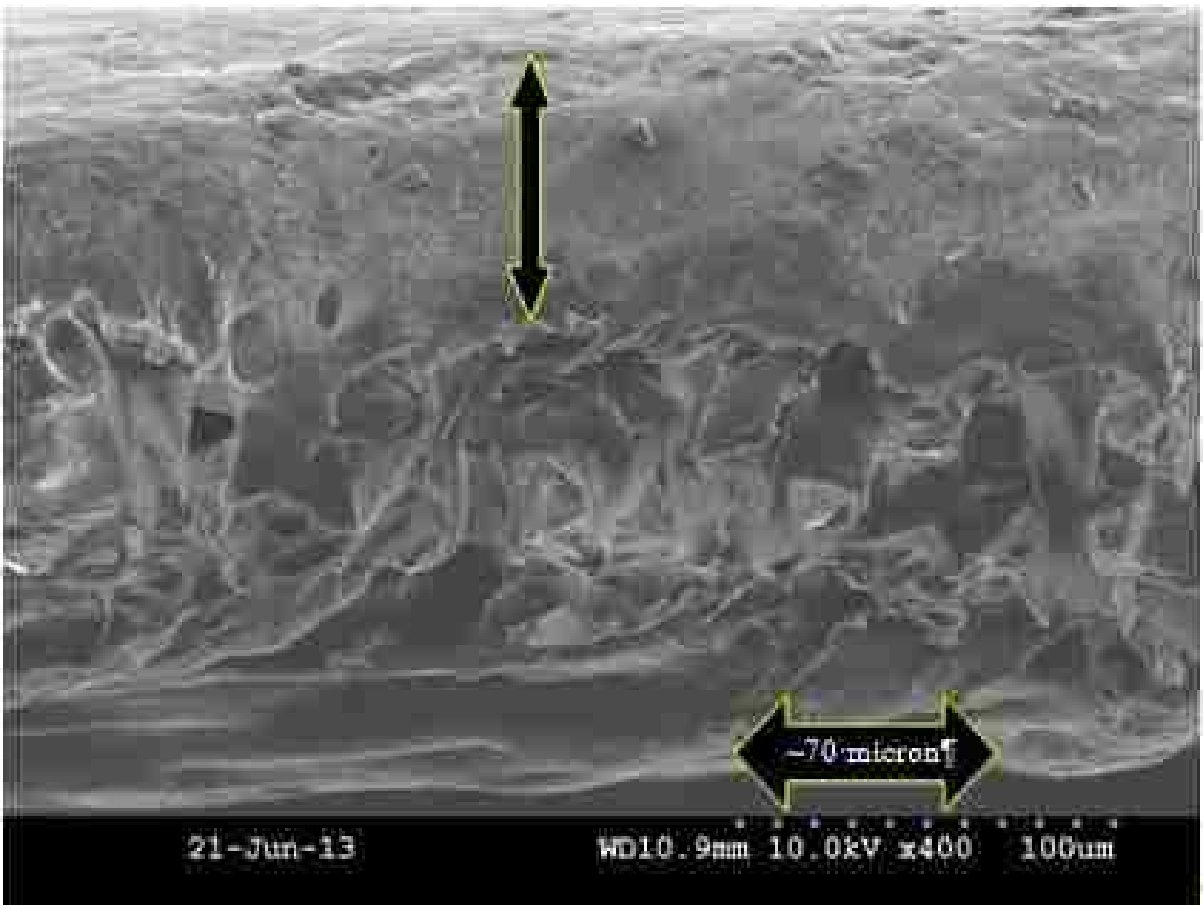

Figure 6.5. SEM cross-section image of a PVDF400HA-PAA membrane under 10 kV. Note that the PVDF functional layer thickness is approximately 70 μm. The bottom layer is polypropylene.

6.3.1 Characterization of Surface PAA Functionalization using SEM and EDS

The presence of carboxyl functionality (PAA) upon the membrane surfaces was observed with SEM coupled with EDS. Bare PVDF and PVDF-PAA membranes (Millipore) were convectively introduced to an aqueous solution of lanthanum (III) chloride ($LaCl_3$) at pH = 6. Since La^{3+} is a trivalent cation, in theory it has a relatively high affinity for ion exchange with $–COO^-$. The ion exchange of La^{3+} with PAA functionality was compared to that of a bare PVDF membrane upon the membrane surfaces. As is shown in Figure 6.6 and Figure 6.7, the adsorption magnitude of La^{3+} was relatively different for PVDF and PVDF-PAA membranes. This signifies that the presence of La in the EDS spectrum indicates the functionalization of the membrane surfaces with PAA [53]. The amount of La^{3+} that adsorbed to the PVDF-PAA membrane in this case was determined to be 0.2 mg. In the presented example, the membrane was not saturated with La^{3+}, such that the molar ratio of La^{3+} to $-COO^-$ would be misleading.

An added benefit of PVDF-PAA ion exchange with La^{3+} is that the former is highly electrically conductive. Therefore, electron beam interactions with the surface of PVDF-PAA-La^{3+} membranes result in a high collision frequency and outstanding SEM image resolution.

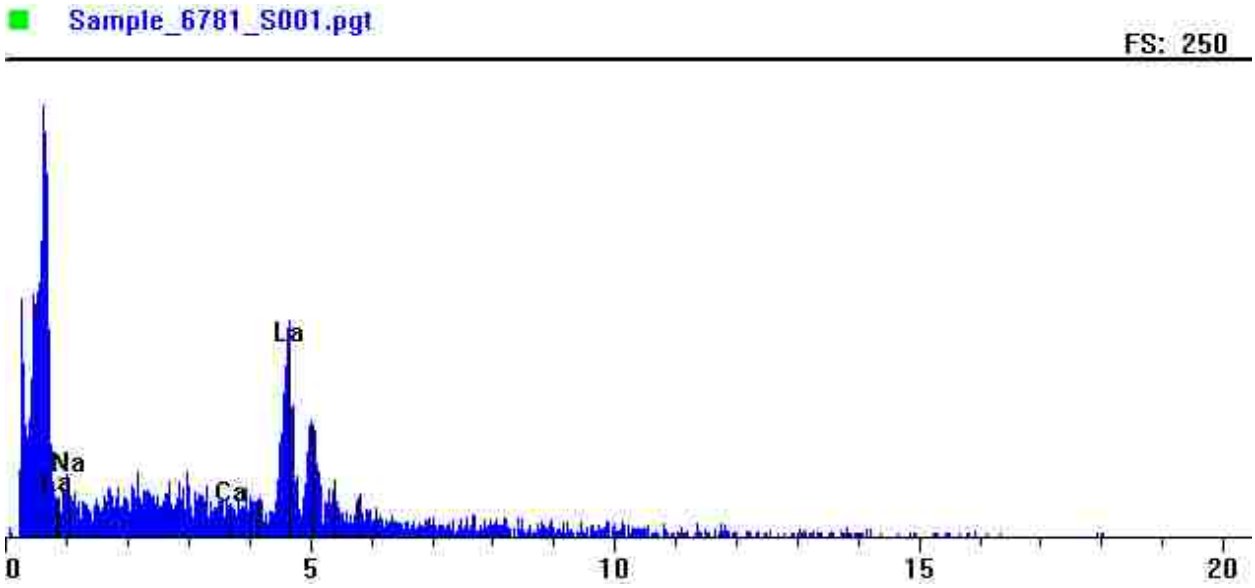

Figure 6.6. EDS spectrum showing the Kα peaks for Na, Ca, and La based off of relative intensities for an SEM surface analysis of a PVDF-PAA-La^{3+} membrane. Note the relative high peaks for La at 4.65 keV. The peaks expressed to the far left are organic-phase energies for C, O, and F.

Table 6.1. Compilation of relative EDS data represented in Figure 6.6.

Element	Line	keV	KRatio	Wt%	At%	At Prop	ChiSquared
Na	KA1	1.041	0.0000	0.00	0.00	0.0	
Ca	KA1	3.691	0.0000	0.00	0.00	0.0	
La	LA1	4.650	1.0000	100.00	100.00	0.0	5.10

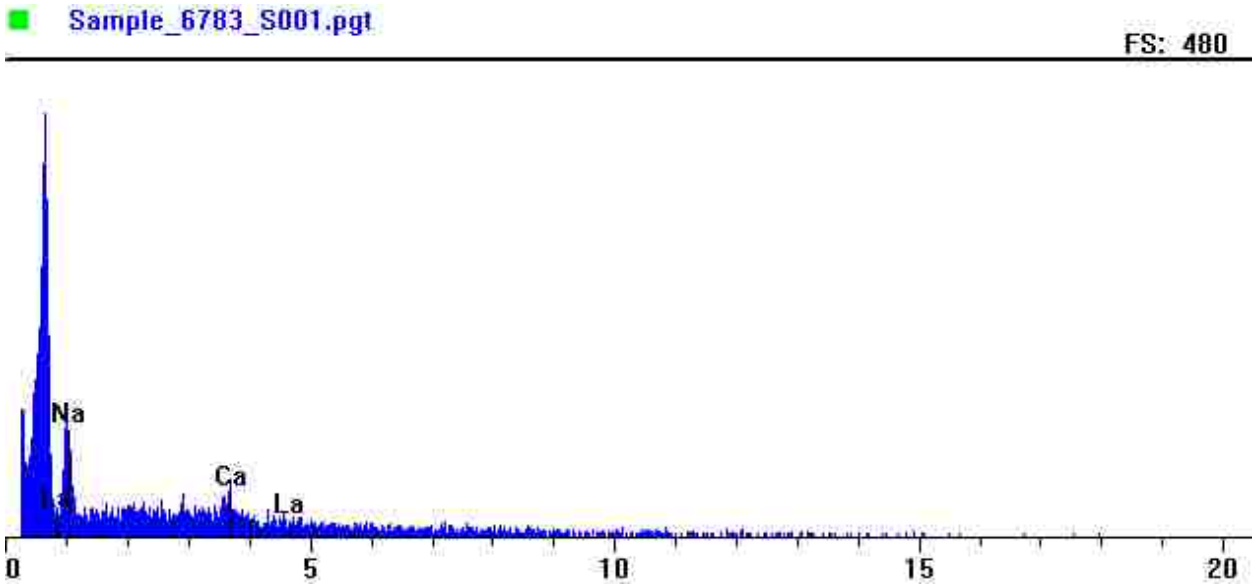

Figure 6.7. EDS spectrum showing the Kα peaks for Na, Ca, and La based off of relative intensities for an SEM surface analysis for a bare PVDF membrane. The peaks for Na^{+} and Ca^{2+} are somewhat above noise values, but should only be representative of physisorption (fouling) of these salts, rather than ion exchange with non-existent $-COO^{-}$. Note that there is no relative La^{3+} adsorption.

Table 6.2. Compilation of relative EDS data represented in Figure 6.7.

Element	Line	keV	KRatio	Wt%	At%	At Prop	ChiSquared
Na	KA1	1.041	0.1269	35.26	48.70	0.0	153.99
Ca	KA1	3.691	0.6333	64.74	51.30	0.0	1.36
La	LA1	4.650	0.0000	0.00	0.00	0.0	

Table 6.3. Table overview of sample La^{3+} mass balance data for experiment outlined in this section.

Sample Labels	La 408.671	La 379.082	La 398.852	La 333.749	La 379.477
Feed	14.14	14.6791	13.967	14.5322	14.718
Permeate	13.9516	14.4397	13.7676	14.3196	14.4815

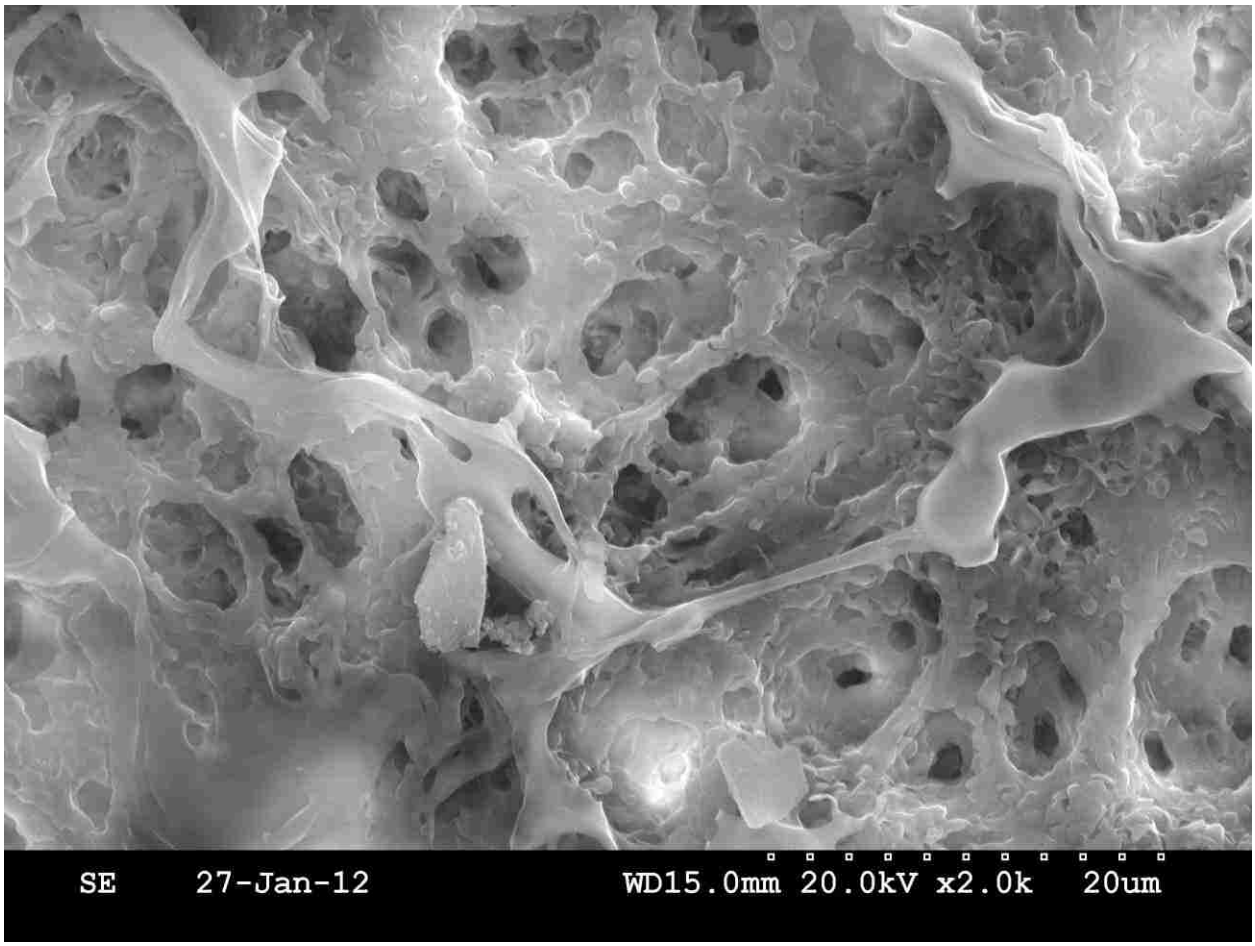

Figure 6.8. SEM image of a (Millipore) PVDF-PAA-La^{3+} membrane surface at 20 kV. Note the very high resolution capabilities of these membranes. For these particular membranes, resolution is not dictated by membrane properties, but rather by SEM capabilities.

6.3.2 Characterization of Axial Distribution of Immobilized GOx using CLSM

It is of importance that the axial distribution of GOx within the functionalized PVDF membrane be determined, if at least qualitatively, for the purpose of allowing the assumption for an even distribution of enzymatic immobilization to be valid. If, for instance, only the top surface of the membrane were subject to convective flow was functionalized with GOx rather than the entire membrane, than most of the membrane would contain "dead" space and the reactor volume would be significantly reduced. This would affect the way in which the specific activity of the immobilized-form reaction would be calculated, and may result in an analysis more prone to error by introducing a.GOx gradient throughout the membrane.

In recent years, confocal laser scanning microscopy has been a characterization technique of choice for probing membrane-based immobilizations [54] Approximately 10 mL of a FITC-functionalized GOx (see Materials and Methods) was permeated through a PVDFHE400-PAA-AA membrane at pH = 6 using a solvent-resistant stirred cell. Samples were visualized at 488 nm with a HCX PL APO lambda blue 63x aqueous-phase objective lens. As can be seen in Figure 6.9 and Figure 6.10, GOx is present upon both the top and bottom surfaces of the PVDF400HE-PAA-AA-PAH-GOx membrane. This implies that the interior of the membrane is functionalized as well, and therefore an axial distribution of GOx is prevalent for the functionalized PVDF domain. Additional images were taken using CLSM at 488 nm with penetration depths of up to 25 um into both surfaces, which qualitatively validates this hypothesis. For example, see Figure 6.11.

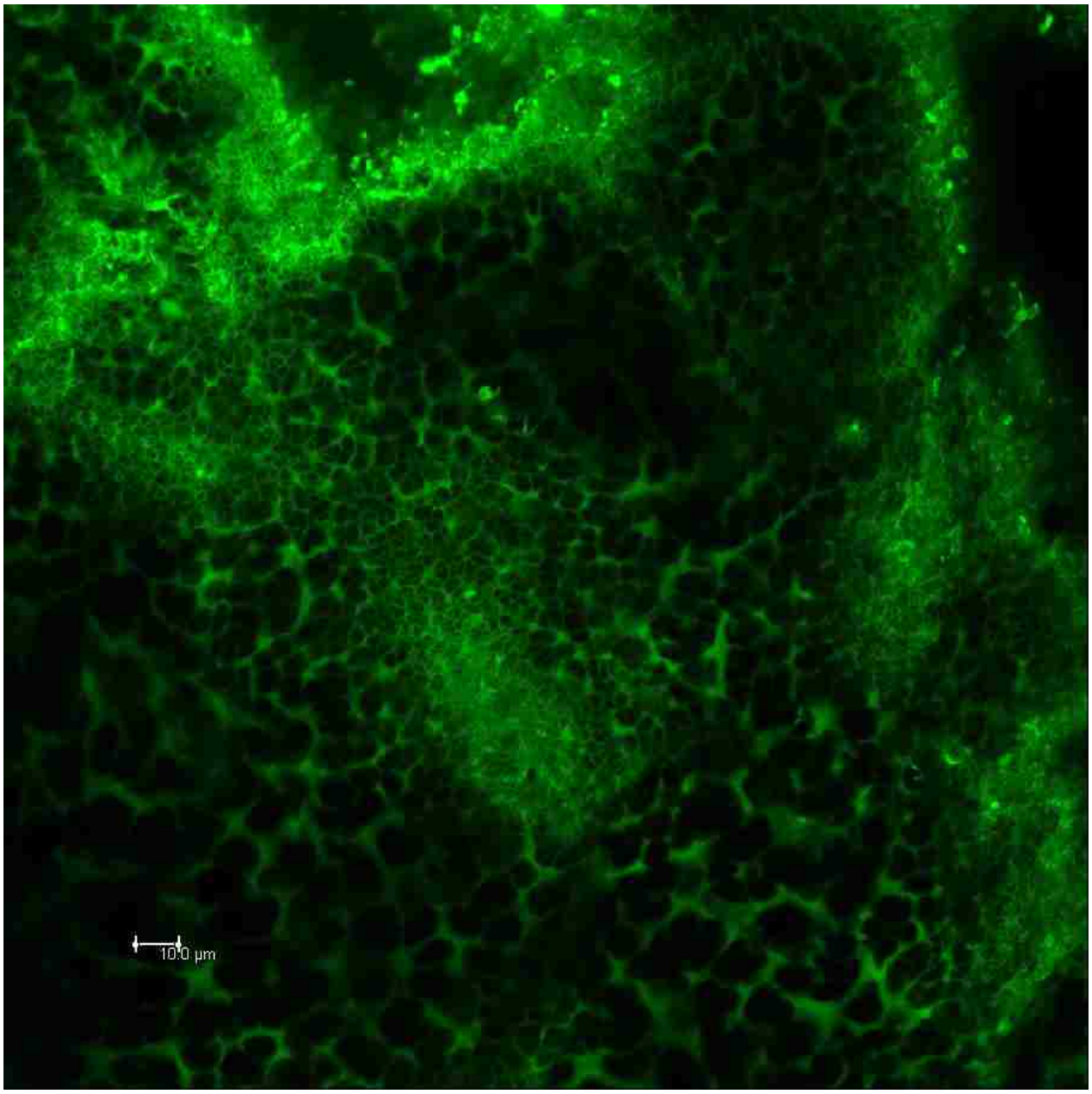

Figure 6.9. CLSM image of the top surface of a PVDF400HE-PAA-AA-PAH-GOx membrane at 488 nm. Note the "cobweb-like" behavior of the GOx immobilization due to the functionalized PVDF structure.

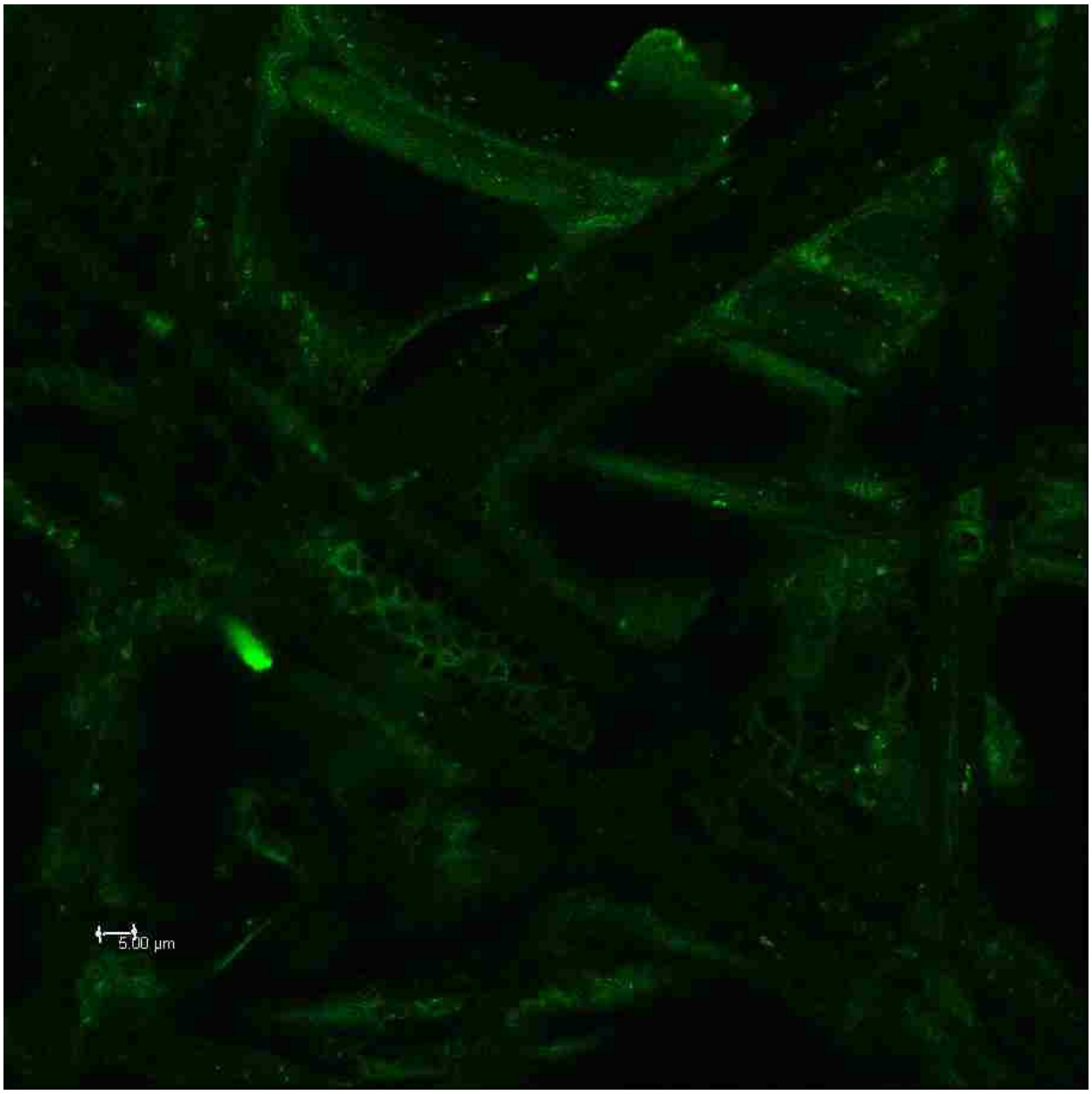

Figure 6.10. CLSM image of the bottom surface of a PVDF400HE-PAA-AA-PAH-GOx membrane at 488 nm. Note the cylindrical behavior of the GOx immobilization due to the partially-functionalized polyester structure. Also note the presence of PAA functionalization between some of the PE strands. Even though there the presence of GOx immobilization is apparent, it is qualitatively less than that experienced within the PVDF domain.

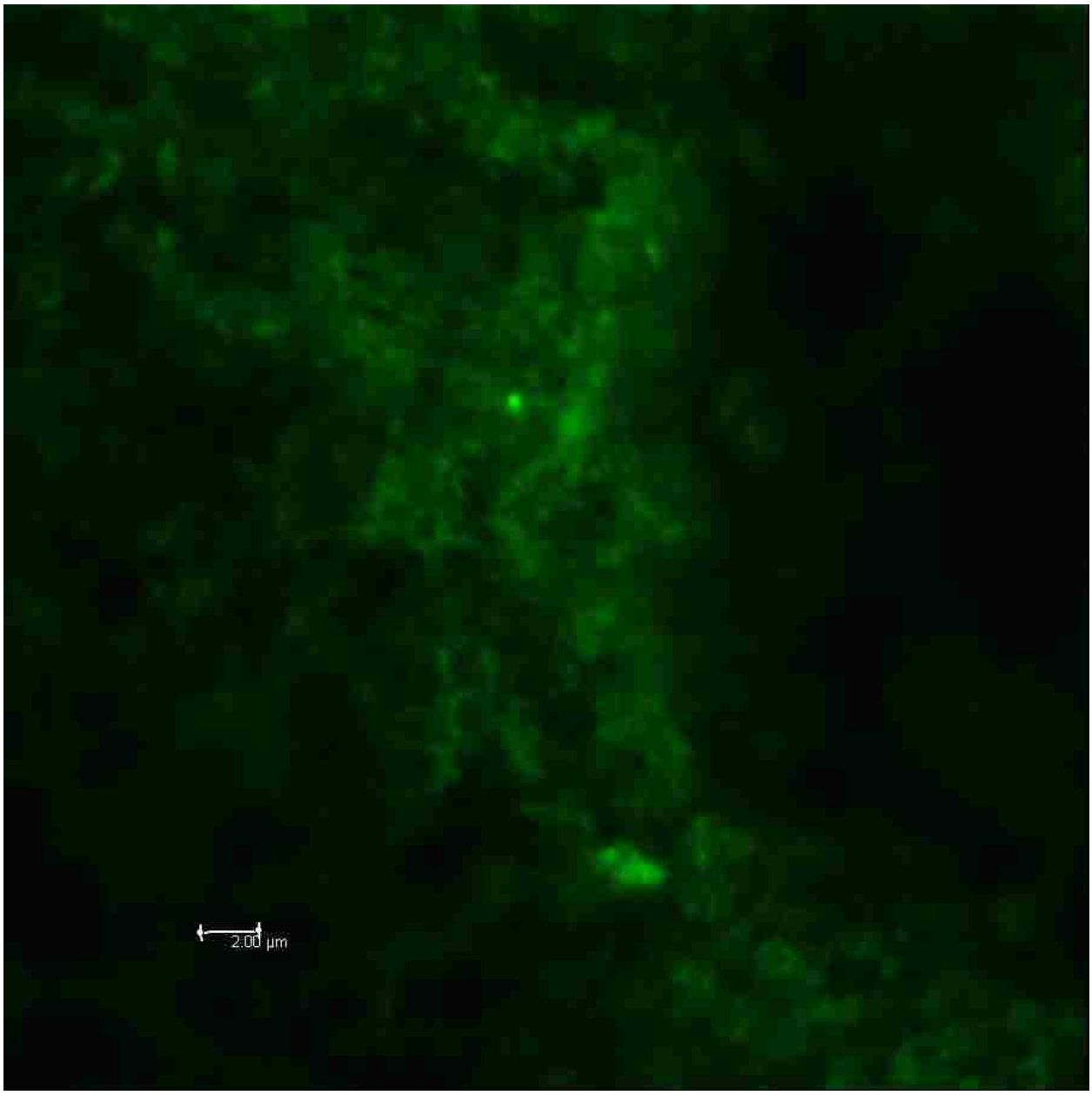

Figure 6.11. CLSM image of the PVDF domain in a PVDF400HE-PAA-AA-PAH-GOx membrane at 488 nm and a penetration depth of approximately 15 µm from the top surface. Note that the image resolution is sacrificed, most likely due to light scattering through the membrane, but the important fact is that GOx immobilization is present at this depth.

6.4 Effect of Operating Pressure on the Permeate Flux of LbL-Functionalized PVDF Membranes

It is fundamentally well-known that the measurable fluid flux through any medium is linearly proportional to the pressure gradient applied to that fluid across the medium. This is expressed by the following:

$$J_v = A\Delta P \quad (6.1)$$

where A is the membrane permeability, which is a function of the sum of resistances to pressure-driven flow, normalized by membrane geometry and fluid properties. Therefore, changes in A encompass any changes in flux resistance, given a constant membrane thickness, such as due to an increased number of LbL immobilizations within the membrane. What is happening in reality with increased LbL immobilization is that the membrane porosity decreases. This is more accurately encompassed by the Darcy formulations of the relationship between permeate flux and applied pressure.

Since, as given by Equation (5.8), membrane permeability is proportional to the fourth power of effective pore diameter for an idealized cylindrical pore, all one needs to calculate the porosity at different stages of LbL functionalization are the original bare membrane porosity, average pore diameter, and permeability; and the membrane permeability at any given level of LbL functionalization at constant pH. The corrected porosity can then be used to estimate the functional volume within the membrane for use in immobilized kinetic modeling.

All of the data summarized in Figure 6.12 and Figure 6.13 were collected with D.I.U.F. H_2O at pH = 6 and a membrane cross-section of 31.7 cm^2. The membrane used in this case was PVDF400HA-PAA-(PAH)-(GOx)-(GOx) with a flux-determining layer (PVDF) thickness of 70 μm, as estimated from Figure 6.5. In this case, the pressure applied to the feed side of the stirred tank is provided by pressurized air, where the pressure differential is in the range of 0.2 to 3.5 bar. For the case of the PVDF400HA-PAA-PAH functional membrane, permeability data were first recorded immediately after PAH immobilization. For these data the permeate pH = 4.4. After convectively permeating at least 2 L of D.I.U.F. H_2O at pH = 6 through this membrane, the permeate pH = 6, and the permeability was again measured. Note that the ratio of these two values is approximately 3:1 :: pH = 4.4:pH = 6, which is in accordance with the PAA pH-responsive data presented in Figure 6.1.

For Figure 6.12 and Figure 6.13, the amount of PAH immobilized was determined to be and 4.03 ± 0.64 mg PAH, and the amounts of GOx immobilized were determined to be 1.53 ± 0.19 mg for GOx(1) and 1.66 ± 0.20 mg for GOx(2).

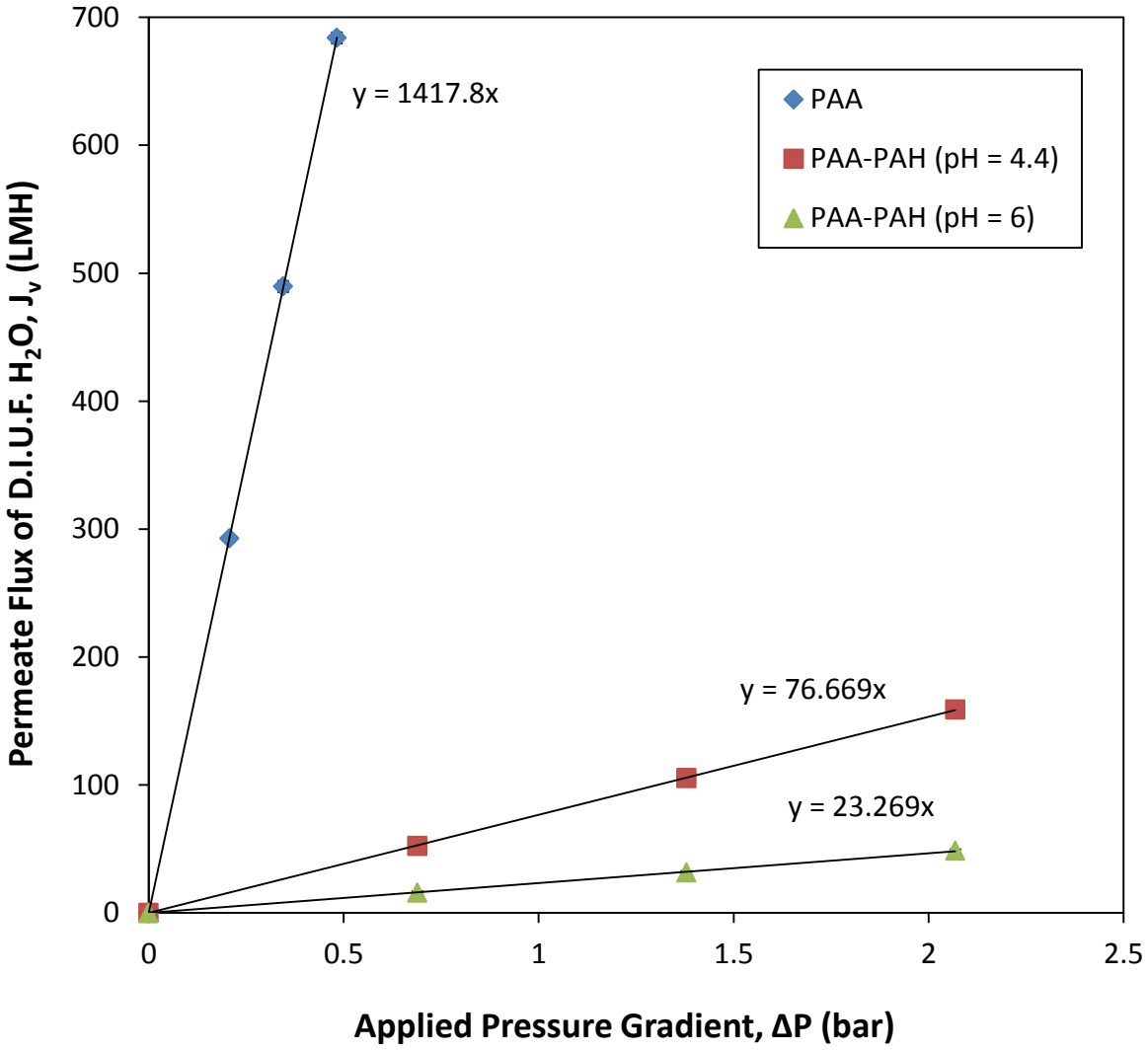

Figure 6.12. Effect of applied pressure gradient on permeate flux of D.I.U.F. H_2O for a number of layers in LbL functionalization for the determination of effective membrane geometries for a PVDF400HA-PAA-(PAH) membrane. Note the effect of permeate (interior) pH on the flux of the membrane, as encompassed by the last two data sets. Feed conditions: T = 23^{0}C; pH = 6. Membrane dimensions: A_c = 31.7 cm^2; l = 70 μm; ε_0 = 0.5 and d_{e0} = 420 nm for bare PVDF400HA. Amounts immobilized: 4.03 ± 0.64 mg PAH.

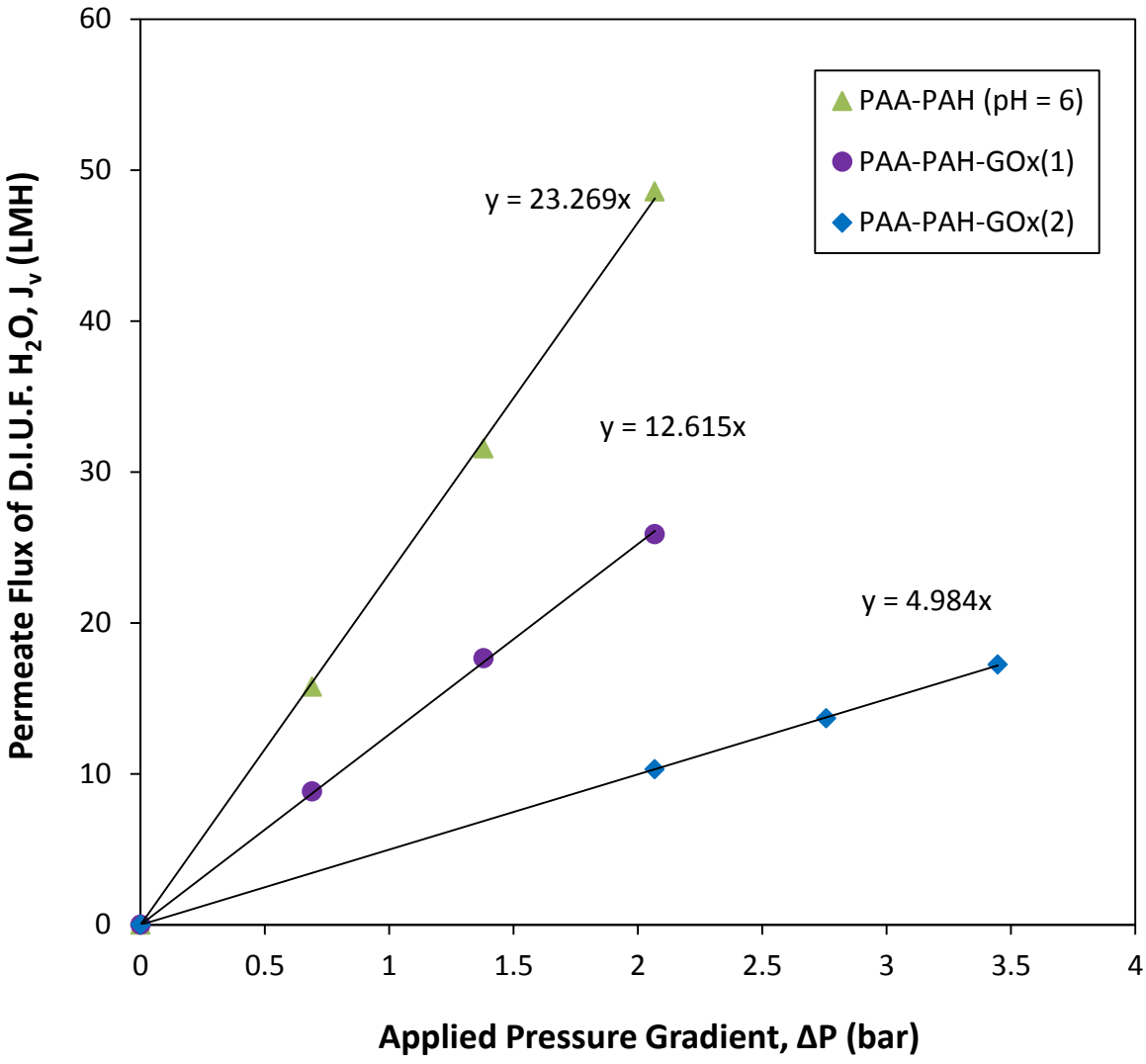

Figure 6.13. Effect of applied pressure gradient on permeate flux of D.I.U.F. H_2O for a number of layers in LbL functionalization for the determination of effective membrane geometries for a PVDF400HA-PAA-PAH-(GOx)-(GOx) membrane. This is a continuation of Figure 6.12. Feed conditions: T = 23^{0}C; pH = 6. Membrane dimensions: A_c = 31.7 cm^2; l = 70 μm; ε_0 = 0.5 and d_{e0} = 420 nm for bare PVDF400HA. Amounts immobilized: 1.53 ± 0.19 mg for GOx(1) and an additional 1.66 ± 0.20 mg for GOx(2).

6.5 Effect of Immobilized Enzymatic Mass on Membrane Permeability

The permeabilities calculated from the previous section can be compiled to form a comprehensive analysis such as the one presented in Figure 6.14. It is crucial to note that the reported permeability values in this figure are normalized against the permeabilties of the PVDF400HA-PAA-PAH membranes prior to GOx functionalization for each data point, respectively. This is because, explicitly, the last two data points are from the membrane characterized in Figure 6.12 and Figure 6.13, while the first data point is from another PVDF400HA-PAA-PAH-GOx membrane entirely. Therefore, the *y*-axis in Figure 6.14 is indicative of the volume of GOx immobilized within a given functionalized membrane.

Ultimately, the trend shown in Figure 6.14 is, by definition, proportional to the immobilization density of GOx. It is very significant that this density is constant from membrane to membrane, given that each membrane has been previously functionalized with identical conditions, i.e., at pH = 6 and with the immobilization order of PVDF400HA-PAA-PAH. Therefore, holding these conditions constant, it is relatively safe to estimate that the GOx immobilization configuration is also constant within the functionalized membranes.

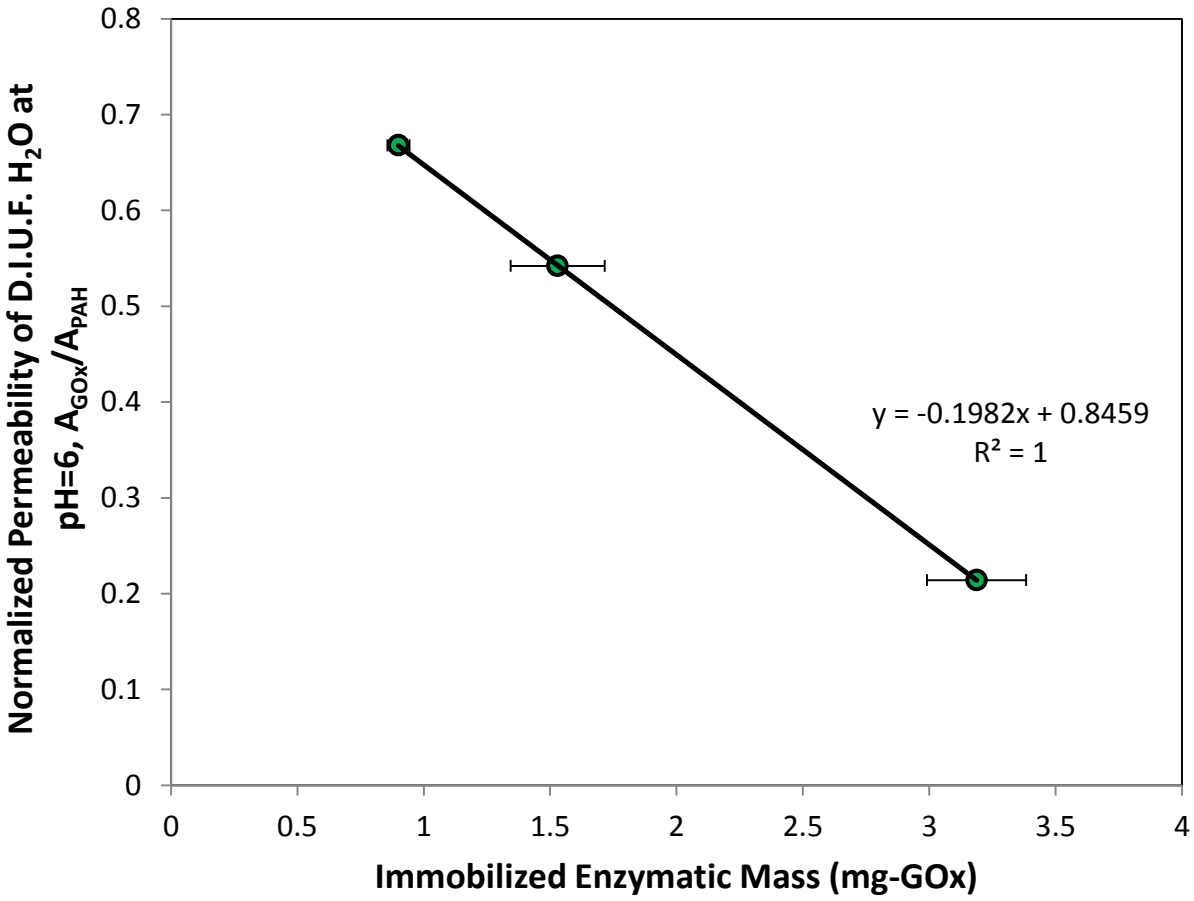

Figure 6.14. Membrane permeability of D.I.U.F. H_2O as a function of the amount of GOx immobilized within PVDF400HA-PAA-PAH-GOx membranes. Feed conditions: T = 23^0C; pH = 6, pressure gradient induced by pressurized air. Membrane dimensions: A_c = 31.7 cm^2; l = 70 μm; ε_0 = 0.5 and d_{e0} = 420 nm for bare PVDF400HA. The last two data points are from one functionalized membrane sample, while the first data point is from another. This implies that immobilization density is constant across any similarly-functionalized membrane.

6.6 Short-Term Reproducibility of Kinetic Data

The reproducibility of the production of H_2O_2 was observed for a PVDF400HE-PAA-AA-PAH-GOx functionalized membrane (without a barrier membrane, see Section 6.9) in order to determine the precise effects that multiple consecutive reactive runs have on immobilized enzyme stability, substrate transport, and overall membrane activity. As can be seen in Figure 6.15, for three consecutive runs there is relatively little change in the rate that H_2O_2 is produced as a function of permeation time. The key point to make here is that the concentration of reaction products (i.e., H_2O_2 and gluconic acid) did not reach some critical value, at which the LbL and enzymatic stability would adversely degenerate [55-58]

As is shown in Section 6.9, the presence of a barrier membrane greatly increases this critical product concentration by essentially eliminating reaction product accumulation in the feed-side solution. This, in turn, allows for localized LbL and GOx exposure to reaction products to be minimized. However, it should be noted that this exposure is not completely eliminated (see Section 6.10).

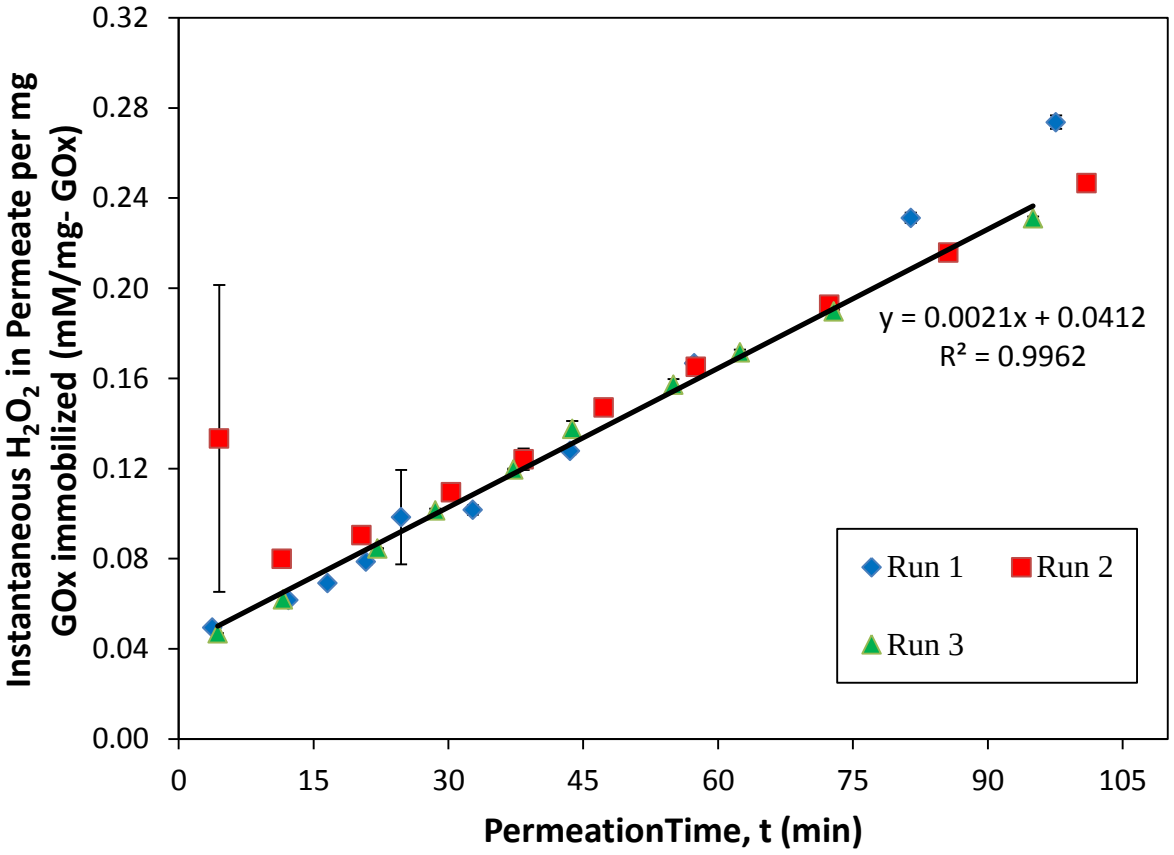

Figure 6.15. Concentration of H_2O_2 in the permeate as a function of permeation time for three consecutive runs. . Feed conditions: T = 23^0C; pH = 6, constant pressure gradient induced by pressurized air. Membrane dimensions: A_c = 31.7 cm^2; l = 70 µm; ε_0 = 0.5 and d_{e0} = 420 nm for bare PVDF400HE.

6.7 Long-Term Stability of Immobilized Enzymatic Activity

The effect that enzymatic catalysis has on the long-term stability of membrane-immobilized enzymatic activity is hypothesized to be a strong function of the residence time of the reaction products, in this case, H_2O_2 and gluconic acid (see deliberation in Section 6.6). Overall, it was observed that high permeate residence times (greater than 60 seconds) and low permeate flow rates under constant flux resulted in degenerative conditions, which were subsequently measured by comparing the activity during the following experiment with the same setup and membrane.

In addition, the nature in which these functionalized membranes are stored is an important factor in their preservation. It was observed that the storage of these membranes in conditions of -20^{o}C and sealed within a glass container allowed for > 95 % activity retention over a long period of time (up to three weeks, when the trial ended); whereas storage at room temperature (approx. 21-23^{o}C @ 1 atm) within the stirred chamber cell with daily DIUF H_2O exchanges resulted in a net activity loss that exceeded 30 % normalized activity over the course of one week. It is hypothesized that this loss in activity is due to the formation of a natural biological layer on the surface of the functionalized membranes.

This latter hypothesis is supported by the following experiment: Three PVDF400HE-PAA-AA-PAH-GOx membranes were synthesized and singularly placed within the stirred tank cell. All three functionalized membranes were introduced to a DIUF H_2O solution at pH = 6 and approx. 21-23^{o}C @ 1 atm and were left in their vessels for the course of a week, without changing the solution, under constant

stirring. After this time period, the samples were visually inspected for bioaccumulation. All samples had accumulated approximately 5 mm of biofilm after the course of one week and > 0.5 mm of biofilm after 2 weeks of experimentation. After each run, the cell was rigorously cleaned using isopropyl alcohol and DIUF H_2O, and disinfected using microwave. As a control, samples stored in the freezer at -20°C did not accumulate and biomass after up to 3 months of storage.

Table 6.4. Summary of the effects that different storage conditions used in this study had on the long-term activity of GOx.

Storage Conditions	**Activity After One Day of Storage***	**Activity After One Week of Storage***	**Observations / Comments**
Homogenous Phase @ pH = 6 and 21-23°C	< 0.90	N/A	Deactivation due to electrostatic binding, biological consumption / colony formation
LbL-immobilized on PVDF membrane @ approx. -20°C and covered in darkness	> 0.95	> 0.90	Slight increase in DIUF permeability @ pH = 6, [o] liters of DIUF @ pH = 6 required to return to previous configuration and permeability upon removal from storage
LbL-immobilized on PVDF membrane in aqueous conditions @ pH = 6 and 21-23°C	> 0.95	< 0.70	Very large increase in DIUF permeability @ pH = 6, > 0.5 mm of biological fouling layer formation on top of membrane

*Normalized against activity of corresponding GOx immobilization method at t = 0

6.8 Effect of Feed Solution Dissolved Oxygen Concentration on Permeate H_2O_2 Concentration

The effect of the feed-side solution concentration of (theoretically) dissolved oxygen (DO) on the production of H_2O_2 was observed in order to gain a better understanding of the mechanisms associated with O_2 transport within a membrane reactor. For a first-pass estimate, simple gas-liquid phase interactions were predicted using Henry's Law.

$$x_i H_i = y_i P \quad (6.2)$$

where x_i and y_i are the fraction of species *i* in the liquid and gas phases, respectively, H_i is the Henry's Law constant, and P is the total gas phase pressure

As can be seen by observing Table 6.5, the effect that the hypothetical concentration of dissolved oxygen is pronounced for a substrate concentration of 25 mM glucose, as compared to nonmeasurable for a substrate concentration of 2 mM glucose (for all other operating conditions and membrane characteristics held constant). This is expected, as a higher concentration of glucose within the feed increases the overall reaction rate of the immobilized enzymatic mass with respect to glucose. However, this behavior, when described by first order Michaelis-Menten kinetics, is asympotitic and will eventually reach the reaction rate limit of v_{max} at $2K_m$ (see Chapter 5).

Since the first order Michaelis-Menten model used in this work is only used as a first-pass scenario, it does not take into account the consumption of oxygen as a secondary reaction substrate. In fact, many have described the reaction of GOx using

a second-order Michaelis Menten model that includes both oxygen and glucose as substrates [59] . If this were considered, one would see that the true v_{max} occurs at high levels of both glucose and DO. Therefore, the apparent v_{max} measured in this study must only be allowed to be a function of feed [glucose]. This function becomes more pronounced at higher levels of [DO]; thus the function resolution increases. This is the primary justification as to why a majority of reaction experiments were conducted using pressurized O_2 instead of industrial grade air.

Another justification for using O_2 as a pressurization gas instead of air is to demonstrate the true capability of the reaction performance of these membranes. Using pressurized air alone for demonstration, as shown above, does not fully use the enzymatic reaction capability to its maximum and lessens the marketability of this technology.

Table 6.5. Effect of feed-side pressure and substrate concentrations of the production of H_2O_2 for ΔP =1.22 bar. Feed conditions: T = 23^0C; pH = 6. Membrane dimensions: A_c = 31.7 cm^2; l = 70 μm; ε_0 = 0.5 and d_{e0} = 420 nm for bare PVDF400HE. 3.12 mg GOx were immobilized. DIUF H_2O permeability at pH = 6 was 17.4 LMH/bar.

Sample	**$[S]_0$ (mM glucose)**	**Gas Source**	**[DO] by Henry's Law (mM)**	**S.S. Permeate Concentration of H_2O_2 (mM)**
1	2	Air	0.33	0.31
2	2	UHPG O_2	1.59	0.38
3	25	Air	0.33	0.31
4	25	UHPG O_2	1.59	0.92

6.9 Effect of Barrier Membranes on Time-Dependent Permeate H_2O_2 Concentration

A combinatory approach was taken in order to troubleshoot an issue that has existed in this research for some time [2]. As has been noted a number of times above, constant enzymatic catalysis without steady, optimal throughput is an adverse phenomena for this technology. In particular, the accumulation of reaction products has the direct ability to degrade the LbL scaffold and reduce enzymatic activity. It is therefore of great interest to direct the reaction towards functional sites that experience relative low residence times for quick permeation of these products before LbL degradation and enzymatic activity depletion. This requirement must be coupled with the requirement of a robust reaction and low pressure permeation (energy conservation). Therefore, there is some *optimal* residence time to operate at for each given membrane at a set value of membrane geometries, LbL properties, feed conditions, and operating parameters that weight these two aforementioned criteria– the analysis of which is outside the scope of this work.

To this end, the initial work encompassed by this report attempts to prevent the accumulation of reaction products alone. Please see Figure 6.16 for a complete synopsis of the membrane system setups used in this work. As is concluded, the composite membrane system consisting of a cellulose acetate (CA) membrane followed by a PVDF400HE-PAA-AA-PAH-GOx membrane has properties that yield the intended outcomes for this experiment. Please see Figure 6.17 for a data analysis

that compares the steady-state GOx enzymatic catalysis capability of these “barrier” membrane systems to that of a single functionalized membrane.

It is important to note that the permeability of the membrane system represented by Setup A decreases as time progresses. It is hypothesized that this is attributed to an adverse buildup of additional LbL features within the pore, particularly from the immobilization of charged gluconic acid species interacting with available LbL amine sites. These species are accumulated within the feed-side solution and subsequently are exposed to the functionalized membrane as permeation occurs. In other words, the pH-sensitive mechanisms that can be attributed to the intelligent LbL design are responding to a change in environmental solution conditions. This is shown by the trend observed in the permeate concentration of H_2O_2. This accumulation also changes the pH of permeate, which changes the internal structure of the LbL scaffold.

In comparison, Setup B and Setup C did not experience this behavior, primarily due to the presence of the “barrier” membrane. This latter membrane serves to prevent backwashing of permeate in to the feed, which is accompanied by an accumulation of reaction products. The “barrier” membrane directs flow to the reactive LbL membrane and increases the pathlength between the feed and the reactive sites. The difference between the permeability of Setup B and Setup C can be attributed to the structure of the “barrier” membrane used for each setup. In Setup B, a PVDF400HE-PAA-AA membrane was used, while in Setup C a CA membrane was used. In the case of the former, the membrane has a PE backing that causes rerouting of permeate around the second reactive membrane due to non-

constrained volumetric flow. In the case of the former, the CA membrane is held in series tightly enough to prevent any adverse channeling.

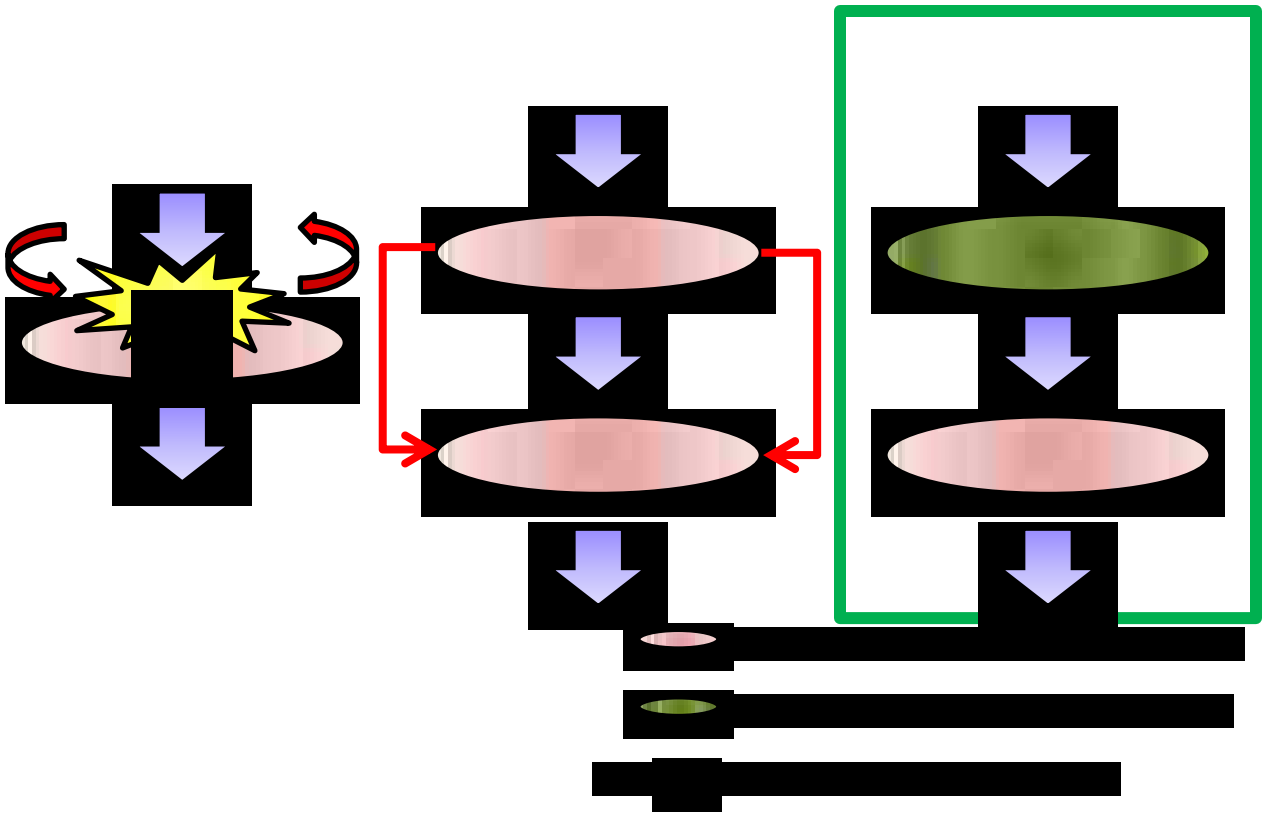

Figure 6.16. Schematic of the different "barrier" membrane set-ups used during this experiment. *Left*: The standard permeation of aqueous solution through a hydrophilized PVDF-PAA-PAH-GOx at given feed conditions results in the production and accumulation of (in this case) H_2O_2 and gluconic acid, which has a negative impact on LbL stability and enzymatic longevity. *Middle*: Two stacked PVDF-PAA membranes, with the bottom one being PVDF-PAA-PAH-GOx result in non-measurable accumulation of reaction products in the feed side of the reactor. However, the PE backing on these particular membranes adversely allows for flow channeling around the bottom, GOx-functionalized membrane, which, in turn decreases apparent overall system effectiveness and increase system permeability. *Right*: A successful membrane system combination, where the "barrier" membrane is composed of CA. In this case, no measurable reaction product concentrations were detectable in the feed and no measurable adverse flux increases were incurred.

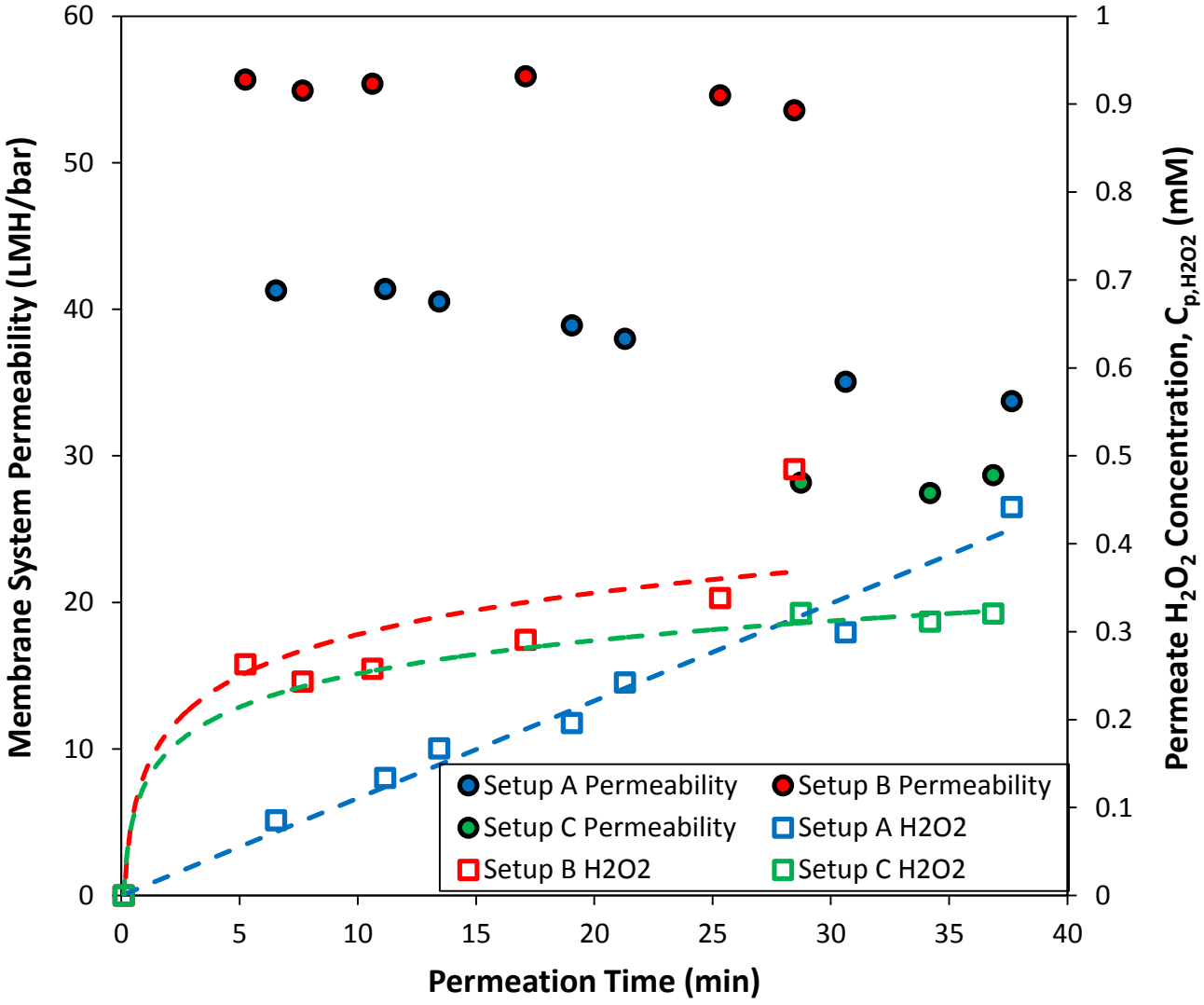

Figure 6.17. Time-dependent data analysis that demonstrates the steady-state enzymatic catalysis of GOx for CA:PVDF400HE-PAA-AA-PAH-GOx (Setup C) and dual PVDF400HE: PVDF400HE-PAA-AA-PAH-GOx (Setup B) composite membrane systems, when compared to a single PVDF400HE-PAA-AA-PAH-GOx (Setup A) membrane alone. Constant operating pressure of ΔP = 1.03 bar generated from pressurized air. Feed conditions: T = 21^{0}C; pH = 6, constant glucose substrate concentration at 2 mM and 100 mL volume. Membrane dimensions: A_c = 31.7 cm^2; l = 70 µm; ε_0 = 0.5 and d_{e0} = 420 nm for bare PVDF400HE. 3.3 mg GOx were immobilized in this study. DIUF H_2O permeability of the reactive membrane alone at pH = 6 was 19.22 LMH/bar.

6.10 Effect of Functionalized Membrane Characteristics on Steady-State Membrane Permeability during Enzymatic Catalysis

As has been a reoccurring theme is this work, product generation within the feed-side of the reactor has an effect on membrane permeability, overall activity, and stability. To a relatively lessened degree, the same can be concluded about product generation *within* the bulk volume of the functionalized membranes. In this work, this latter phenomenon can be observed by the effect that the combination of immobilized enzymatic mass and normalized functionalized membrane permeability (measured as DIUF H_2O permeability) have on reaction solution permeability. While the effect that product generation within the membrane has on permeate flux is relatively small compared to the effect that feed-side generation has on membrane performance, it is still noticeable and measurable as a function of the applied pressure gradient. Note that this does not equate to a function of permeate flux since, as has been shown, there is a direct effect that feed-side pressure has on the dissolved oxygen concentration, thus enzymatic turnover. In summary, since the pH of the solution passing through the membranes is constantly changing, i.e., becoming more acidic due to the production of gluconic acid and H_2O_2 during catalysis, the flux of the membranes will locally change due to the pH-responsive LbL.

Fortunately, due to the level of immobilized enzymatic mass and applied permeation pressure used in this particular experiment, there was not enough reaction product accumulation to allow for any measurable degradation of the LbL scaffold or deactivation of the immobilized enzymes. As can be seen by comparing

Figure 6.18 and Figure 6.19, normalized membrane permeability plays an important role in determining stable conditions for flow-driven, immobilized enzymatic catalysis. In figure Figure 6.18, the functionalized membrane shown has a DIUF H_2O permeability of 10.07 LMH/bar at pH = 6.0 and approximately 3.2 mg GOx immobilized. For the applied pressure gradient range shown, this membrane exhibits an asymptotically-increasing trend of permeability with respect to applied pressure gradient. It is hypothesized that this is primarily due to two factors: A higher partial pressure of feed-side oxygen (resulting in a higher activity pressure, thus an increased permeate flux), and a relatively faster degree of membrane system stabilization and steady-state conditioning due to a larger magnitude of permeation volume. At the low pressure end of Figure 6.18, where the partial pressure of dissolved oxygen and permeate flux are relatively low, it is observed that the permeability of the membrane is directly affected.

On the other hand, in Figure 6.19, the functionalized membrane shown has a DIUF H_2O permeability of 7.02 LMH/bar at pH = 6.0 and approximately 1.4 mg GOX immobilized. For the applied pressure gradient range shown, this membrane exhibits a much different trend than the former from Figure 6.18. In this case, the asymptotically-increasing trend of permeability with respect to applied pressure gradient is observed for the last three points of each data set, which indicates that similar fundaments are present, but not for, roughly, the first two data points of each set. As can be seen, the permeability *increases* for this subset. This indicates that there are other phenomena assuming a paramount role at low pressure gradients. It is hypothesized that for a membrane of relatively low permeability, this

is due to the *same* phenomenon that adversely affects membrane performance during permeation without a barrier membrane present. It is possible that, for denser membranes, the permeate residence time of the catalysis products becomes long enough that the interactions between the products with the LbL scaffold and the immobilized enzymes becomes significant. Since H_2O_2 and gluconic acid allow for an acidic environment, the LbL will respond accordingly by converting from salt form to a hydrated state. This allows for a higher permeability. While not shown here, this effect may be compounded by having a larger amount of immobilized enzymatic mass within a relatively dense membrane.

All of these observations imply that there exists a critical functionalization condition regarding an optimal amount of immobilized LbL and enzymatic mass for a particular membrane at which the immobilized enzymatic catalysis performs without adverse effects, but yields maximum mass-normalized activity.

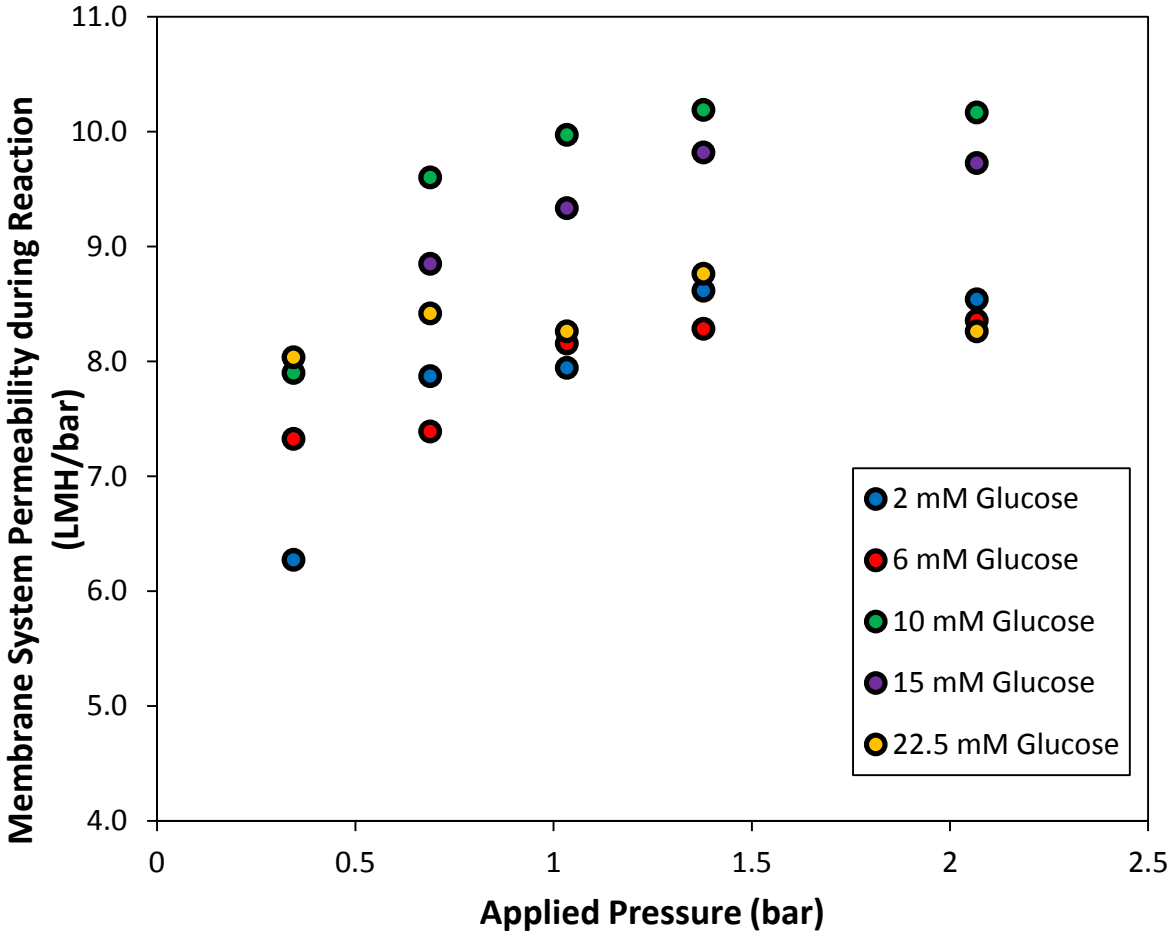

Figure 6.18. Effect of applied pressure gradient on functionalized membrane permeability during enzymatic catalysis of GOx for a CA:PVDF400HE-PAA-AA-PAH-GOx membrane system. Membrane dimensions: A_c = 31.7 cm^2; l = 70 µm; ε_0 = 0.5 and d_{e0} = 420 nm for bare PVDF400HE. Pressure was driven by UHPG O_2. Pure DIUF H_2O permeability was measured to be 10.07 LMH/bar at pH = 6.0. Approximately 3.2 mg GOx was immobilized within this membrane.

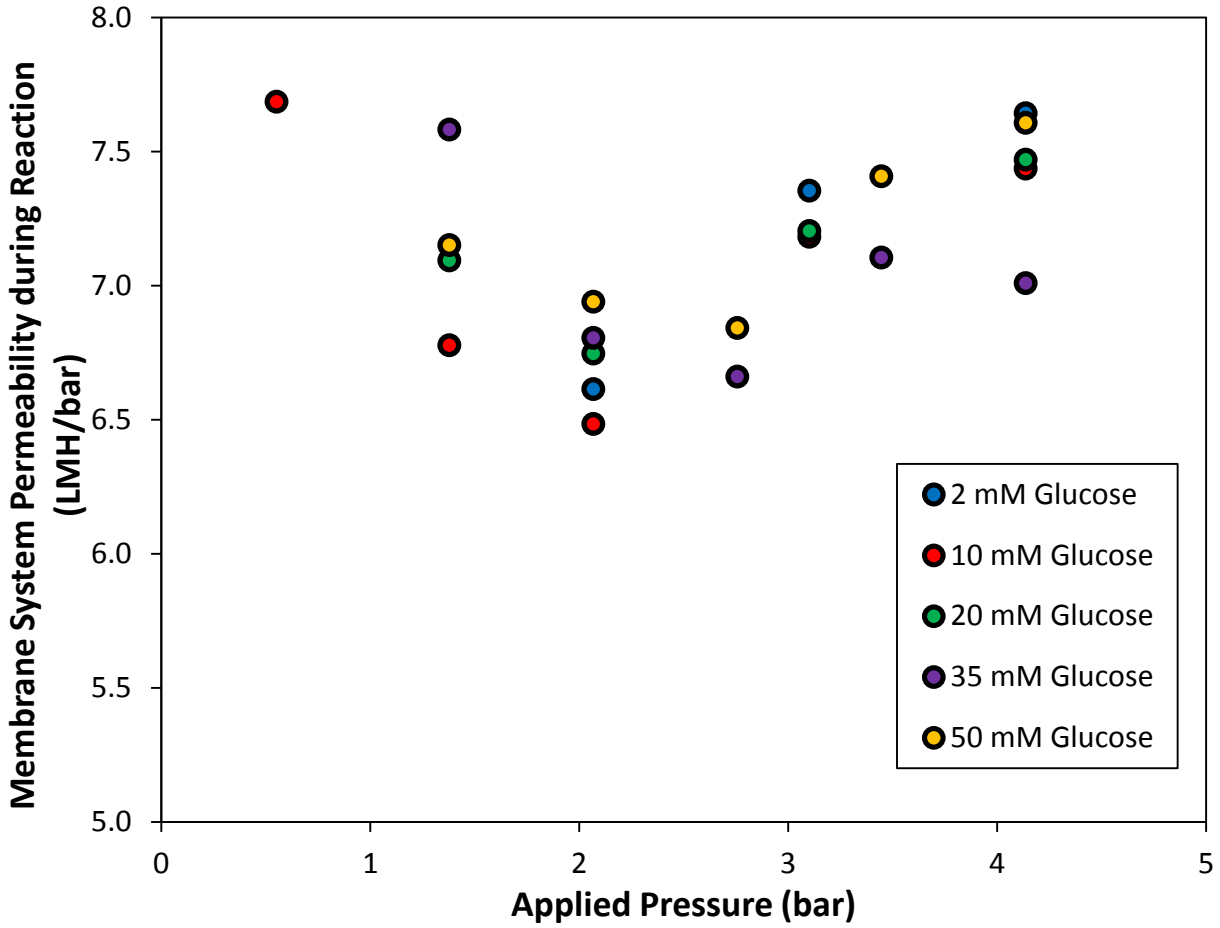

Figure 6.19. Effect of applied pressure gradient on functionalized membrane permeability during enzymatic catalysis of GOx for a CA:PVDF400HE-PAA-AA-PAH-GOx membrane system. Pressure was driven by UHPG O_2. Membrane dimensions: A_c = 31.7 cm^2; l = 70 μm; ε_0 = 0.5 and d_{e0} = 420 nm for bare PVDF400HE. Pure DIUF H_2O permeability was measured to be 7.02 LMH/bar at pH = 6.0. Approximately 1.4 mg GOx was immobilized within this membrane.

6.11 Effect of Permeate Residence Time on Permeate H_2O_2 Concentration

As given by Equation (5.20), the conversion of glucose into H_2O_2 can be written as a simple CSTR approximation for certain operating condition ranges. The following figures (Figure 6.20 to Figure 6.25) depict exactly that: Generally speaking, for estimated permeate residence times of less than 15 seconds; this linear approximation is valid with $R^2 > 0.95$. This approximation allows for a straightforward evaluation of the reaction rates for different magnitudes of glucose substrate concentration and LbL-immobilized GOx. As described in the theory, this is due to the dominance of the CSTR approximation of the PFR.

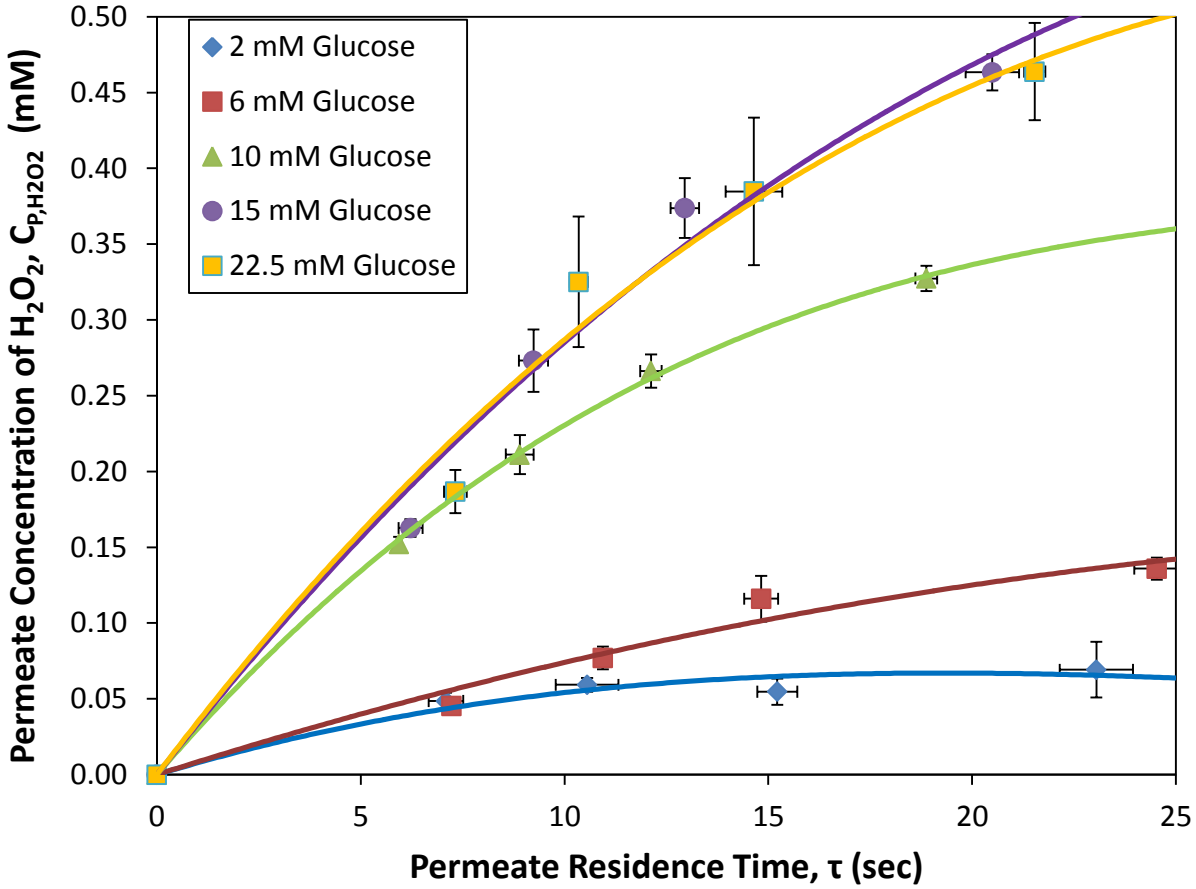

Figure 6.20. Effect of estimated steady-state permeate residence time on immobilized GOx enzymatic kinetics for LbL-functionalized CA:PVDF400HA-PAA-PAH-GOx membrane systems. Pressure was driven by UHPG O_2. Membrane dimensions: A_c = 31.7 cm^2; l = 70 µm; ε_0 = 0.5 and d_{e0} = 420 nm for bare PVDF400HA. Feed conditions: T = 21^{0}C; pH = 6, variable glucose substrate concentration at 300 mL volume. Approximately 0.90 mg GOx were immobilized within this membrane.

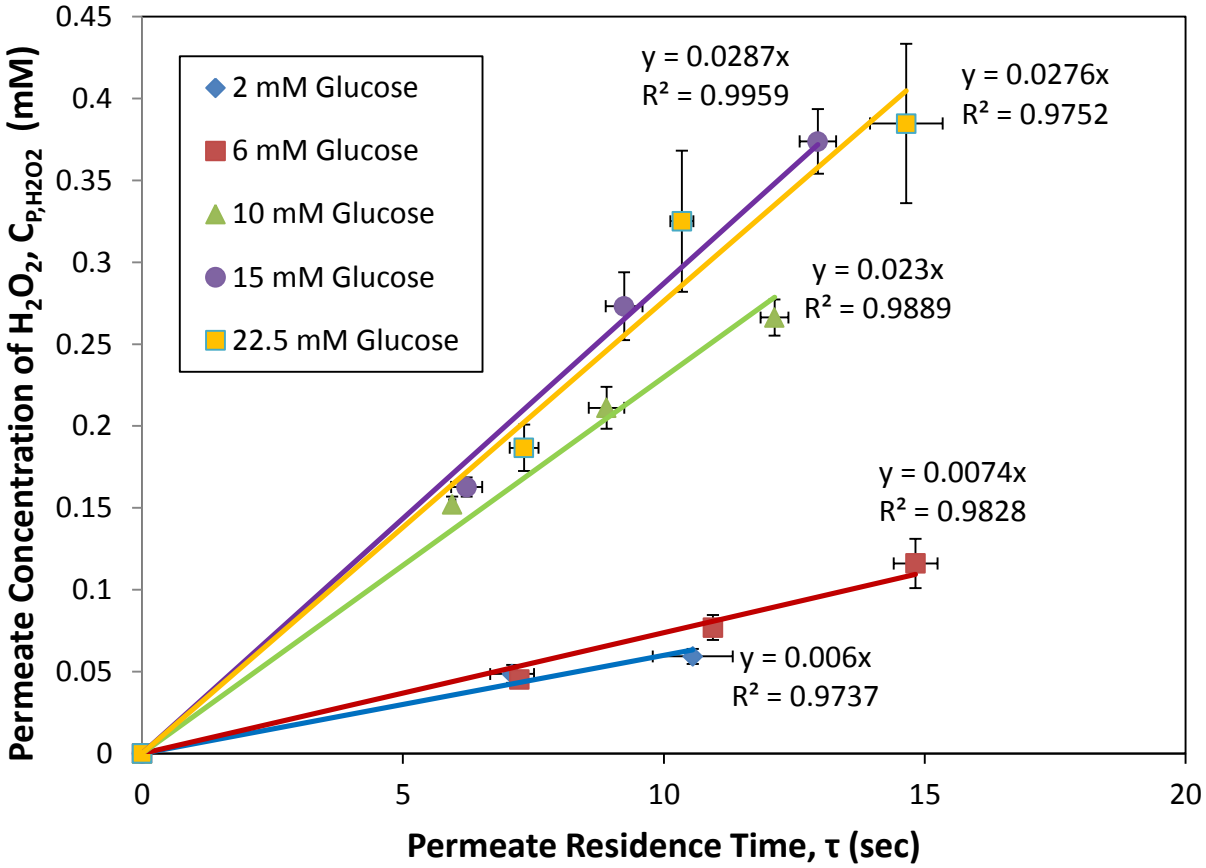

Figure 6.21. Effect of estimated steady-state permeate residence time on immobilized GOx enzymatic kinetics for LbL-functionalized CA:PVDF400HA-PAA-PAH-GOx membrane systems. Note that the linear approximation is for the data of Figure 6.20 that apply to the CSTR model described in the theory. Pressure was driven by UHPG O_2. Membrane dimensions: A_c = 31.7 cm^2; l = 70 μm; ε_0 = 0.5 and d_{e0} = 420 nm for bare PVDF400HA. Feed conditions: T = 21^{0}C; pH = 6, variable glucose substrate concentration at 300 mL volume. Approximately 0.90 mg GOx were immobilized within this membrane.

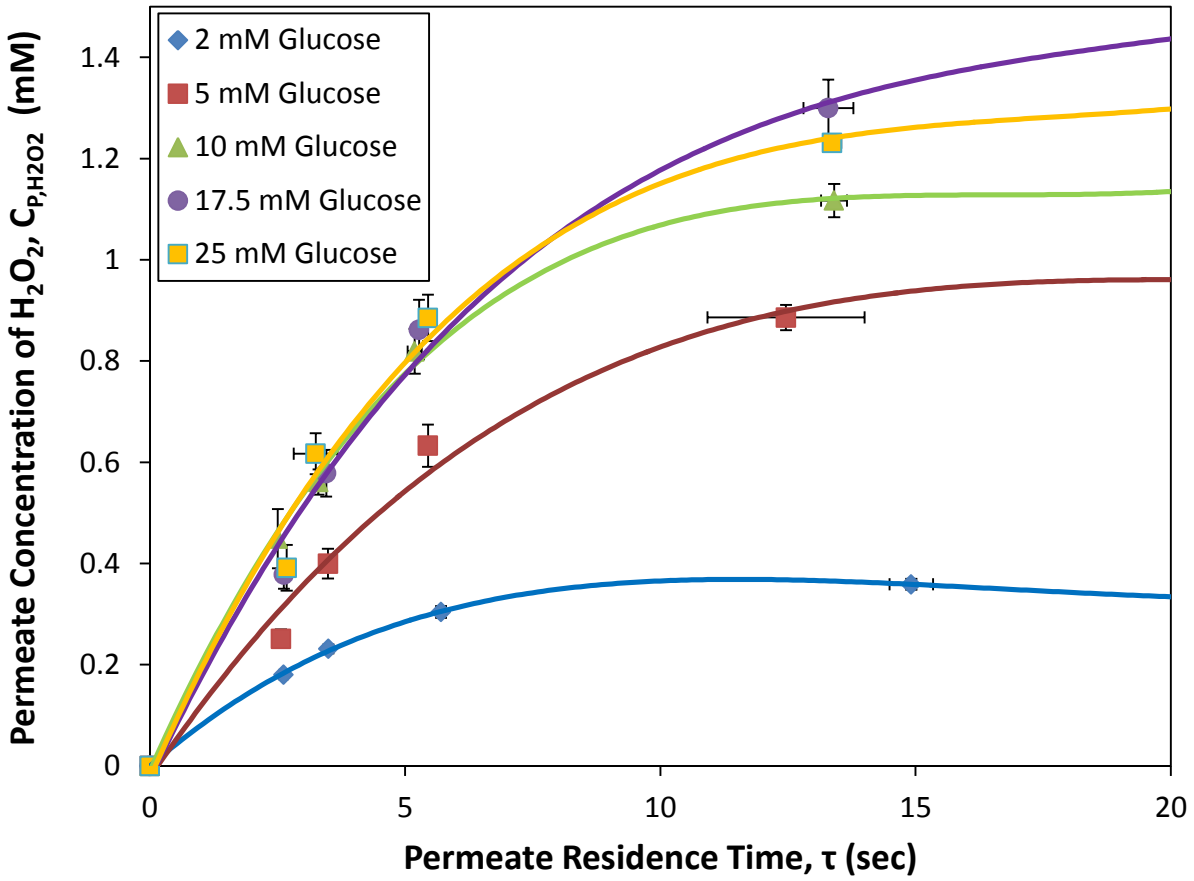

Figure 6.22. Effect of estimated steady-state permeate residence time on immobilized GOx enzymatic kinetics for LbL-functionalized CA:PVDF400HA-PAA-PAH-GOx membrane systems. Pressure was driven by UHPG O_2. Membrane dimensions: A_c = 31.7 cm^2; l = 70 μm; ε_0 = 0.5 and d_{e0} = 420 nm for bare PVDF400HA. Feed conditions: T = 21^{0}C; pH = 6, variable glucose substrate concentration at 300 mL volume. Approximately 1.53 mg GOx were immobilized within this membrane.

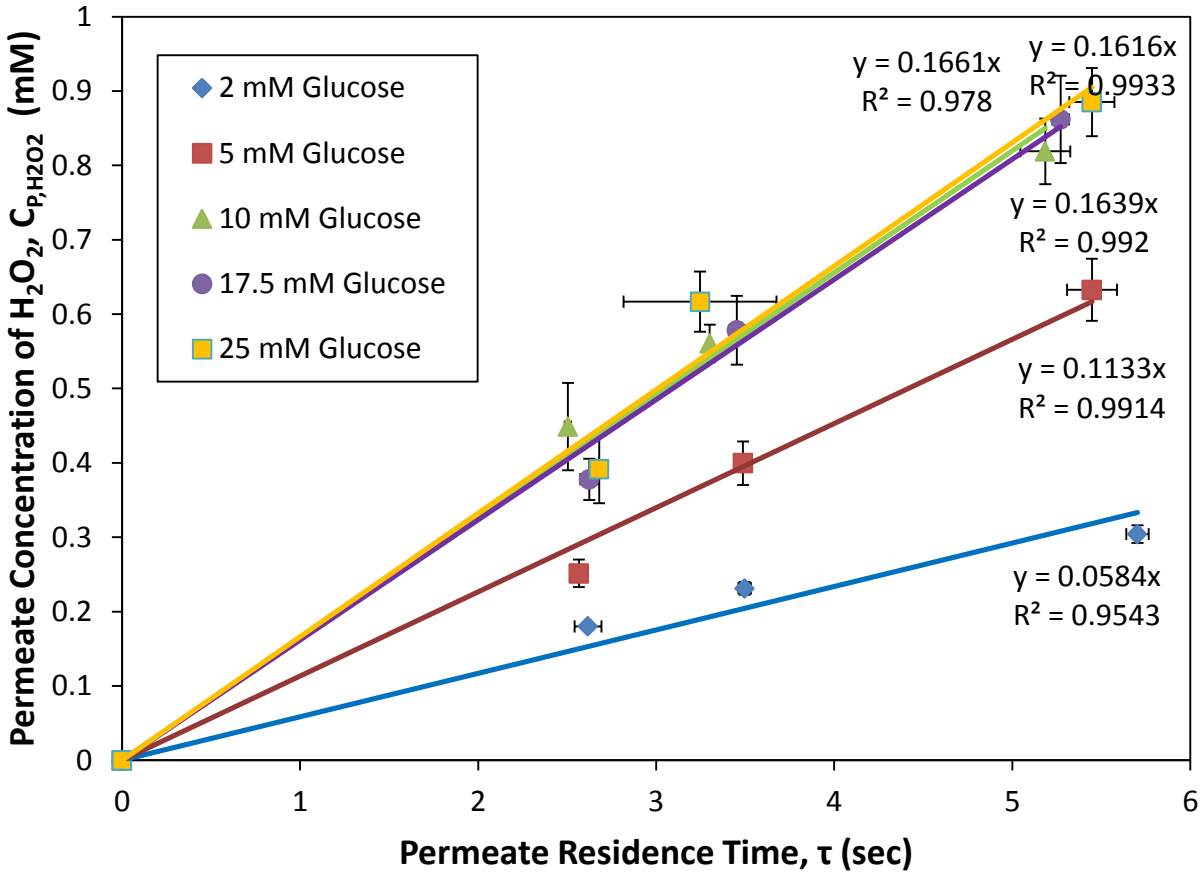

Figure 6.23. Effect of estimated steady-state permeate residence time on immobilized GOx enzymatic kinetics for LbL-functionalized CA:PVDF400HA-PAA-PAH-GOx membrane systems. Note that the linear approximation is for the data of Figure 6.22 that apply to the CSTR model described in the theory. Pressure was driven by UHPG O_2. Membrane dimensions: A_c = 31.7 cm^2; l = 70 μm; ε_0 = 0.5 and d_{e0} = 420 nm for bare PVDF400HA. Feed conditions: T = 21^{0}C; pH = 6, variable glucose substrate concentration at 300 mL volume. Approximately 1.53 mg GOx were immobilized within this membrane.

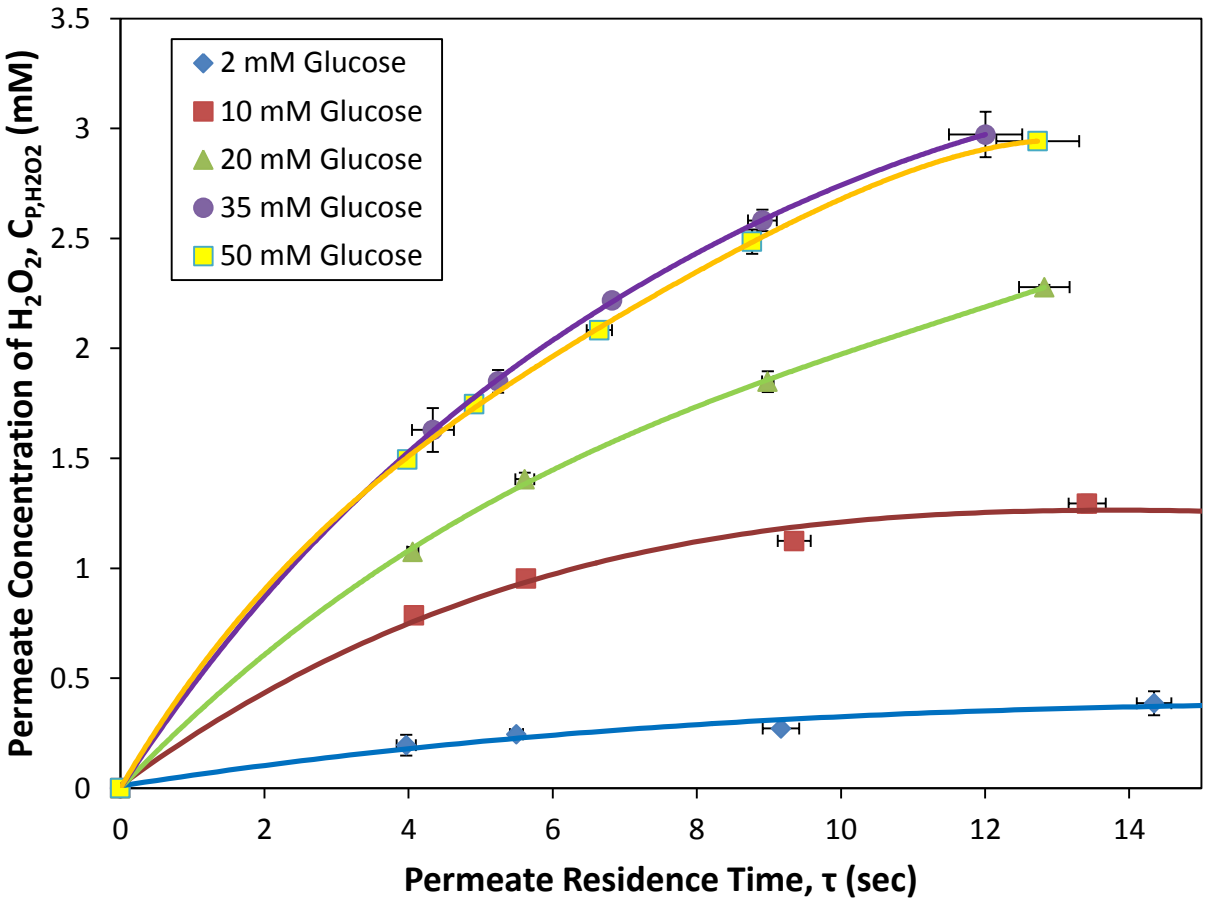

Figure 6.24. Effect of estimated steady-state permeate residence time on immobilized GOx enzymatic kinetics for LbL-functionalized CA:PVDF400HA-PAA-PAH-GOx membrane systems. Pressure was driven by UHPG O_2. Membrane dimensions: A_c = 31.7 cm^2; l = 70 µm; ε_0 = 0.5 and d_{e0} = 420 nm for bare PVDF400HA. Feed conditions: T = 21^{0}C; pH = 6, variable glucose substrate concentration at 300 mL volume. Approximately 3.19 mg GOx were immobilized within this membrane.

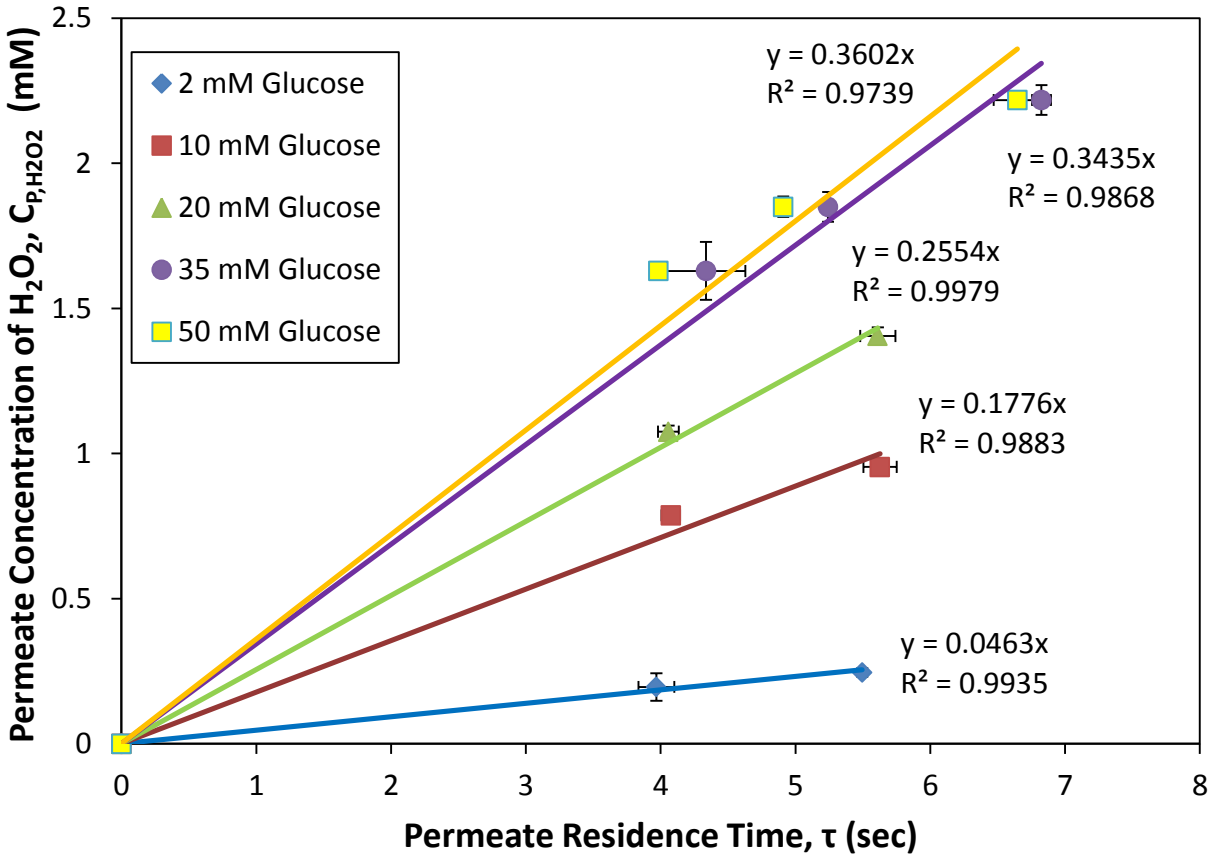

Figure 6.25. Effect of estimated steady-state permeate residence time on immobilized GOx enzymatic kinetics for LbL-functionalized CA:PVDF400HA-PAA-PAH-GOx membrane systems. Note that the linear approximation is for the data of Figure 6.24 that apply to the CSTR model described in the theory. Pressure was driven by UHPG O_2. Membrane dimensions: A_c = 31.7 cm²; l = 70 μm; ε_0 = 0.5 and d_{e0} = 420 nm for bare PVDF400HA. Feed conditions: T = 21°C; pH = 6, variable glucose substrate concentration at 300 mL volume. Approximately 3.19 mg GOx were immobilized within this membrane.

6.12 Effect of Initial Glucose Substrate Concentration on Reaction Rate

The effect that the initially-charged concentration of glucose has on the reaction rate of the enzymatic catalysis was studied as a compilation of the regressions generated in the previous section. The linear regression data were plotted against the corresponding initial concentrations of glucose, for a specified amount of LbL-immobilized GOx. These data were fit by a MATLAB function, MMFit, which can be viewed in Appendix A. As can be seen, a standard Michaelis-Menten model is appropriate for an estimation of reaction parameters K_m and v_{max}.

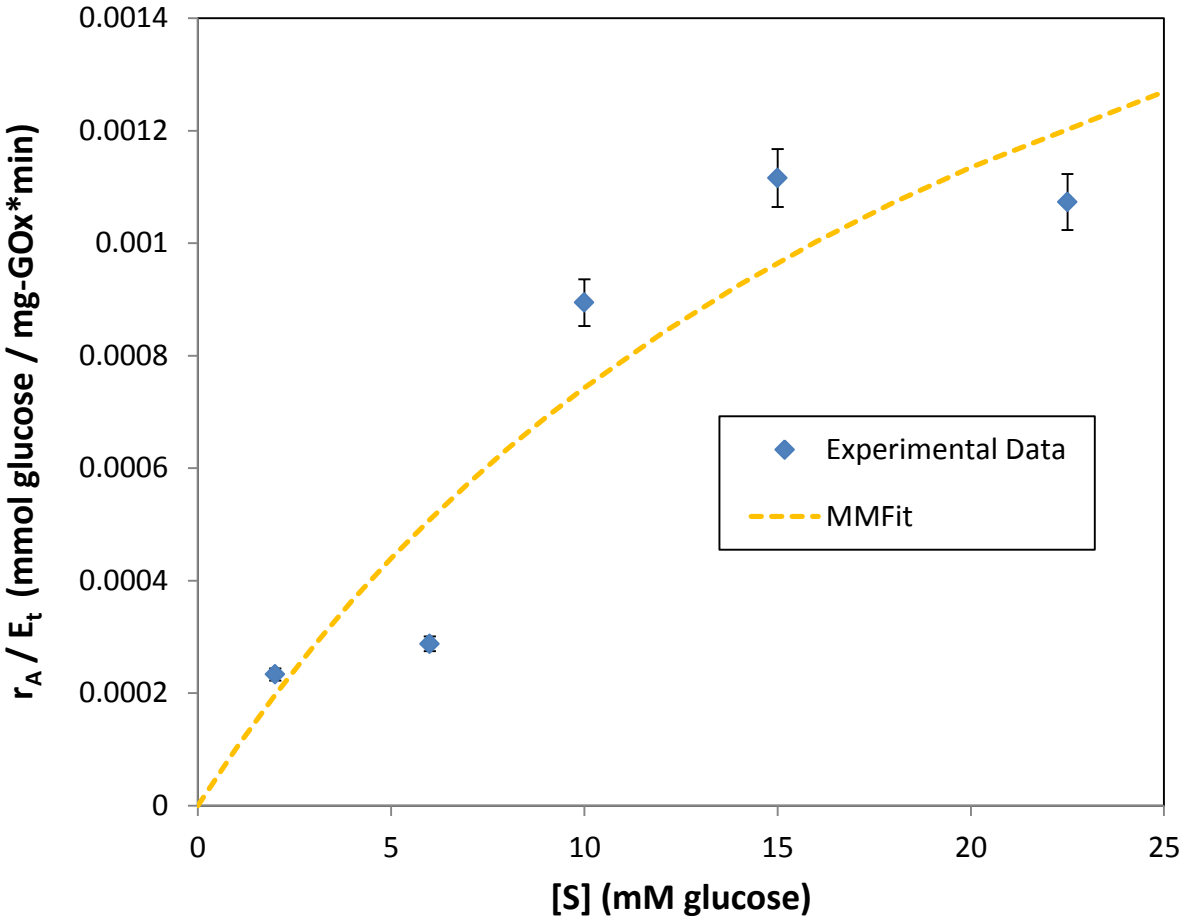

Figure 6.26. Effect of initially-charged glucose concentration on immobilized GOx enzymatic kinetics for LbL-functionalized CA:PVDF400HA-PAA-PAH-GOx membrane systems. These data were generated from the linear regressions in Figure 6.21. Pressure was driven by UHPG O_2. Membrane dimensions: A_c = 31.7 cm^2; l = 70 μm; ε_0 = 0.5 and d_{e0} = 420 nm for bare PVDF400HA. Feed conditions: T = 21^{0}C; pH = 6, variable glucose substrate concentration at 300 mL volume. Approximately 0.90 mg GOx were immobilized within this membrane.

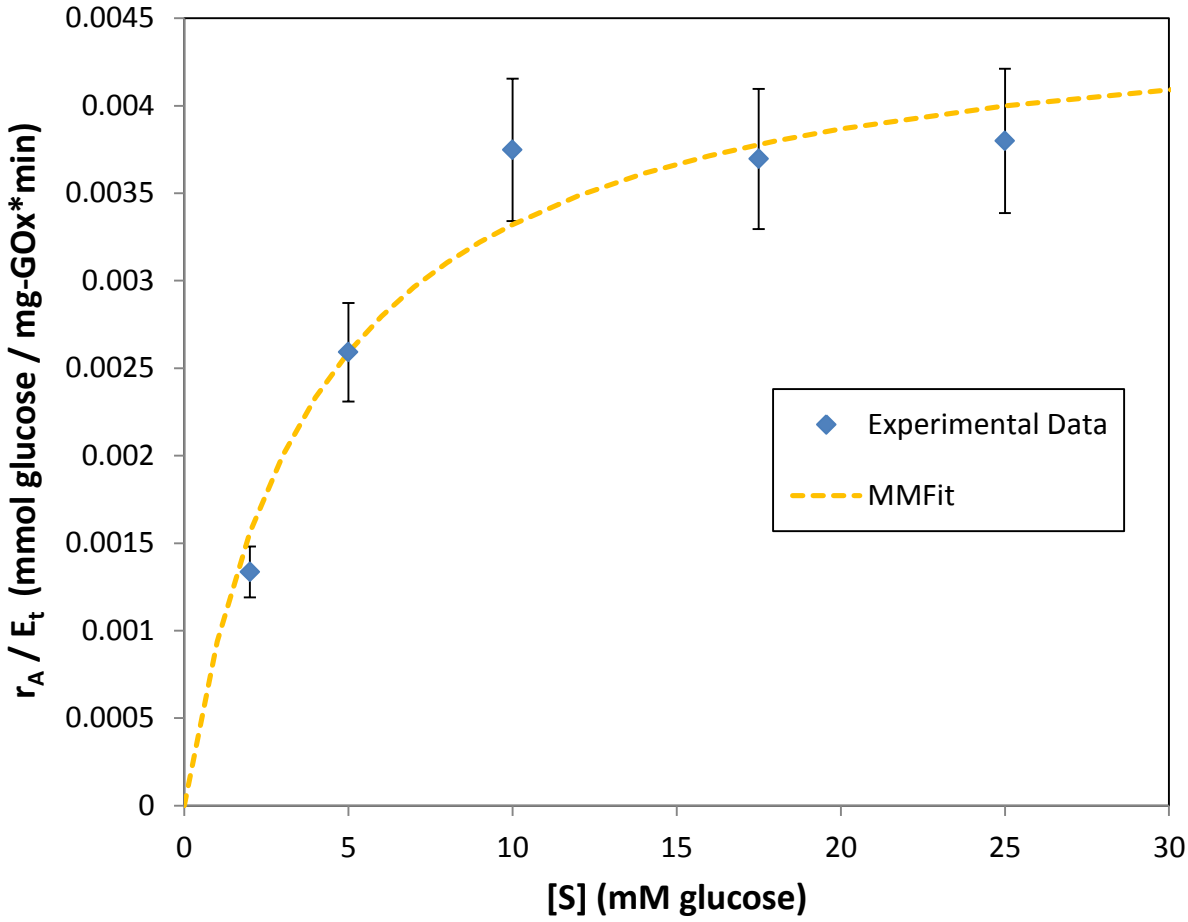

Figure 6.27. Effect of initially-charged glucose concentration on immobilized GOx enzymatic kinetics for LbL-functionalized CA:PVDF400HA-PAA-PAH-GOx membrane systems. These data were generated from the linear regressions in Figure 6.23. Pressure was driven by UHPG O_2. Membrane dimensions: A_c = 31.7 cm^2; l = 70 μm; ε_0 = 0.5 and d_{e0} = 420 nm for bare PVDF400HA. Feed conditions: T = 21^{0}C; pH = 6, variable glucose substrate concentration at 300 mL volume. Approximately 1.53 mg GOx were immobilized within this membrane.

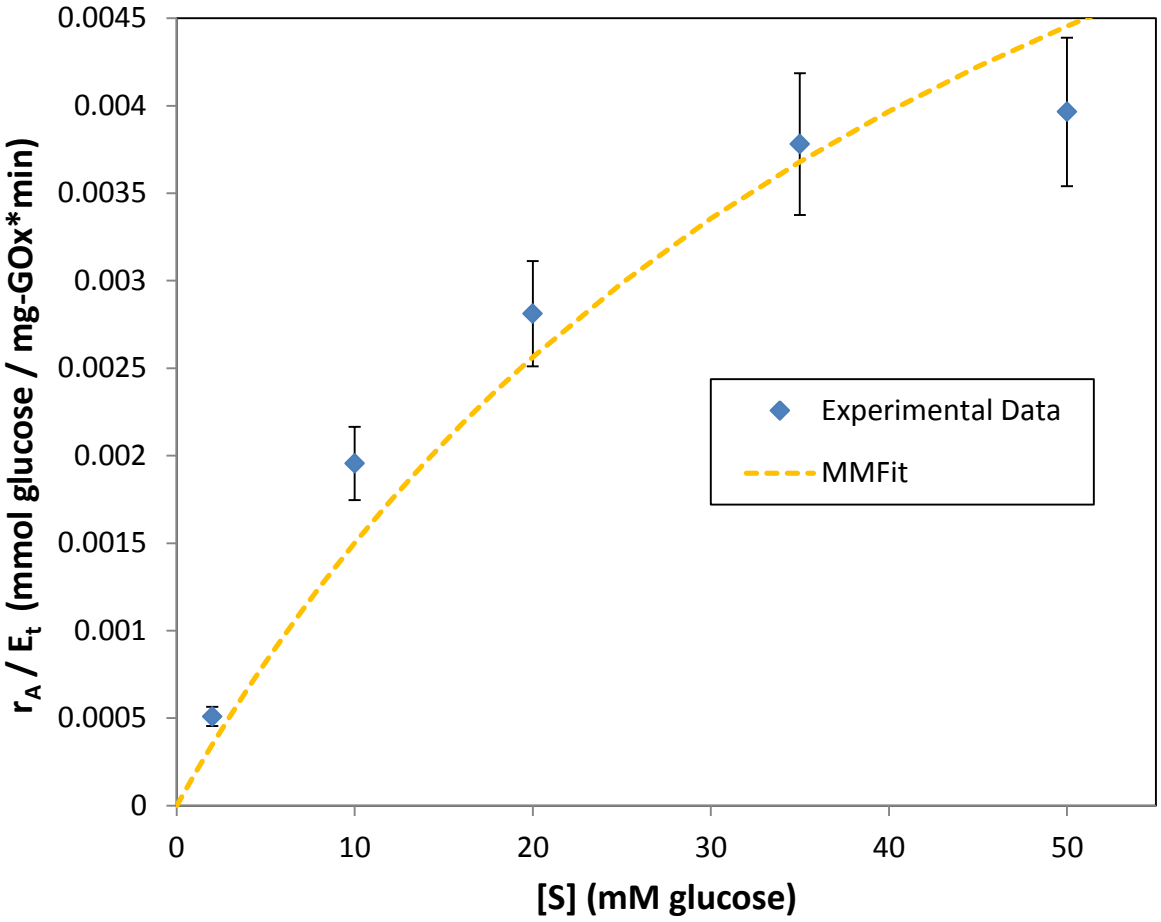

Figure 6.28. Effect of initially-charged glucose concentration on immobilized GOx enzymatic kinetics for LbL-functionalized CA:PVDF400HA-PAA-PAH-GOx membrane systems. These data were generated from the linear regressions in Figure 6.25. Pressure was driven by UHPG O_2. Membrane dimensions: A_c = 31.7 cm^2; l = 70 μm; ε_0 = 0.5 and d_{e0} = 420 nm for bare PVDF400HA. Feed conditions: T = 21^{0}C; pH = 6, variable glucose substrate concentration at 300 mL volume. Approximately 3.19 mg GOx were immobilized within this membrane.

6.13 Effect of Immobilized Mass of Enzyme on Activity

By using the MMFit function (Appendix A), the MM parameters were able to be estimated for both homogeneous kinetics and LbL-immobilized kinetics (CSTR model). Of relevance to this study is the comparison of the turnover ratio parameter, k_3, which can easily be estimated by plotting the parameter v_{max} against the amount of enzymes loaded into the corresponding reactive volume, E_tV. It is important to note that this product is used, rather than just E_t itself, because the reactive volume is variable from homogeneous to membrane-immobilized kinetics, and also between different functionalized membranes.

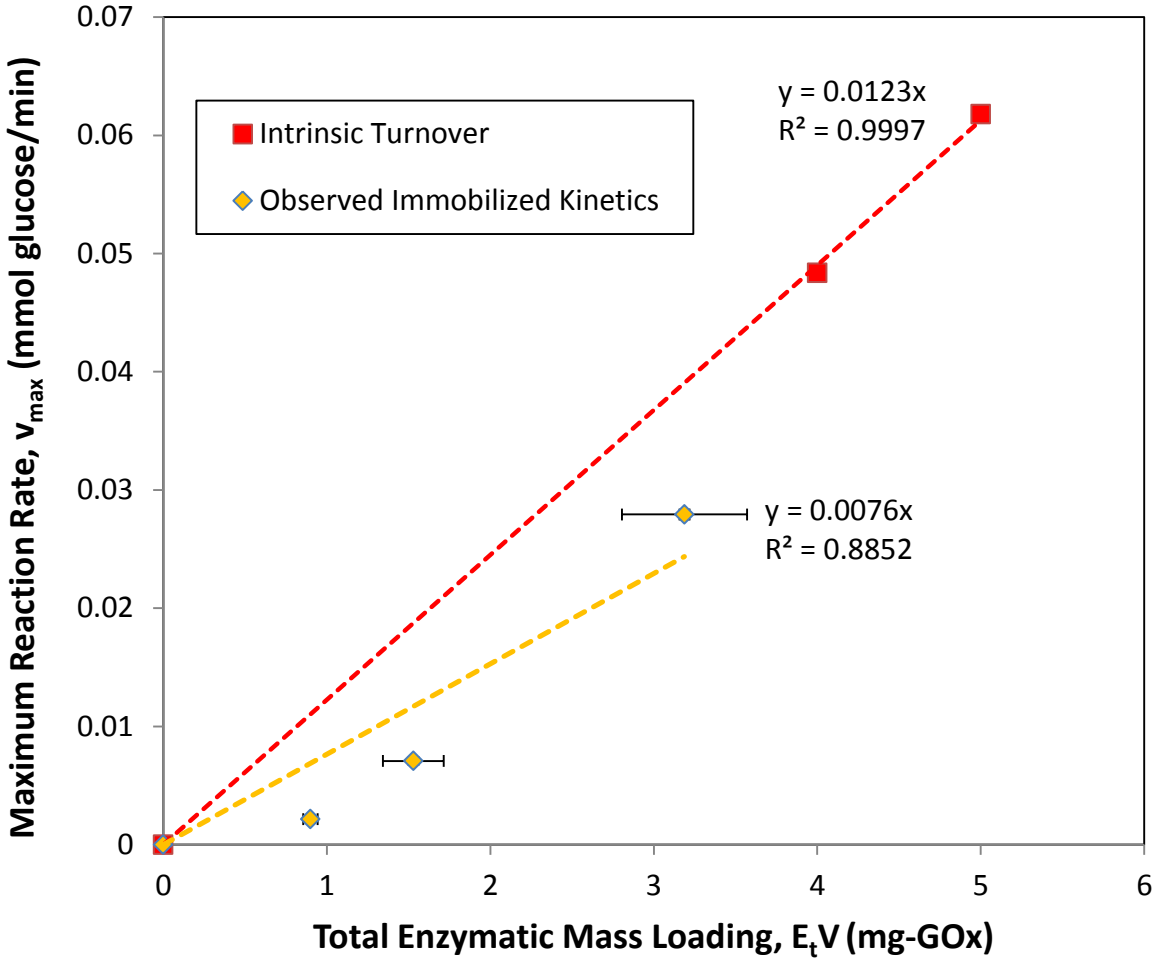

Figure 6.29. Comparison of volume-denormalized enzymatic loading on between immobilized GOx enzymatic kinetics for LbL-functionalized CA:PVDF400HA-PAA-PAH-GOx membrane systems and homogeneous-phase kinetics of the same kind. The data regarding the former case were generated from the function MMFit and the data shown in Figure 6.26, Figure 6.27, and Figure 6.28. For the former case, pressure was driven by UHPG O_2. Membrane dimensions: A_c = 31.7 cm^2; l = 70 μm; ε_0 = 0.5 and d_{e0} = 420 nm for bare PVDF400HA. Feed conditions: T = 21^0C; pH = 6, variable glucose substrate concentration at 300 mL volume. Homogeneous-phase kinetics were carried out in DIUF H_2O at T = 21^0C; pH = 6 and 60 rpm of magnetic stir under normal atmospheric pressure.

Chapter 7. Conclusions

The field of membrane-immobilized enzymatic catalysis is lush and fertile, primarily due to new advances in understanding the most appropriate conditions for enzymatic immobilizations and reactions. It has been shown that the effectiveness, Ω, of membrane-based LbL-immobilized enzymatic kinetics actually *increases* with immobilized mass. Specifically, it is apparent (Figure 6.29) that an increase in immobilized catalytic mass results in a quasi-linear effect on maximum reaction rate. This is derived from a number of causes: First, in the case of immobilized kinetics, not all immobilizations are alike. Rather, some active sites may be unavailable due to inherently unfavorable biological immobilization configurations, which generate local mass-transfer rate-determining effects on reaction rates, and cause variability in overall reaction robustness. The extent of this phenomenon may be derived from the departure that the LbL scaffold has from native biological conditions, namely, the ratio of available amine to carboxyl functionalization sites, as well as the relative distance from each function group. A scaffold that minimizes this effect will biomimic the cell membrane conditions that surround GOx *en vivo*. Second, not all reaction domains within the functionalized microfiltration membrane are alike, at least, in terms of volumetric size. Since there is an intrinsic polydispersity amongst the pore diameters in such a membrane as hydrophilized PVDF, there also exists an inherent residence time distribution. This is especially true in the case of a catalytically-functionalized membrane, where the immobilized enzymes themselves contribute to an additional variance, this time in terms of functionalized mass from pore to pore (best visualized in Figure 6.9). Third,

due to the effect of dissolved oxygen on the reaction rate (Table 6.5), the v_{max} shown for the immobilized kinetics is somewhat of an all-encompassing parameter that includes contributions from both glucose and oxygen variability in the reactive solution. Since, with varying applied pressure, the concentration of dissolved oxygen varies linearly, this contribution to the overall reaction kinetics cannot be circumvented in such am experimental setup as the one used in this study. It is most likely that this phenomenon contributes the most to the quasi-linear effect of immobilized catalytic mass of maximum reaction rate, and, more interestingly, the increase in Ω with an increase in immobilized mass, since $\Omega = \Omega(v_{max})$.

In addition, this work has demonstrated that, for this experimental setup, it is of utmost importance to prevent significant reaction product accumulation on the feed-side of the membrane reactor. This phenomenon results in aqueous condition changes, such as in pH and redox state, which not only have effects on catalytic conditions, but also on LbL stability and longevity. In this study, the accumulation was significantly stemmed due to the use of the coined "barrier" membranes that preceded, in series, the membrane reactor.

Equally important is how, with the appropriate storage conditions, LbL immobilized enzymatic catalysis within a membrane scaffold can be carried out for extended periods of time without issues regarding LbL degradation of enzymatic destabilization. Herein lies one of the greatest benefits and potentials of this field: A significantly increased catalytic lifespan as compared to the homogeneous phase, particularly when immobilized upon an optimally biomimetic surface, and protected from external vectors (such as a microfiltration membrane provides).

Overall, due to the robustness and versatility of these platforms, membrane-based, functionalized LbL scaffolds for enzymatic catalysis has shown to be a promising approach for process-dependent, long-term use applications. Additional work is required in order to delineate the local phenomena that occur within the membrane domain. The biologically-inspired optimization of physical and operating conditions for maximum immobilized reaction effectiveness will prove crucial for demonstration of the ultimate potential of this technology, which is on the cusp of being realized.

Appendix A. MATLAB Program Code

Shown below are examples of the MATLAB program MMFit.m and its function MMFunction.m developed by Andrew Tomaino. Note that the data entered are shown for example purposes only.

MMFit.m

```
clear
clc

% This script file (MMFit.m) is a MATLAB-coded project that calls upon
% a function, MMFunction, which fits two column (x = glucose substrate
% concentration, y = kinetic rate) data vectors to a nonlinear rational
% function of the Michaelis-Menten kind. This script is used for solving
% for the Michaelis-Menten batch kinetic constants, Km and v_max, at
% pH = 6, T = 23 deg C, and constantly-stirred conditions.

% Initial glucose concentration [mM glucose]
MMxData = [2; 5; 10; 17.5; 25];

% Kinetic rate [mM glucose/(min*mg-GOx)]

MMyData = [0.000252061; 0.000489015; 0.00070741; 0.000697483; 0.000716905];

[ratFit, gof2] = MMFunction(MMxData, MMyData);

ratFit
gof2

plot(ratFit, 'b')
```

MMFunction.m

```
function [cRate, g] = MMFunction(x,y)

% MMFunction.m Fits assigned data vectors to a function of type
% (a*x)/((x+b)^n), where n = -1. Returns the fitted curve vector using the
% built-in MATLAB function fit().

plot(x, y, 'o')
hold on

s = fitoptions('Method', 'NonlinearLeastSquares',...
        'Lower', [0,0],...
        'Upper', [Inf, Inf],...
        'Startpoint', [0.000716905,25]);
f = fittype('(a*x)*((x+b)^n)','problem','n','options',s);

[cRate,g] = fit(x,y,f,'problem', -1);

end
```

References

[1] A. D. Taylor, M. Michel, R. C. Sekol, J. M. Kizuka, N. A. Kotov, and L. T. Thompson, "Fuel Cell Membrane Electrode Assemblies Fabricated by Layer-by-Layer Electrostatic Self-Assembly Techniques," *Advanced Functional Materials,* vol. 18, pp. 3003-3009, 2008.

[2] S. Datta, C. Cecil, and D. Bhattacharyya, "Functionalized Membranes by Layer-By-Layer Assembly of Polyelectrolytes and In Situ Polymerization of Acrylic Acid for Applications in Enzymatic Catalysis," *Industrial & Engineering Chemistry Research,* vol. 47, 2008.

[3] Z. Tang, Y. Wang, P. Podsiadlo, and N. A. Kotov, "Biomedical Applications of Layer-by-Layer Assembly: From Biomimetics to Tissue Engineering," *Advanced Materials,* vol. 18, 2006.

[4] F. Crespilho, V. Zucolotto, O. Oliveira, and F. Nart, "Electrochemistry of layer-by-layer films: a review," *Int. J. Electrochem. Sci,* 2006.

[5] K. Ariga, J. Hill, and Q. Ji, "Layer-by-layer assembly as a versatile bottom-up nanofabrication technique for exploratory research and realistic application," *Physical chemistry chemical physics : PCCP,* vol. 9, pp. 2319-2340, 2007.

[6] S. P. Jiang, Z. Liu, and Z. Q. Tian, "Layer-by-Layer Self-Assembly of Composite Polyelectrolyte–Nafion Membranes for Direct Methanol Fuel Cells," *Advanced Materials,* vol. 18, 2006.

[7] T. R. Farhat and P. T. Hammond, "Designing a New Generation of Proton-Exchange Membranes Using Layer-by-Layer Deposition of Polyelectrolytes," *Advanced Functional Materials,* vol. 15, 2005.

[8] C. Jiang, S. Markutsya, Y. Pikus, and V. Tsukruk, "Freely suspended nanocomposite membranes as highly sensitive sensors," *Nature materials,* vol. 3, pp. 721-728, 2004.

[9] P. K. Deshmukh, K. P. Ramani, S. S. Singh, A. R. Tekade, V. K. Chatap, G. B. Patil, and S. B. Bari, "Stimuli-sensitive layer-by-layer (LbL) self-assembly systems: targeting and biosensory applications," *J Control Release,* vol. 166, pp. 294-306, Mar 28 2013.

[10] W. Zhao, J.-J. Xu, and H.-Y. Chen, "Electrochemical Biosensors Based on Layer-by-Layer Assemblies," *Electroanalysis,* vol. 18, pp. 1737-1748, 2006.

[11] C. Yang, E. E. Nuxoll, and E. L. Cussler, "Reactive barrier films," *AIChE Journal,* vol. 47, 2001.

[12] V. Hornok, A. Erdőhelyi, and I. Dékány, "Preparation of ultrathin membranes by layer-by-layer deposition of layered double hydroxide (LDH) and polystyrene sulfonate (PSS)," *Colloid and Polymer Science,* vol. 283, pp. 1050-1055, 2005.

[13] J. R. Siqueira, F. N. Crespilho, V. Zucolotto, and O. N. Oliveira, "Bifunctional electroactive nanostructured membranes," *Electrochemistry Communications,* vol. 9, pp. 2676-2680, 2007.

[14] L. Krasemann and B. Tieke, "Selective Ion Transport across Self-Assembled Alternating Multilayers of Cationic and Anionic Polyelectrolytes," *Langmuir,* vol. 16, 2000.

[15] D. Wandera, S. R. Wickramasinghe, and S. M. Husson, "Modification and characterization of ultrafiltration membranes for treatment of produced water," *Journal of Membrane Science,* vol. 373, pp. 178-188, 2011.
[16] K. Hu and M. J. Dickson, "Modelling of the pore structure variation with pH for pore-filled pH-sensitive poly(vinylidene fluoride)–poly(acrylic acid) membranes," *Journal of Membrane Science,* vol. 321, 2008.
[17] K. Hu and J. M. Dickson, "In vitro investigation of potential application of pH-sensitive poly(vinylidene fluoride)–poly(acrylic acid) pore-filled membranes for controlled drug release in ruminant animals," *Journal of Membrane Science,* vol. 337, 2009.
[18] P. Pardeshi and A. A. Mungray, "Synthesis, characterization and application of novel high flux FO membrane by layer-by-layer self-assembled polyelectrolyte," *Journal of Membrane Science,* vol. 453, pp. 202-211, 2014.
[19] S. Guedidi, Y. Yurekli, A. Deratani, P. Déjardin, C. Innocent, S. A. Altinkaya, S. Roudesli, and A. Yemenicioglu, "Effect of enzyme location on activity and stability of trypsin and urease immobilized on porous membranes by using layer-by-layer self-assembly of polyelectrolyte," *Journal of Membrane Science,* vol. 365, pp. 59-67, 2010.
[20] D. M. Dotzauer, M. L. Bruening, and L. Sun, "Catalytic Membranes Prepared Using Layer-by-Layer Adsorption of Polyelectrolyte/Metal Nanoparticle Films in Porous Supports," *Nano Letters,* vol. 6, 2006.
[21] D. Wandera, S. R. Wickramasinghe, and S. M. Husson, "Stimuli-responsive membranes," *Journal of Membrane Science,* vol. 357, 2010.
[22] V. Smuleac, D. Butterfield, and D. Bhattacharyya, "Layer-by-layer-assembled microfiltration membranes for biomolecule immobilization and enzymatic catalysis," *Langmuir : the ACS journal of surfaces and colloids,* vol. 22, pp. 10118-10124, 2006.
[23] M. Bruening, D. Dotzauer, P. Jain, L. Ouyang, and G. Baker, "Creation of functional membranes using polyelectrolyte multilayers and polymer brushes," *Langmuir : the ACS journal of surfaces and colloids,* vol. 24, pp. 7663-7673, 2008.
[24] K. Caridis and T. Papathanasiou, "Pressure effects in cross-flow microfiltration of suspensions of whole bacterial cells," *Bioprocess and Biosystems Engineering,* 1997.
[25] Perry's, "Microfiltration," *Perry's Chemical Engineer's Handbook,* vol. 8, pp. 54-57.
[26] Y. Su, Y. Liang, C. Mu, and Z. Jiang, "Improved Performance of Poly(Vinylidene Fluoride) Microfiltration Membranes Prepared by Freeze and Immersion Precipitation Coupling Method," *Industrial & Engineering Chemistry Research,* vol. 50, pp. 10525-10532, 2011.
[27] D. P. Go, A. Hung, S. L. Gras, and A. J. O'Connor, "Use of a short peptide as a building block in the layer-by-layer assembly of biomolecules on polymeric surfaces," *J Phys Chem B,* vol. 116, pp. 1120-33, Jan 26 2012.
[28] C. Zhao, S. Nie, M. Tang, and S. Sun, "Polymeric pH-sensitive membranes—A review," *Progress in Polymer Science,* vol. 36, pp. 1499-1520, 2011.

[29] B. Zeeb, C. Thongkaew, and J. Weiss, "Theoretical and Practical Considerations in Electrostatic Depositioning of Charged Polymers," *Applied Polymer Science,* vol. 231, 2014.

[30] Fujiwara, Grubbs, and Baldeschwieler, "Characterization of pH-Dependent Poly(acrylic Acid) Complexation with Phospholipid Vesicles," *Journal of colloid and interface science,* vol. 185, pp. 210-216, 1997.

[31] R. Messing, "Simultaneously immobilized glucose oxidase and catalase in controlled-pore titania," *Biotechnology and bioengineering,* vol. 16, pp. 897-908, 1974.

[32] S. Lewis, S. Datta, M. Gui, E. Coker, F. Huggins, S. Daunert, L. Bachas, and D. Bhattacharyya, "Reactive nanostructured membranes for water purification," *Proceedings of the National Academy of Sciences of the United States of America,* vol. 108, pp. 8577-8582, 2011.

[33] G. M. Rios, M. P. Belleville, D. Paolucci, and J. Sanchez, "Progress in enzymatic membrane reactors – a review," *Journal of Membrane Science,* vol. 242, 2004.

[34] B. Swoboda and V. Massey, "Purification and properties of the glucose oxidase from Aspergillus niger," *Journal of Biological Chemistry,* 1965.

[35] H. Hecht, H. Kalisz, J. Hendle, R. Schmid, and D. Schomburg, "Crystal structure of glucose oxidase from Aspergillus niger refined at 2.3 A resolution," *Journal of molecular biology,* vol. 229, pp. 153-172, 1993.

[36] S. Hayashi and S. Nakamura, "Multiple forms of glucose oxidase with different carbohydrate compositions," *Biochimica et Biophysica Acta (BBA)-Enzymology,* 1981.

[37] H. Tsuge and O. Natsuaki, "Purification, Properties, and Molecular Features of Glucose Oxidase from Aspergillus Niger," *J Biochem,* vol. 78, pp. 835-843, 1975 1974.

[38] X. Wang, K.-X. Zhu, and H.-M. Zhou, "Immobilization of glucose oxidase in alginate-chitosan microcapsules," *International journal of molecular sciences,* vol. 12, pp. 3042-3054, 2011.

[39] H. Xue, Z. Shen, and C. Li, "Improved selectivity and stability of glucose biosensor based on in situ electropolymerized polyaniline-polyacrylonitrile composite film," *Biosensors & bioelectronics,* vol. 20, pp. 2330-2334, 2005.

[40] H. Bright and M. Appleby, "The pH dependence of the individual steps in the glucose oxidase reaction," *Journal of Biological Chemistry,* 1969.

[41] T. D. Dziubla, V. V. Shuvaev, N. K. Hong, B. J. Hawkins, M. Madesh, H. Takano, E. Simone, M. T. Nakada, A. Fisher, S. M. Albelda, and V. R. Muzykantov, "Endothelial targeting of semi-permeable polymer nanocarriers for enzyme therapies," *Biomaterials,* vol. 29, pp. 215-27, Jan 2008.

[42] Y. Yao, R. Li, Y. Ma, X. Wang, C. Li, X. Zhang, R. Ma, Z. Ding, and L. Liu, "alpha-Lipoic acid increases tolerance of cardiomyoblasts to glucose/glucose oxidase-induced injury via ROS-dependent ERK1/2 activation," *Biochim Biophys Acta,* vol. 1823, pp. 920-9, Apr 2012.

[43] A. J. Gow and F. Branco, "Immunotargeting of glucose oxidase: intracellular productino of H2O2 and endothelial oxidative streaa," *Am J Physical Lung Cell Mol Physiol,* vol. 277, pp. 271-281, 1999 1999.

[44] K. Hu and J. M. Dickson, "Development and characterization of poly(vinylidene fluoride)–poly(acrylic acid) pore-filled pH-sensitive membranes," *Journal of Membrane Science,* vol. 301, 2007.

[45] M. Bradford, "A rapid and sensitive method for the quantitation of microgram quantities of protein utilizing the principle of protein-dye binding," *Analytical biochemistry,* vol. 72, pp. 248-254, 1976.

[46] P. J. Fraker and J. C. Speck, "Protein and Cell Membrane Iodinations with a Sparingly Soluble Chloromide, 1,4,3,6-tetrachloro-3a,6a-diphenylgylcoluril," *Biochemical and Biophysical Research Communications,* vol. 80, pp. 849-857, 1978.

[47] P. A. Clapp, D. F. Evans, and T. S. S. Sheriff, "Spectrophotometric determination of hydrogen peroxide after extraction with ethyl acetate," *Analytica Chimica Acta*, vol. 218, pp. 331-334, 1989.

[48] A. Blandino, M. Macias, and D. Cantero, "Immobilization of glucose oxidase within calcium alginate gel capsules," *Process Biochemistry,* pp. 601-606, 2000.

[49] S. Rauf, A. Ihsan, K. Akhtar, M. A. Ghauri, M. Rahman, M. A. Anwar, and A. M. Khalid, "Glucose oxidase immobilization on a novel cellulose acetate-polymethylmethacrylate membrane," *J. Biotechnology,* pp. 351-360, 2006.

[50] A. Hollman and D. Bhattacharyya, "Pore assembled multilayers of charged polypeptides in microporous membranes for ion separation," *Langmuir,* 2004.

[51] V. Smuleac, L. Bachas, and D. Bhattacharyya, "Aqueous - Phase Synthesis of PAA in PVDF Membrane Pores for Nanoparticle Synthesis and Dichlorobiphenyl Degradation," *J Memb Sci,* vol. 346, pp. 310-317, Jan 15 2010.

[52] M. Gui, L. E. Ormsbee, and D. Bhattacharyya, "Reactive Functionalized Membranes for Polychlorinated Biphenyl Degradation," *Industrial & Engineering Chemistry Research,* vol. 52, pp. 10430-10440, 2013.

[53] D. Bhattacharyya, J. A. Hestekin, P. Brushaber, L. Cullen, L. Bachas, and S. K. Sikdar, "Novel poly-glutamic acid funcitonalized microfiltration membranes for sorption of heavy metals at high capacity," *Journal of Membrance Science,* vol. 141, pp. 121-135, 1998.

[54] H. C. Chenette, J. R. Robinson, E. Hobley, and S. M. Husson, "Development of high-productivity, strong cation-exchange adsorbers for protein capture by graft polymerization from membranes with different pore sizes," *J Memb Sci,* vol. 432-424, pp. 43-52, Dec 15 2012.

[55] S. Vaddiraju, D. J. Burgess, F. C. Jain, and F. Papadimitrakopoulos, "The role of H2O2 outer diffusion on the performance of implantable glucose sensors," *Biosens Bioelectron,* vol. 24, pp. 1557-62, Feb 15 2009.

[56] C. Mai, A. Majcherczyk, and W. Schormann…, "Degradation of acrylic copolymers by Fenton's reagent," *Polymer degradation and …,* 2002.

[57] K. Sato, Y. Naka, and J. Anzai, "Effects of hydrogen peroxide on the electrochemical decomposition of layer-by-layer thin films composed of 2-iminobiotin-labeled poly(ethyleneimine) and avidin," *J Colloid Interface Sci,* vol. 315, pp. 396-9, Nov 1 2007.

[58] S. Tomita, K. Sato, and J. Anzai, "Layer-by-layer assembled thin films composed of carboxyl-terminated poly(amidoamine) dendrimer as a pH-sensitive nano-device," *J Colloid Interface Sci,* vol. 326, pp. 35-40, Oct 1 2008.

[59] J. P. Roth and J. P. Klinman, "Catalysis of electron transfer during activation of O2 by the flavoprotein glucose oxidase," *Proc Natl Acad Sci U S A*, vol. 100, pp. 62-7, Jan 7 2003.

Vita

Andrew Tomaino was born in Red Bank, New Jersey in 1988. He completed his Bachelor of Science in Chemical Engineering at Rowan University in 2010. He entered the graduate program at the University of Kentucky in Fall 2011 in the Dept. of Chemical and Materials Engineering under the advisement of Prof. Dibakar Bhattacharyya. Andrew now lives in Lexington, KY with his girlfriend, Ashley Sofia.